Advanced Functionalization of Polyethylene via Catalyzed Chain Growth: Tailored Surfaces and Cationic End-Groups

Dissertation

zur Erlangung des mathematisch-naturwissenschaftlichen Doktorgrades
"Doctor rerum naturalium"
der Georg-August-Universität Göttingen

im Promotionsprogramm Catalysis for Sustainable Synthesis (CaSuS)
der Georg-August University School of Science
(GAUSS)

vorgelegt von
Jannik Wagner
aus Kassel

Göttingen, 2019

Thesis committee

Prof. Dr. Philipp Vana, MBA	Institute of Physical Chemistry Georg-August-University Göttingen
Prof. Dr. Franc Meyer	Institute of Inorganic Chemistry Georg-August-University Göttingen

Members of the examination board

Supervisor

Prof. Dr. Philipp Vana, MBA	Institute of Physical Chemistry Georg-August-University Göttingen

Co-supervisor

Prof. Dr. Franc Meyer	Institute of Inorganic Chemistry Georg-August-University Göttingen

Further members of the examination board

Prof. Dr. Dietmar Stalke	Institute of Inorganic Chemistry Georg-August-University Göttingen
Dr. Tim Schäfer	Institute of Physical Chemistry Georg-August-University Göttingen
Dr. Thomas Zeuch	Institute of Physical Chemistry Georg-August-University Göttingen
Dr. Florian Rehfeldt	3rd Institute of Physics - Biophysics Georg-August-University Göttingen

Date of the oral examination: February 04, 2019

Acknowledgement

First of all, I would like to thank my supervisor Prof. Dr. Philipp Vana for his guidance during my work and for giving me the freedom to follow my own ideas. I also want to thank my co-supervisor Prof. Dr. Franc Meyer for useful discussions, his support and especially for his engagement regarding the CaSuS Phd program. Prof. Dr. Dietmar Stalke, Dr. Tim Schäfer, Dr. Thomas Zeuch and Dr. Florian Rehfeldt are gratefully acknowledged for completing my thesis committee.

I was lucky to get a lot of support during my thesis. In this context I want to thank Wentao Peng and Darius Rohleder for providing me their nanoparticles, for TEM measurements and a lot of useful discussions. Dr. Martin Königsmann and Dr. Dennis Hübner are gratefully acknowledge for sharing their support and sharing expertise about wood and silica surface modification. A special thank goes to Byron Staudt for a close and wonderful cooperation and all the discussions we had. Lukas Emmerich and Volker Radisch are great fully acknowledged for conducting DVS and SEM analysis. I would like to thank Stella Weber, Lara Riemann, Annika Nitschke, Martin Königsmann, Darius Rohleder, Judith Steinhoff, Katharina Dabow and Byron Staudt for useful discussions and all their support improving this manuscript. Hans-Peter Vögele, Sandra Lotze, Heike Rohmann and the mechanical department are acknowledged for technical support. I would like to thank also my former bachelor student Niklas Eisele for a nice cooperation. All members of the MMC group and all CaSuS students are gratefully acknowledged for the nice working atmosphere.

I would like to thank Alex Groschopp, Dennis Hübner and Judith Steinhoff for the great time we had.
Finally, I want to thank my lovely wife Lorina, my great family and my friends for believing in me and all their support and help in every condition of life.

Abstract

Well-defined, end-functional polyethylene (PE) was synthesized in a catalyzed chain growth (CCG) polymerization and applied in novel synthetic routes for PE modified surfaces as well as in the manufacturing of multifunctional charged PE.

Polyethylene was covalently attached to the surface of prefunctionalized wood particles via different coupling reactions. Amine and azide end-functional polyethylene was grafted onto the surface via an amide-coupling or [3+2]-cycloaddition, respectively. Attenuated total reflectance Fourier-transform infrared (ATR-FTIR) spectroscopy of treated wood particles confirmed their successful modification. Differential scanning calorimetry (DSC) revealed the formation of a crystalline polyethylene layer with a decreased melting temperature range compared to non-bound PE. The decomposition temperature of PE modified wood shows combined characteristics of both components examined by thermogravimetric analysis TGA. Caused by the permanent attachment of polyethylene, a strong enhancement of the surface's hydrophobicity was achieved and validated by water contact angle (WCA) measurements and dynamic vapor sorption (DVS) analysis. Based on the developed strategies, surface modifications of silica nanoparticles were performed. TGA and dynamic light scattering (DLS) analysis confirmed the successful modification, further underlining the versatility of the designed system.

A novel route for the fabrication of polyethylene grafted gold- and silver nanoparticles (AuNPs and AgNPs) was developed by an efficient ligand exchange procedure using trithiocarbonate and thiol end-functional PE. DLS analysis revealed a strong increase in the hydrodynamic diameter of the nanoparticles caused by the strongly attached polyethylene-shell. The stability of the grafted nanoparticles over a wide temperature and time range was confirmed by DLS and UV-vis analysis. A perfect separation of the formed polyethylene–nanoparticle hybrids was observed and vali-

dated by transmission electron microscopy (TEM). Furthermore, these hybrid materials were well dispersible into a PE matrix even at high particle contents. Polyethylene capped AuNPs and AgNPs exhibited a reversible temperature-dependent aggregation/disaggregation behaviour, entirely attributed to the critical solution temperature of the attached polyethylene layer. The complete reversibility and the corresponding critical disaggregation temperature were confirmed by UV-vis analysis, demonstrating polyethylene's potential as thermoresponsive polymer. The investigated approach was subsequently transferred to palladium nanocrystals to further expand the field of polyethylene–noble metal nanohybrids.

The synthesis of charged end-functional polyethylene was performed based on iodo terminated PE in combination with an efficient nucleophilic substitution using various amines. The introduction of a permanent cationic end-group enables matrix-assisted laser desorption/ionization (MALDI) and electrospray ionisation (ESI) mass spectrometry of the investigated compounds, extending the field of PE end-group characterization via mass spectrometry. Mass spectra with excellent signal-to-noise ratios were obtained without the addition of any auxiliary metal salt. Caused by the introduction of an additional hydroxyl group, further transformation reactions on charged polyethylene were conducted. For this purpose, an alkyl-bromide moiety was introduced, resulting in a PE-based charged macroinitiator which was applied in a controlled radical polymerization, leading to the formation of a block copolymer. Moreover, the developed charged end-functional PE was applied in phase transfer catalysis. The results obtained by NMR spectroscopy revealed similar or superior activities compared to well-established phase transfer catalysts. In addition, the PE-based catalyst was completely recovered by simple filtration due to the solution properties of PE. Based on the phase transfer properties, an anionic dye could be introduced efficiently into cationic polyethylene. Caused by strong ion–ion interactions, the designed material showed an excellent solvent resistance without observing any migration of the incorporated compound.

Table of Content

1 Introduction and Motivation

With more than 50 weight percent of the overall produced polymers, polyolefins hold an outstanding relevance in modern industry.[1] Polyethylene and polypropylene represent the quantitatively most important polyolefin-based thermoplastics.[2] The physical and chemical properties of polyolefins, especially of polyethylene, depend strongly on their crystallinity and possible chain branching.[3] In 1955, *Ziegler* and coworkers developed a synthetic procedure for strictly linear polyethylene via a catalytic polymerization, resulting in high density polyethylene (HDPE).[4] This polymer is a cost-efficient material which is characterized by its magnific strength-to-density ratio, a relatively low toxicity[5] as well as excellent mechanical, UV- and thermal stability.[2,6,7] Based on these outstanding features a wide range of commercially available products has been established.[8] One special property of polyethylene is its thermomorphic behavior meaning a drastic change of its solubility within a small temperature range.[9–11]

Nonetheless, a direct chemical modification of polyethylene and therefore its usage as functional polymer for special applications is still restricted. One technique to overcome this limitation is the catalyzed chain growth (CCG) polymerization.[12,13] This method provides easy access to narrowly distributed polyethylene terminated by tunable functional groups.[14] Up to now, a wide range of different functional moieties was introduced, resulting in well-defined polyethylene for various applications.[15–18] For this purpose, an accurate examination of the end-group structure via different analytic methods is required. A general technique for polymer characterization is mass spectrometry that is mostly unsuitable for PE due to the lack of polar or coordinating moieties.[19–21]

Beside the fabrication of functional polymers, composite materials consisting of polymer and fillers are in the focus of academic and industrial research. These hybrid materials combine the characteristics of both components and therefore enhance their overall properties such as their mechanical, thermal, solubility or electrical behavior.[22] Typical reinforcing fillers such as silica[23,24] or wood[25,26] are well-established in

material science and are mostly applied for mechanical improvement of the composites. Additionally, the usage of nanoparticles for the formation of hybrid materials is of special interest due to their excellent surface-to-volume ratios.[27] Especially, noble metal nanoparticles such as gold and silver are in the focus of research caused by their antibacterial or outstanding optical properties and therefore are used e.g. for biomedical applications.[28–31]

Composites can be either formed by simply blending the respective filler into polymer matrices or by surface modification of the reinforcing material via a permanent attachment of polymers.[22,32] The latter strategy, mostly conducted for particles, results in stable and fine-tunable surfaces.[33] Nonetheless, the formation of covalently bound polymer brushes requires a strong interaction to the surface and therefore suitable functionalization of polymers.[33] Due to the lack of appropriate functional end-groups, polyethylene modified surfaces have not been properly developed yet.[34,35]

The purpose of this work was to demonstrate the versatility of various well-defined end-functional polyethylene synthesized via CCG for different approaches. Herein, the incorporation of charged end-groups was explored in order to expand the field of analysis for polyethylene by mass spectrometry. Beside a full characterization of PE, the phase transfer properties of cationic polyethylene in combination with its thermoresponsive behavior was investigated in detail. Moreover, a novel synthetic route for the modification of hydrophilic surfaces is presented. These tailored surfaces and their modified properties such as the change of hydrophobicity were examined. Another major project was the development of polyethylene grafted noble metal nanoparticles and thus the combination and enhancement of their outstanding characteristics.

2 Theoretical Background

In this chapter the theoretical and historical background of polyethylene polymerization will be summarized. In addition, more complex concepts and methods such as mass spectrometry, optical properties of metal nanoparticles and surface modifications, applied in this work, will be discussed and classified into the field of PE. Further discussions as well as additionally applied concepts will be explained in the main part of this thesis on the point it is required.

2.1 Conventional Polymerization of Polyethylene

Various polymerization methods for the production of polyethylene are established. One main technique is the radical polymerization of ethylene.[2,36] Although high pressures up to 1500 bar and high temperatures are required, this polymerization technique is widely used in industry. Via this method low density polyethylene (LDPE) can be produced caused by chain branching during the radical polymerization process.[36] For the production of high density polyethylene (HDPE) with negligible chain branching alternative polymerization methods are required. In the 1960s a polymerization system based on so-called *Philipps* catalysts was developed.[8] This catalyst type, based on chromium, is still used in industry scale and produces HDPE in combination with several advantages e.g. enabling of long-chain branching.[37,38] Another – probably the most famous – polymerization technique for PE is called Ziegler–Natta polymerization and the mechanism based on this method will be discussed in detail within the next paragraphs.

In 1955 *Ziegler* and *Natta* reported a procedure for the polymerization of ethylene (*Ziegler*) and other α-olefins (*Natta*) independently from each other.[39–41] The Ziegler–Natta process offers the possibility to polymerize at low temperature as well as low pressure and was awarded with the Nobel Prize in 1963.[4,42] The first reported systems were based on a mixed catalyst system consisting of a transition metal (group IV-VIII), commonly applied as halides (e.g. $TiCl_4$), and a main group metal (group

I-III) alkyl (e.g. AlR_3).[8] This process has been implemented on an industrial scale and has been steadily developed through the investigation of new catalysts and co-factors.[2,8,43,44]

Basics of Ziegler–Natta Polymerization

Typically, the classical Ziegler–Natta polymerization is carried out in heterogeneous phase. In this case, the titanium catalyst is mostly bound to a supporting material and afterwards activated. Due to the similar crystalline structure, magnesium chloride is often used as a carrier for $TiCl_3$ precatalysts.[44–46] Within crystalline $TiCl_3$ each titanium ion exhibits an octahedral environment of six chloride ions. On the surface, certain titanium ions offer a free coordination site regarding to crystallographic defects as well as exposed positions.[47] *Cossee* and *Arlman* developed a model mechanism for the ethylene polymerization using a $TiCl_3$ surface in combination with AlR_3 that works as an activator (Scheme 2-1).[47,48] The main group organic compound (AlR_3) is able to abstract a chloride ion from the surface and substitute it with an alkyl-group resulting in an alkylated titanium surface bearing a free coordination site. Onto the resulting coordination site, the respective monomer coordinates followed by an insertion of ethene into the metal–carbon bond yielding again an alkylated and unsaturated titanium surface.[47] Repeating of the coordination and insertion leads to a polymerization.[8,44]

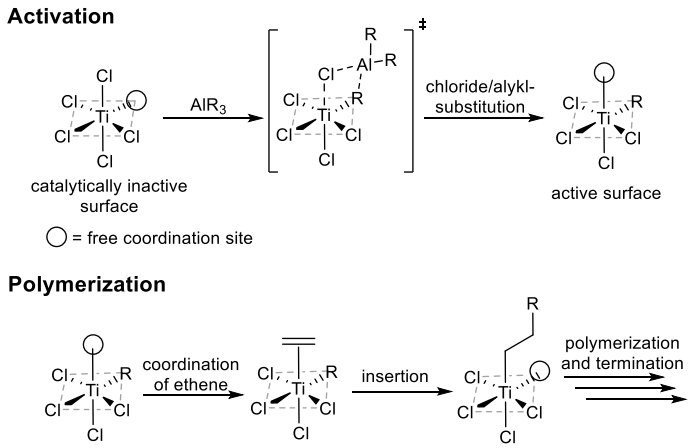

Scheme 2-1. Simplified Ziegler–Natta polymerization of ethylene using $TiCl_3$ and AlR_3.

Metallocene Catalyst in Olefin Polymerization

Another class of catalysts for the polymerisation of olefins was introduced in the 1980s in combination with the development of novel activation compounds (for further discussions see chapter 2.2).[49,50] Caused by the applied ligand system (cyclopentadienyl (cp) or pentamethylcyclopentadienyl (cp*)) these catalyst species are called metallocene catalyst or simply metallocene. The precatalysts ($(cp)_2MX_2$, M = transition metal, X = halide) are soluble in organic solvents and allow homogeneous reactions with defined catalytically active centers.[50–53] Commonly, transition metals of group IV (Ti, Zr, Hf) are used.[54]

Through the usage of homogeneous single-site catalysts, the activity and selectivity of the polymerization of α-olefins can be controlled by tuning the applied ligand systems. Thus, by employing chiral catalysts it is possible to achieve a stereoselective polymerization e.g. of propene. Ansa-metallocenes are usually used as chiral catalysts, which are characterized by a rigid and defined symmetry of the active center.[54,55] In Figure 2-1 exemplary zirconium-based catalysts, their symmetry and the resulting stereoselectivity are summarized.

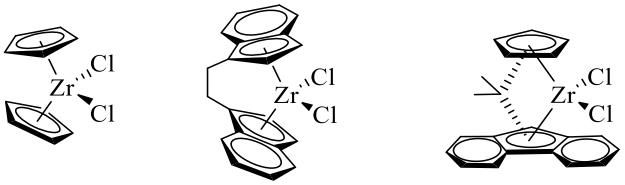

symmetry	C_{2v}	C_2	C_s
resulting tacticity	atactic	isotactic	syndiotactic

Figure 2-1. Examples of stereoselective metallocene catalysts.

For the polymerization of ethene, stereoselectivity is irrelevant and therefore synthetically easier accessible complexes with a C_{2v}-symmetry can be applied. In addition to metallocenes, a broad variation of ligand systems and multinuclear catalysts has been developed.[43,55,56]

Within this work a metallocene catalyst with C_{2v}-symmetry was applied, and therefore, other catalyst classes were not discussed furthermore.

Although single-site and heterogenous multi-site catalysts differ in activity and possible selectivity, both belong to a comparable mechanism that is discussed in the next subchapter.

2.2 Mechanism of Homogenous Ethylene Polymerization

In general, the main mechanistic steps of the polymerization using homogeneous catalysts are comparable to the Ziegler–Natta procedure further underlining the importance of its investigation (Scheme 2-2).[8] The activation, propagation and termination reactions of the mechanism will be discussed step-by-step.

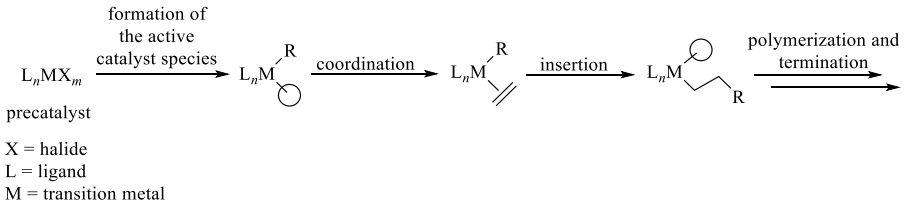

Scheme 2-2. Simplified polymerization mechanism of ethylene.

Activation

The first part of the mechanism is the formation of an active catalyst species. Nowadays variable activators are accessible ranging from simple aluminium alkyls to more complex, but highly active compounds (e.g. $[Ph_3C]^+[B(C_6F_5)_4]^-$).[57,58] The development and investigation of methylaluminoxane (MAO), namely by *Kaminsky* and *Sinn*, was one of the major achievements within this field.[45,50,59] Both have shown that the usage of partially hydrolysed trimethylaluminum (MAO) drastically increases the overall activity of various catalyst systems as well as expends the field of applicable catalysts.[57,59–61] The structure and the impact of MAO is multifaceted due to its heterogeneity. Nevertheless, it is one of the most applied activators and used in large industry scale.[59] The activation using MAO in combination with a metallocene based catalyst is a two-step process (Scheme 2-3).

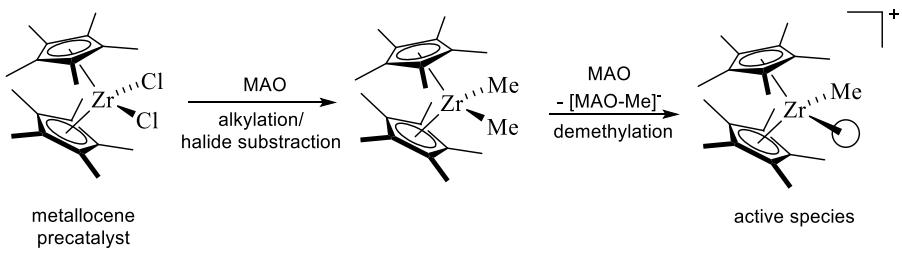

Scheme 2-3. Activation of a metallocene catalyst using MAO.

In the first step MAO acts as a lewis acid and substitutes two chloride ions bound to zirconium with two methyl groups yielding a double methylated complex. In the following step MAO reacts as a demethylating agent resulting a positively charged complex bearing a free coordination site.[60] This species is extremely efficient for the polymerization of ethylene.[57,62,63] Conclusively, activators like MAO act as a lewis acid and as a methylating as well as a demethylating agent.[57,64]

Propagation

After the formation of a catalytic active species, a monomer can coordinate to the free binding site followed by an insertion reaction (Scheme 2-2). The key step of the propagation mechanism is the insertion of the olefin into the M–C bond. A more accurate and generally accepted description of this step was introduced in the 1960s by *Arlman* and *Cossee* (Scheme 2-4).[47,48] In this model it is assumed that the insertion step takes place via a 4-electron–4-center transition state. Based on the insertion step the growing chain migrates from one binding site to another.[8] Besides the *Cossee–Arlman* mechanism, different models were discussed in literature. For instance, *Rooney* and *Green* postulated a carbene intermediate via a hydride transfer from carbon to the metal centre. After coordination, the monomer reacts with this intermediate followed by a reductive elimination of the hydride complex yielding again an active catalyst.[65,66]
A further development of the *Cossee–Arlman* mechanism was performed by *Brookhart* and *Green*. This model includes the concept of α- and β-agostic interactions into the consideration of the mechanism (Scheme 2-4).[67,68] These weak intramolecular interactions between a C–H-bond and the transition-metal centre stabilize the coordinatively unsaturated complex and the transition state.[69,70]

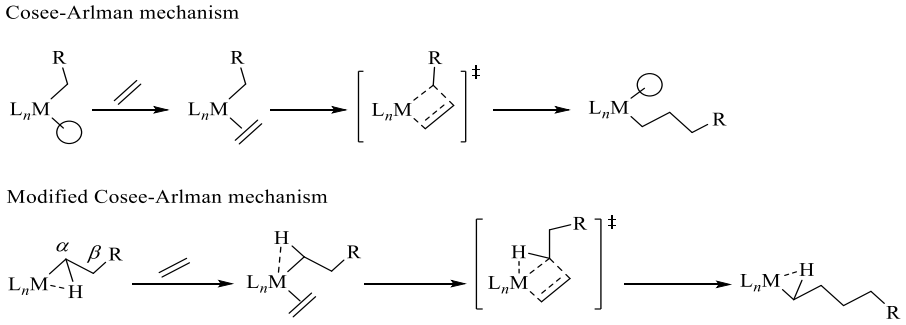

Scheme 2-4. Coosee–Arlman mechanism of ethylene insertion.

Termination

The last step of the mechanism considers possible chain termination or transfer reactions (Scheme 2-5).[71] Proceeding from the via *β*-agostic-bond stabilized complex a second reaction can occur in the absence of monomer coordination. This *β*-hydride elimination yields a hydrido complex and a vinylic terminated polymer chain (Scheme 2-5 middle).[72] Another possible side reaction is the *β*-hydride transfer from a bound polymer chain to a coordinated monomer, yielding a vinylic terminated polymer as well but in addition an alkylated complex (Scheme 2-5 top).[44] A third termination reaction, that is discussed herein, is the transfer from the coordinated polymer chain to the activator (e.g. MAO). This transfer results in an active alkylated complex and a polymer chain mostly irreversible bounded to the cofactor. The described termination or transfer reactions do not necessarily lead to a full ending of the polymerization process, since hydrogen or chain transfer yield to other catalytically active alkyl complexes.[8,71]

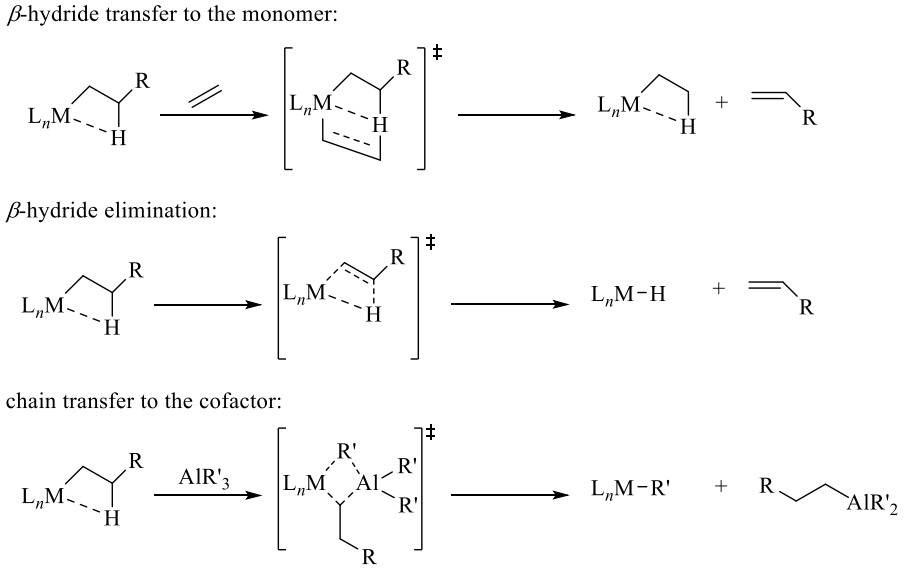

Scheme 2-5. Possible termination and transfer reactions.

2.3 Catalyzed Chain Growth

Limitations of the conventional, statistically occurring coordination-insertion polymerization are high-dispersed products (for heterogenous Ziegler-Natta catalysts: $Đ$ = 8-30, for homogenous catalysts: $Đ$ = ~2) and on the other hand strongly limited functionalizations of polyethylene.[3,73] One technique to overcome these limitations is the coordinative chain transfer polymerization that is based on a transition metal catalyst in combination with a chain transfer agent (CTA) (Scheme 2-6).[13]

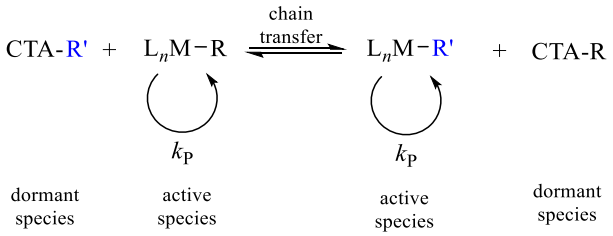

Scheme 2-6. Simplified mechanism of coordinative chain transfer polymerization.

Basic Mechanism of CCTP and CCG

The mechanism of the coordinative chain transfer polymerization (CCTP) differs from the conventional polymerization in one major element. As described in chapter 2.2, the polymer chain is growing on the active catalyst in a typical coordination-insertion polymerization. In an additional step, the growing chain is reversible exchanged with another polymer that is bound on a catalytically inactive chain transfer agent (dormant species, see Scheme 2-6).[74] One special feature of this method is the possible usage of two catalysts which are selective to different monomers in combination with only one suitable CTA. By implementing this approach block copolymers are accessible via CCTP.[75]

Within this field the related concept of catalyzed chain growth (CCG) was established by *Gibson* and coworkers.[12] The first system introduced by this group is based on a bis(imido)pyridyl iron catalyst in combination with diethyl zinc as chain transfer agent.[76,77] It was demonstrated that in the absence or suppression of termination processes and under consideration of an efficient and completely reversible transfer between the CTA and the catalyst, all chains have the same probability to grow.[77,78] In addition, by using efficient CTAs working also as activators, multiple chains grow on one catalyst molecules parallelly whereas in a conventional system only one chain per catalyst can grow at the same time.[79] Furthermore, after the CCG polymerization process occurred, nearly all polymer chains are bound to the main group cofactor. Based on the resulting metal-organic group, CCG provides access towards end-group functionalization as well as the possibility to synthesize block copolymers by the subsequent addition of another monomer.[13,74,79] The

basic concept of catalyzed chain growth is comparable to RAFT (reversible addition-fragmentation chain transfer polymerization) polymerization, a well-established controlled radical polymerization technique.[80] For the reasons mentioned, catalyzed chain growth can be considered as living-type polymerization.[12,81]
In CCG and CCTP various transition metal catalysts e.g. chromium[82], iron[76], different lanthanides like lanthanocene[83], zirconium[84], cerium[85], neodymium[86] or hafnium[87] were applied. Established chain transfer agents are commonly based on aluminium[74,87], magnesium[88] or zinc[77].
A suitable combination of the catalyst/cocatalyst depends on e.g. the sterically hinderance. Furthermore, the binding energy of the polymer to the CTA has to be comparable to the stability of the polymer–catalyst bond in order to achieve a fast and full reversibility of the transfer reaction.[13,78]

Catalyzed Chain Growth based on Neodymium and Magnesium

One highly active precatalyst that is suitable for the polymerization of ethylene is $[(cp^*)_2NdCl_2Li(OEt)_2]$.[89] In combination with a dialkylmagnesium compound, that works both as CTA and activator, the resulting system is able to polymerize ethylene in a controlled fashion. This well-established and investigated system was applied in this work and therefore will be presented herein.[88] The catalyzed chain growth mechanism of ethylene using a [Nd] catalyst is shown in Scheme 2-7.

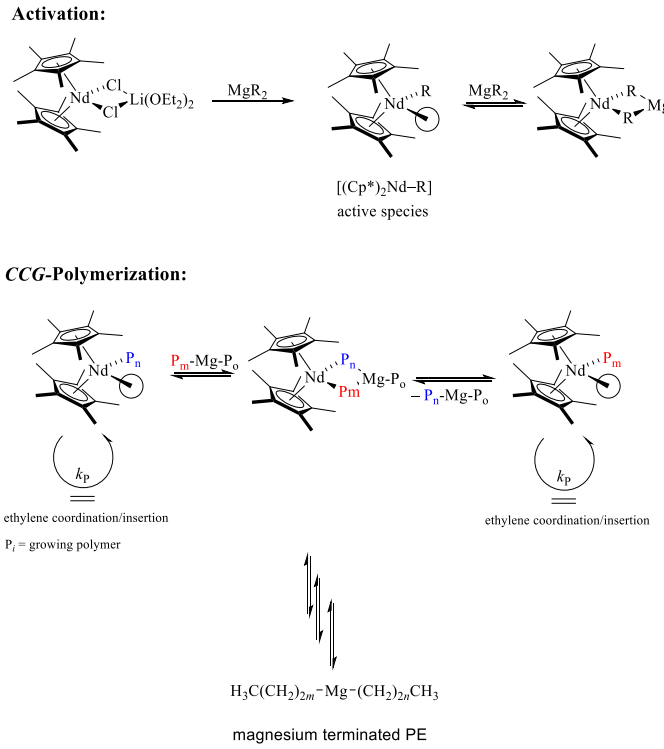

Scheme 2-7. CCG polymerization mechanism of ethylene using dialkylmagnesium and [(cp*)$_2$NdCl$_2$Li(OEt)$_2$].

Analogous to the discussions made before, the first mechanism-step is the activation of the precatalyst via a diorganomagnesium compound forming an active, unsaturated complex (Scheme 2-7 upper site).[90,91] Proceeding from this species the ethylene polymerization occurs in a typical coordination-insertion mechanism (chapter 2.2, Scheme 2-4). As described above, within the CCG system the diorganomagnesium compound exhibits an additional function and acts as a chain transfer agent via a bimetallic intermediate.[88,91] Based on the efficient and completely reversible exchange of growing polymer chains a uniform molecular weight distribution is achievable under those conditions.[83,90] In addition, the polymerization degree is linearly proportional to the reaction time and monomer conversion.

End-group Functionalization of Polyethylene

Besides the mentioned improvements, the major advantage of CCG is the formation carbon–magnesium bonds at all chains (PE–Mg–PE) after propagation. This terminated polyethylene intermediate provides a strong electrophilic behavior and can react in *Grignard*-type reactions. Based on this highly reactive species various end groups has been introduced (Scheme 2-8).[14]

For instance, elemental iodine reacts efficiently with PE–Mg–PE resulting in iodo terminated polyethylene (PE-I) with excellent yields up to 95 %.[15] PE-I can be converted into an azide end-group (PE-N_3) by the reaction with NaN_3 that can be applied for instance in a *Huisgen* cycloaddition.[15,92] Another pathway based on PE-N_3 is the quantitative reduction providing an amine end-functional polyethylene (PE-NH_2) that can be subsequently converted e.g. into an macroinitiator for the synthesis of well-defined block copolymers via controlled radical polymerization techniques.[14,15] Based on the Grignard type intermediate also macroalkoxyamines are accessible for the application in nitroxide-mediated radical polymerization.[90,93] Also PE-based macroinitiators for further polymerization methods were successfully synthesized via a CCG procedure in combination with multiple step end-group modifications.[16] Furthermore, by using prefunctionalized diorganomagnesium compounds even α-ω-functional polyethylene bearing different end-groups are accessible.[17,18,94] In addition, by the reaction with sulfur or oxygen[14] respective thiol or hydroxyl functional groups can be introduced into polyethylene.[95] Alkene groups in combination with thiol groups were subsequently used in thiol *Michael*- or thiol-ene-reactions offering a novel reaction pathway for various end-group transformations.[95,96] The reaction of di-polyethylene magnesium directly with disulfides of trithiocarbonates leading in trithiocarbonate functionalized PE (Scheme 2-8).[97]

These examples demonstrate the versatility of the catalyzed chain growth polymerization for the efficient end-group modification of polyethylene. Several of these strategies were applied and further developed in this work.

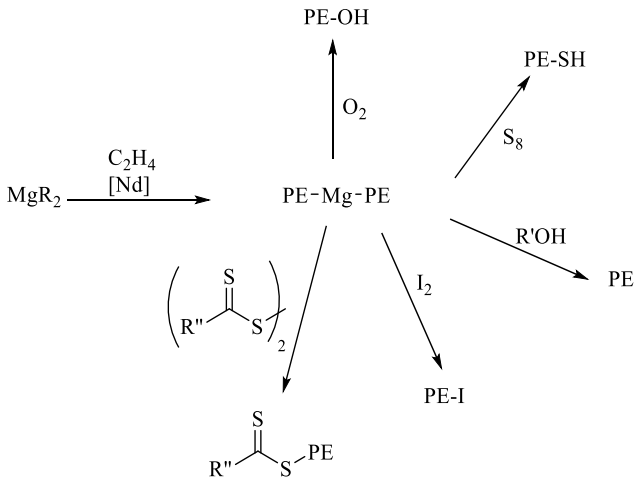

Scheme 2-8. Possible end-group functionalization based on CCG.

2.4 Mass-Spectrometry in Polymer Science

Mass spectrometry (MS) is a widely used technique in academic research as well as in industry for the analysis of various compounds. Up to now, a broad range of detection methods and ionization processes were developed and therefore only those applied in this work will be discussed in a simplified fashion.[98,99]

The basic principle of a mass spectrometer can be divided into different parts (Figure 2-2).[98] First of all the sample has to be introduced into the mass spectrometer. In mass spectrometry the conversion of the analyte into the gas phase as well as its ionisation is required. The resulting gaseous and ionized compounds are separated based on their mass-to-charge (*m*/*z*) ratio and subsequently analysed by a detector. The ionisation process, the separation and the detection of the sample are carried out *in vacuo*.

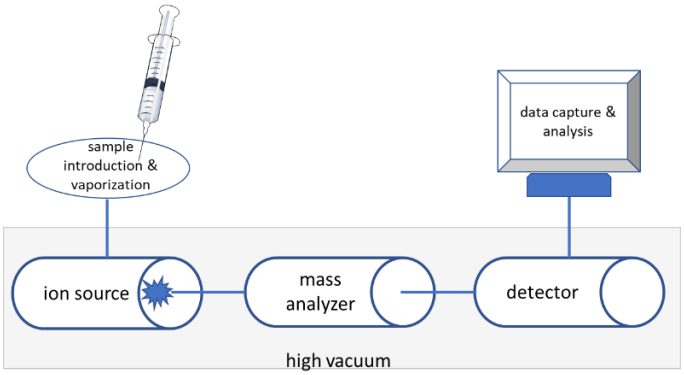

Figure 2-2. Simplified set-up of a mass spectrometer.

Basics of ESI-MS & MALDI-TOF-MS

Within the field of ionisation procedures electrospray ionisation mass spectrometry (ESI-MS) and matrix-assisted laser desorption mass spectrometry (MALDI-MS) are two of the most established techniques. These soft-ionisation methods were awarded with the Noble Prize in the year 2003.[100,101]

In case of ESI, the sample has to be dissolved homogenously using a polar and volatile solvent (for further discussion see chapter 5). This solution is transferred through a capillary with a decreasing diameter. The capillary is charged with a high voltage via an electrode tip and the analyte is sprayed into the mass analyser. This procedure results in highly charged droplets.[102] Through repulsion electric forces as well as the evaporation of the solvent a downsizing of the droplet occurs until a unsolvated single analyte molecule is obtained which is analysed (Figure 2-3).[98,99,103]

In contrast to ESI, in MALDI-MS the analyte is supported by a matrix in the solid state. Therefore, the choice of a suitable matrix and a careful sample preparation are fundamental in MALDI.[19] Often organic molecules with an aromatic π-system are applied in combination with an acid that is able to ionize the analyte during the MALDI process.[99,104] The matrix is irradiated with using a laser.[99] The absorption of the laser energy leads to local heating and the matrix as well as the ionized analyte are transferred into the gas-phase.[104–106] Via an applied accelerating voltage the analyte is introduced to the detector system (Figure 2-4).[106]

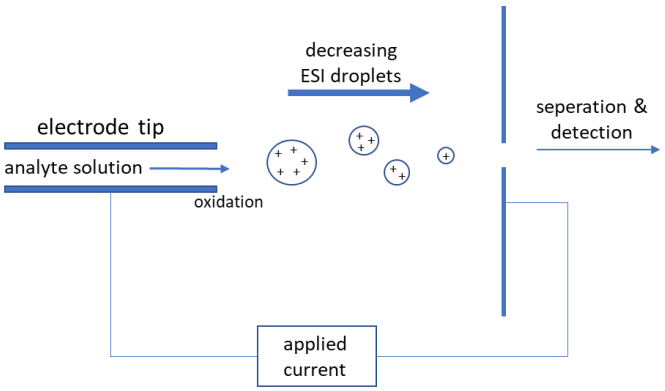

Figure 2-3. Simplified mechanism of electrospray ionisation.[98]

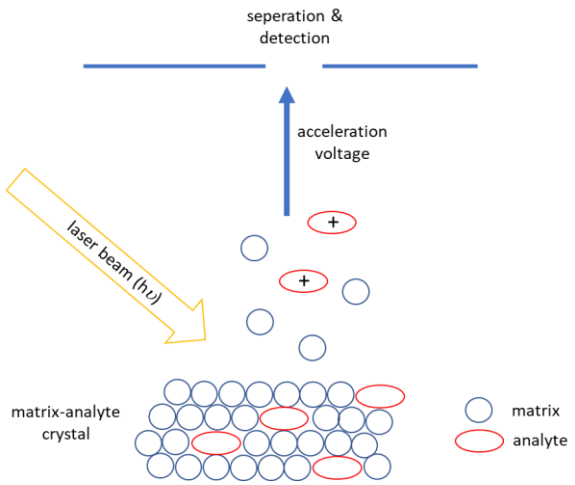

Figure 2-4. Simplified mechanism of matrix-assisted laser desorption ionization.

The mass analyser used in this work is based on the separation of the ions through an applied electric field. Via this field the ionized analytes were accelerated and due to the diversity in the *m*/*z*-ratio a difference in the (electric-field-free) flight duration occurred. This leads to a separation of the analytes followed by their detection. This technique is called time-of-flight mass spectrometry (TOF-MS).[107]

Mass Spectrometry of Polymers and Polyethylene

Mass spectrometry has a wide range of applications.[98] In the field of polymer characterization mass spectrometry is well-established.[20] Due to the high sensitivity of MS, distinct chains are separated and well resolved spectra and mass distributions can be achieved.[20,108] Consequently, both MALDI-MS and ESI-MS offer the possibility for a detailed end-group characterization of polymers.[19] It has to be considered that the obtained spectra of ESI and MALDI can differ, e.g. in case of ESI multiple charged chains whereas in MALDI only single charged molecules can be detected. In addition to end-group characterization, mass spectrometry gives access to molecular weight distribution, although a divergence compared to molecular weight distribution obtained from site-exclusion chromatography (SEC) is observed.[19,108] This is explainable because of mass discrimination effects in MS. Polymers with higher molar masses are more difficult to evaporate and the transport efficiency of such polymers is reduced. For this reason, molar mass distributions obtained from MS are typically shifted to lower molar masses compared to SEC.[109–111] The most established route for the formation of polymer ions is the adductions of auxiliary ions like alkali metals (specially Na^+) in case of hydrophilic polymers or silver ions for more nonpolar polymers like polystyrene bound via π-interactions.[108,109]

Due to the lack of polar groups in polyolefins, especially for PE, mass spectrometry is still a challenging topic and is commonly not suitable for these classes of polymers.[21] Nevertheless, one possibility to overcome this limitation is the introduction of polar or vinylic groups into PE. Polar groups can be introduced e.g. by using catalyzed chain growth (chapter 2.3). These polar groups offer a coordination site and can be used in MALDI-MS via the explained metal adduct method.[93,97] Vinylic terminated polyethylene can be synthesized using conventional polymerization techniques via β-hydride elimination (see chapter 2.2, Scheme 2-5). These double bonds can be ionized by using e.g. silver ions and therefore partially be detected in MALDI-MS.[112] Another approach, that builds the basis of this work, is the incorporation of a charged group into polyethylene, mainly developed by *Wallace* and coworkers.[113,114] The synthesis of precharged polyethylene gives direct access to MALDI-MS without any additional metal adducts.[21,114] The synthetic procedure is

based on a conventional vinylic terminated polyethylene that is subsequently brominated followed by a nucleophilic substitution using triphenylphosphine yielding a permanent charged PE (Scheme 2-9). The overall yields obtained in this procedure were reported to be around 48 %.[21,113] In addition to the work of *Wallace*, by the introduction of other charged groups or using a cationized catalyst-bound intermediate, a few examples are described in literature for the analysis of polyethylene via ESI-MS that is typically more difficult due to the requirement of a homogenous solution as described above.[115,116] A detailed discussion of charged polyethylene, also its usage for other applications, will take place in chapter 5.

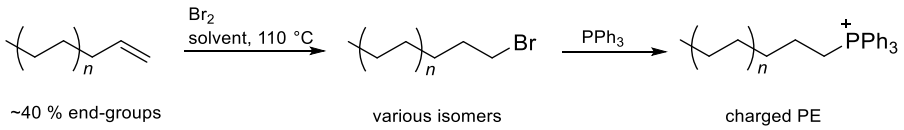

Scheme 2-9. Simplified reaction scheme for the synthesis of charged functional PE based on the work of *Wallace* and coworkers.

2.5 Polyethylene Modified Surfaces

Exemplary Strategies for the Surface Modifications with Polymers

Hybrid materials consisting of polymer and inorganic particles play an important role in scientific research as well as in industrial applications. Different strategies for the formation of such compounds are discussed in literature. In one simple strategy, particles can be introduced by simple blending with a polymer solution or melt followed by evaporation of the solvent and a crosslinking processes of the polymer resulting in composite materials.[22] In this typical coating process the polymer–surface interaction is based on physisorption and therefore only weak attachments can be reached. In contrast to this procedure, polymer chains can be covalently bound to the surfaces forming polymer brushes with a high stability.[22,33] The formation of polymer brushes on the surfaces has a

strong impact on the overall properties of the hybrid material. The characteristics of the polymer and the applied particles can be combined via this approach. Consequently, depending on the type of polymer, the surface's properties can be tailored. For instance, by varying the applied polymer the hydrophilicity or hydrophobicity of the surfaces can be tuned.[117] Also more complex characteristics can be introduced by using e.g. responsive polymers leading in a change of their properties by an external stimulus.[118] These are just two examples of tailoring surfaces and a wide range of polymer and particle combinations were established and developed.[119] In this work only polyethylene and the applied particles will be discussed in the next subchapters. Within the field of hybrid materials, nanoparticles (NP) are of special interest due to excellent surface-to-volume ratios.[119,120] In consequence, by adding only small amounts of respective NPs into polymer matrices a strong impact on the overall properties is achieved.[27]

In a simplified perspective, the basic approaches for the surface modification are comparable independently from the applied polymerization technique and herein, two major strategies will be discussed. The first approach is based on the preformation of a polymer chain bearing a functional group. The advantage is that a full characterization and tailoring of the compound can be achieved independently from the particles. The active end-group can react subsequently with an anchor group bound to the surface resulting in a covalent modification of the respective interface. Due to this two-step mechanism, the method is called grafting-to approach (Scheme 2-10 left-hand side).[121,122] The second synthetic route is called grafting-from approach. In this method either an initiator or a chain transfer agent is bound to the surface. This leads to a growing of the chain directly from the surfaces resulting in polymer brushes covalently bound to the surface as well. Using this approach typically higher grafting densities can be obtained due to less steric hindrance. On the other hand the characterization of the polymer as well as a possible cleavage reactions are more challenging (Scheme 2-10 right-hand side).[22,119,123]

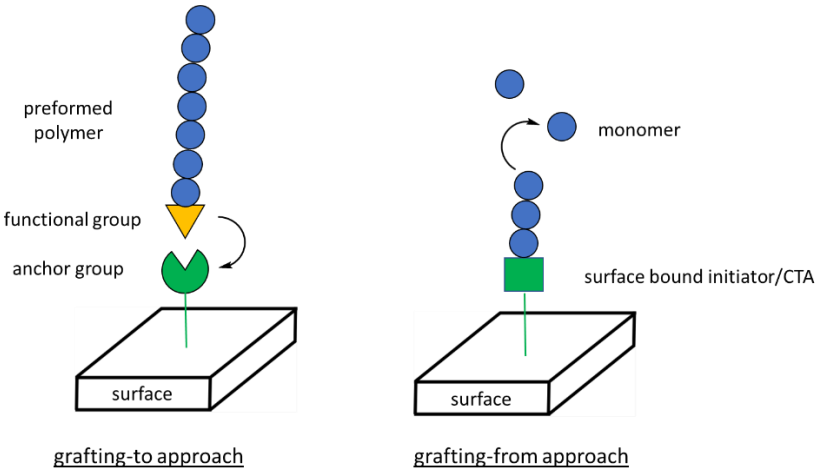

Scheme 2-10. Basic mechanisms of a grafting-to or grafting-from approach.

Polyethylene on Variable Surfaces

Due to the lack of possible binding sites in polyethylene, the surface modification with PE is still challenging, but several composite materials based on polyethylene in combination with variable types of particles have been developed. Commonly the synthesis is either based on in-situ polymerization[124], by using a copolymer containing possible binding moieties[125], the immobilization of an active catalyst on the surface[126,127] or by blending stabilized particles into a polyethylene matrix[32]. Nevertheless, the surface modification using well-defined PE synthesized by CCG is still limited and just a few examples exist up to now. The basic properties and strategies of the materials applied in this work will be discussed in the next paragraphs.

Silica Surfaces

Silica nanoparticles have a wide range of industrial applications ranging from additives in food to reinforcing materials in coating and varnish to the usage in rubber technology.[23,24] Besides the industrial applications, silica particles are in the focus in polymer chemistry reaching from mechanistic studies to the synthesis of novel polymer–silica-

composites.[24,128,129] Two examples for surface modification of either silicon substrates or silica particles with well-defined polyethylene via CCG were introduced. *D'Agosto* and coworkers grafted a planar silicon substrate with poly(glycidyl methacrylate). The so attached epoxide-moiety could afterwards react with an amino end-functionalized polyethylene synthesized via CCG resulting in a homogenous PE coverage of the surface.[35] Recently, a second approach for the synthesis of PE-modified silica nanoparticles was introduced.[130] The group of *Hu* et al. presented different synthetic routes based on variable anchor groups in a grafting-to approach. The silica nanoparticles were converted via tetrachlorosilane into an active Si–Cl surface that could subsequently reacts with prefunctionalized polyethylene. The resulting silica–polyethylene nanocomposites were dispersible in a PE-matrix.[130]

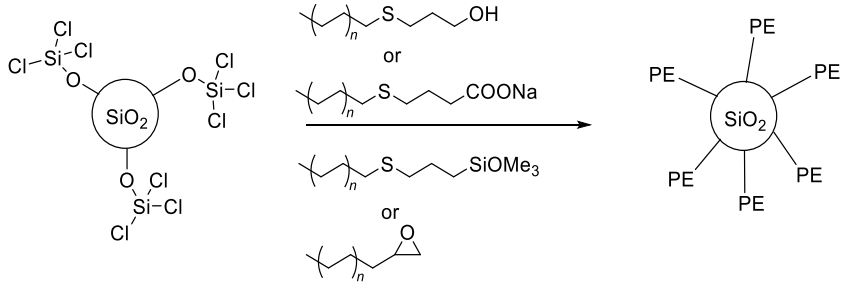

Scheme 2-11. Synthesis of PE-grafted silica based on the work of *Hu* et al.

Wood Surfaces

Wood plastic composites (WPC) have received a strong attention in scientific research and industry. This interest is explainable because wood provides a strong enhancement of the mechanical and thermal properties compared to its relatively low density and its low cost.[25,26] Furthermore, a polymer coating, e.g. using polyolefins, shielded the wood surface against undesired water absorption and microorganism caused degradation.[131] In addition, wood is an environmentally friendly and a renewable source and therefore sustainable. PE–wood hybrid materials are of special interest because they combine the properties of wood with

the versatility, stability and processability of PE mentioned before.[25,132]
The major challenge for the formation of polyethylene–wood hybrid materials is caused by the surface of wood. Due to the high amount of hydrophilic hydroxyl-groups an insufficient interaction with PE occurs and therefore commonly further additives are required.[133] Nevertheless, one major strategy is discussed in literature for the formation of polyethylene brushes on wood surfaces. This strategy used in industry and academic research is based on the functionalization of polyethylene with maleic anhydride moieties (PE-*g*-MA).[25,134] The introduced anhydride can directly react with the surface resulting in PE modified wood. The formation of such PE-*g*-MA polymers starts from saturated, conventional HDPE that is cracked either thermal, via ultrasonic irradiation or by a strong excess of radicals leading in a homolytic cleavage of a C–C- or C–H-bond within the PE backbone (Scheme 2-12).[135,136] This intermediate radical can react with maleic anhydride yielding PE-*g*-MA. The major disadvantage of this process is the variability of side-reaction pathways during the procedure resulting in a strong inhomogeneity of the compound. Possible side reactions are transfer reactions, recombination of two radicals and varying amounts of MA in the resulting polymer.[135]
Up to now a sufficient modification of wood with well-defined polyethylene brushes is still limited and will be discussed in chapter 3.2.

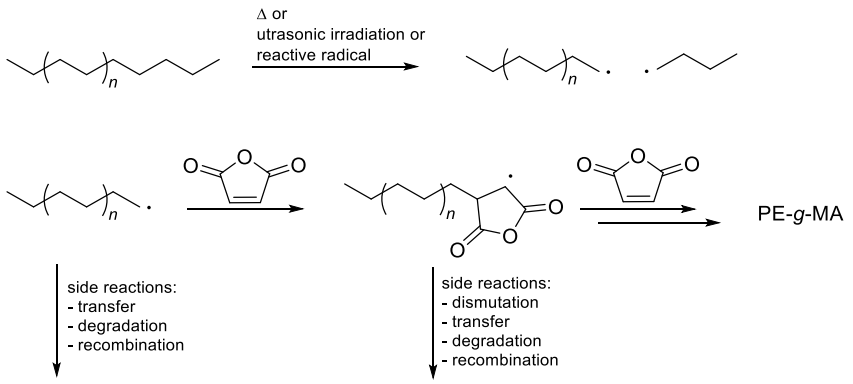

Scheme 2-12. Synthesis of polyethylene-*g*-maleic anhydride.

Metal Nanoparticle Surfaces

As briefly mentioned before, nanoscience and nanotechnology have become a prominent field with raising attention in academic research.[27] The combination of metal NPs with polymer science resulting in metal-polymer hybrid nanostructures provides versatile applications. These materials interconnect the characteristics of functional polymers and applied NPs leading to improved mechanical, optical or electrical properties.[137] In addition to that, polymer brushes on the surface enhance the stability due to steric effects and therefore supress aggregation that typically occurs between nanoparticles due to strong interparticle forces. Furthermore, the polymer shell provides adjustable dispersibility into e.g. solvents or polymer matrices which were unsuitable for blank NPs.[138] In nanoscience, polymer grafted silver and gold nanoparticles are of a major interest. One requirement for the successful formation of these compounds is a strong attachment of the polymer to the surface and an appropriate grafting-density in order to combine both properties and ensure a high stability. To achieve these criteria, strong interactions to the surface are required. For AuNPs and AgNPs sulfur-containing moieties like thiol or trithiocarbonate groups offer a strong attachment to the surface, well-investigated by the group of *Vana*. Therefore, this strategy is also applied within this work (chapter 4).[139–141]

Properties of Gold and Silver Nanoparticles

Silver nanoparticles exhibit outstanding antimicrobial properties and are widely used e.g. in food packaging and in biomedical industry.[29,30] These particles are the most applied antimicrobial filler in polymer–NP-composites.[142] AuNPs are widely introduced in research and in consumer products[28] e.g. in cosmetic industry as well as in the field of catalysis[143] as well. The major application of AuNPs is regarded to the unique optical properties and based on this behaviour established e.g. in biosenseroing.[31] The optical properties are from large importance because it's directly regarded to the structure and environment of gold particles depending e.g. on size, shape, temperature or surrounding medium.[144,145] Therefore, optical spectroscopy (UV-vis) is a powerful tool for the analysis of gold NPs and nanocomposites and is also applied in this work (chapter 4). This feature is assigned to the surface plasmon resonance of gold particles that will be discussed briefly.[144] Surface plasmon resonance

is based on the interaction of light with a specific wavelength and free electrons on the surface resulting in an exciting and vibrating state of those. The oscillation of the electrons is caused by an electromagnetic field induced by light. The conductive electrons move exert from the electromagnetic field towards the surface resulting in a dipole moment in opposite direction. The oscillation frequency corresponds to the applied wavelength typically in the UV range (Figure 2-5). The absorption of a certain wavelength of visible light leads to the colourization of the NPs and is dependent on various factors mentioned above.[144]

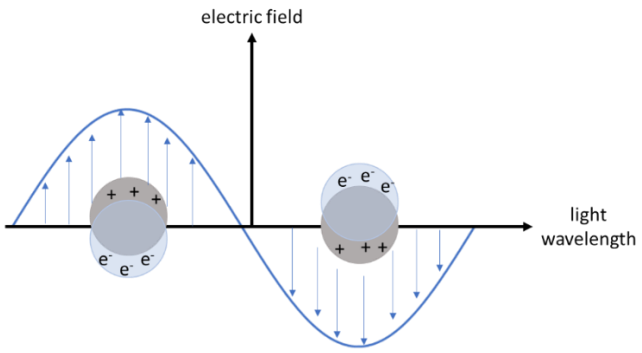

Figure 2-5. Schematic mechanism of surface plasmon resonance.

Polyethylene and Metal Nanoparticles

Up to now, for the synthesis of polyethylene gold and silver composites, AgNPs or AuNPs stabilized by ligands are simply blended with a polyethylene matrix.[32,146] The disadvantage is that migration as well as aggregation of the nanoparticles were observable. The synthesis of metal nanoparticles with a strongly attached polyethylene shell is barely developed. One route for the formation of metal–PE hybrids is based on iron oxide and amino end functional polyethylene synthesised via CCG by a ligand exchange procedure.[34] The resulting nanohybrid is fully dispersible within polyethylene matrices in high dosages without observed aggregation. This is a novel approach towards metal nanocomposites containing polyethylene that will be expanded and discussed in chapter 4 in detail.[34]

3 Polyethylene Modified Wood and Silica Surfaces

3.1 Introduction and Motivation

Composite materials consisting of polymers and reinforcing fillers have gained an outstanding interest in academic research as well as in industrial technology. These hybrid materials combine the characteristics of both polymer and filler and therefore a strong improvement of the overall properties can be achieved.[22,117] One strategy for the formation of hybrid materials is the direct modification of the respective surface by the covalent attachment of polymer brushes.

Due to its outstanding properties, such as high hydrophobicity as well as low cost and great chemical and thermal stability, polyethylene is one of the most important polymers.[1] Within the field of composites, the usage of wood as a reinforcing material is of special interest due to its high durability and – compared to its low density – outstanding improvement of mechanical properties. Furthermore, it is a renewable and therefore sustainable source. Nevertheless, for some applications several disadvantages are attributed to wood such as its highly hydrophilic character resulting in moisture dependent swelling or shrinking and in microorganisms-based degradation.[132] Surface modification of wood and the fabrication of wood plastic composites (WPC) using hydrophobic and stable polymers such as polyethylene can overcome these limitations.

However, due to the high amount of hydroxyl groups on the wood surface, one major challenge for the fabrication of PE-modified wood is attributed to their weak interactions among each other.[25] Up to now, the surface modification is performed using PE-*graft*-(maleic anhydride) (PE-*g*-MA) copolymers. These polymers are synthesized via a cracking process of HDPE under harsh conditions resulting in PE-based macroradicals that react *in situ* with MA. The disadvantage of this process is the formation of an inhomogeneous material due to a high number of side reactions and its high dispersities (see chapter 2.5).[134]

Considering this background, the major intention of this project was the development of a synthetic route for the formation of well-defined polyethylene covalently bound to wood surfaces. To ensure an appropriate grafting density, suitable prefunctionalized PE, synthesized via catalyzed chain growth, were applied which are able to react with suitable anchor groups on the wood surface in a grafting-to approach. The resulting hybrid materials were characterized via different methods in order to validate the enhancement of the WPC's properties, e.g. its wetting and thermal properties.
Beside the surface modification of wood, an investigation was conducted whether the developed strategies are transferable to other hydrophilic surfaces such as silica nanoparticles (SiNPs), a well-established filler material, to demonstrate the versatility of the applied synthetic route.

Predesign and Criteria of the Applied System
As described above, to achieve a sufficient grafting-density of the wood surface a strong driving force for the permanent attachment of polyethylene is required. Therefore, the overall strategy was the synthesis of one prefunctionalized polymer species that acts as a building platform for further transformations into suitable end-groups. Due to the efficient and established synthesis, iodo functionalized polyethylene (PE-I) was a promising starting material.[14]
For the surface modification two major synthetic pathways were aimed. In the first approach, unfunctionalized wood and its high amount of hydroxyl groups on the surface was applied in combination with an auxiliary base that enhances their nucleophilic character. For the subsequent nucleophilic substitution, PE-I might be directly applicable due to the strong leaving group properties of the iodide. Additionally, an epoxide end-functionalized polyethylene (PE_{epo}) was synthesized and applied due to its outstanding reactivity in ring-opening reactions.[147]
The second strategy includes a pretreatment of the wood surface in order to expand possible reactions. Considering the criteria explained before, the introduction of carboxyl moieties on the wood surface was targeted. These groups are expected to react with amine end-functional polyethylene (PE-NH_2) in a coupling reaction. Furthermore, an alkyne prefunctionalized wood surface is applicable in an efficient *click*-reaction

in combination with azide terminated polyethylene (PE-N_3).
In addition to the modification of wood, this approach was planned to be transferred to other hydrophilic surfaces, such as silica. Therefore, the strategy developed for wood surfaces should be implemented for the surface modification of silica nanoparticles (SiNPs). Beside the grafting-to approach a synthetic route for the surface modification of SiNPs by a grafting-from approach was designed.

3.2 Modification of Wood Surfaces

In this subchapter the predesigned synthetic routes will be presented starting from polymer synthesis and the introduction of various end-groups to the application of surface modification reactions. Additionally, the full characterization of PE–wood hybrid materials via different methods will be discussed in detail.

3.2.1 Synthesis of End-Functional Polyethylene

Synthesis and Characterization of Iodo End-functional Polyethylene (PE-I)

Based on the predesign of the grafting-to approach, the first step of the synthetic route was the formation of iodo end-functional polyethylene (PE-I) in a procedure comparable to literature.[14] The polymerization was conducted in a typical catalyzed chain growth process using $(cp^*)_2NdCl_2Li(OEt_2)_2$ in combination with butyloctylmagnesium (Bomag) that acts both as an activator and as a chain transfer agent (for detailed discussion see chapter 2.3). The applied ratio of [Nd] : [Mg] was 1 : 200 and the conduction temperature was set to 80 °C to ensure a high transfer rate and flexibility of the polymer while suppressing termination reactions. In order to achieve high molar masses of the polymer, that are required for an appropriate modification of the surface properties, the polymerization was conducted until precipitation was observed. At this point, the maximal achievable molar mass was reached before termination products became dominant due to the insolubility of the

PE–Mg–PE intermediate (Scheme 3-1).
The second requirement for a sufficient reaction with an adequate anchor group was a high degree of end-group functionality. Therefore, the efficient reaction between PE–Mg–PE and elemental iodine was applied. To avoid possible side reactions, a saturated iodine solution in THF ([I_2] : [Mg] = 1 : 5) was added immediately after precipitation was observed and the reaction was carried out over night by simultaneously cooling down the reaction mixture to room temperature. Afterwards, the polymer was filtered and washed followed by drying, resulting in PE-I that was directly applicable for characterizations and further reactions.

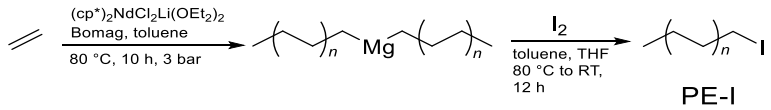

Scheme 3-1. Synthesis of iodo end-functionalized polyethylene.

In order to verify that the conducted polymerization was successful and that it proceeded under controlled conditions, high-temperature size exclusion chromatography (HT-SEC) was performed. The chromatogram revealed a narrow molecular mass distribution ($Đ = 1.1$) (Figure 3-1). From this examination it can be concluded that an excellent control of the polymerization was achieved. Furthermore, the determination of the characteristic values such as $\bar{M}_n$ (1650 g mol^{-1}), $\bar{M}_w$ (1800 g mol^{-1}) and the maximum of the molar mass distribution (M_P = 1900 g mol^{-1}) showed that a sufficient polymerization degree was reached while suppressing high mass termination products.
To ensure that a high degree of end functionality was achieved, the polymer was analyzed via proton nuclear magnetic resonance spectroscopy (^{1}H-NMR) that is one of the most suitable methods for the analysis of polymer end-groups. To achieve a full dissolution of PE, the measurement was conducted at 80 °C using toluene-d8 as solvent. The ^{1}H-NMR spectrum of the product confirmed the successful formation of iodo end functional polyethylene (Figure 3-2). The characteristic signal at $\delta = 2.8$ ppm was assigned to the methylene group adjacent to iodine (~CH_2-I). In addition, a broad multiplet at $\delta = 1.1 – 1.4$ ppm corresponds

to the polymer backbone whereas the triplet at $\delta = 0.88$ ppm can be assigned to the methyl end-group (~CH_3). By comparing the intensities of the integrals of the ~CH_2-I and ~CH_3 signals, an end-group functionality of 91 % was determined.

The characterization of PE-I via HT-SEC and ^{1}H-NMR spectroscopy confirmed the efficient and successful synthesis of PE-I with an extraordinary high end-group functionality. Consequently, further functionalization reactions based on PE-I could be conducted and will be explained in the next paragraphs.

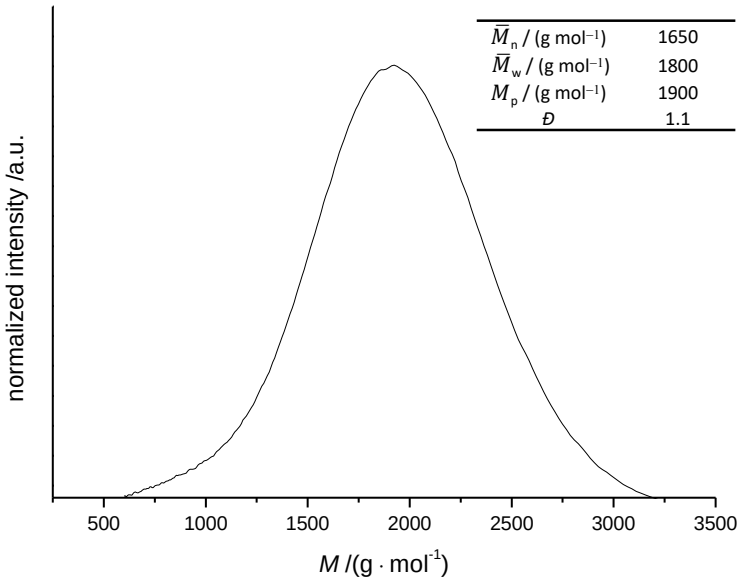

Figure 3-1. HT-SEC analysis of PE-I. The measurement was conducted at 150 °C using 1,2,4-trichlorobenzene as eluent.

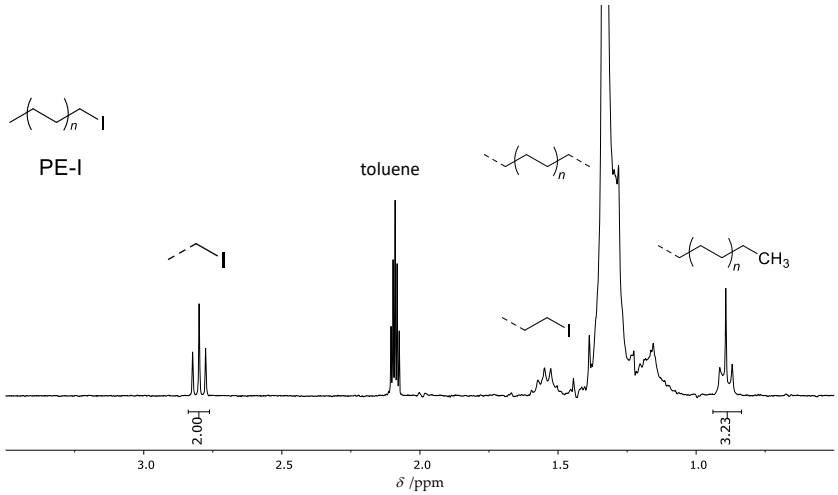

Figure 3-2. ^{1}H-NMR spectrum of PE-I. The measurement was conducted at 80 °C using toluene-d8 as solvent.

Synthesis of Azide- and Amine Terminated Polyethylene

After the successful synthesis of iodo end-functional polyethylene was confirmed, PE-I was applied for further substitution reactions. Due to the excellent leaving-group properties of the iodide, the iodo end-group can be replaced by an azide moiety in a simple nucleophilic substitution reaction using sodium azide (Scheme 3-2).[14] In order to achieve a full dissolution and high flexibility of the polymer chains, the reaction was conducted under reflux conditions. Furthermore, to ensure an appropriate dissolution of both polyethylene and sodium azide, a solvent mixture of toluene and dimethylformamide (DMF) was applied and the reaction was proceeded for 24 h. The azide functionalized polyethylene (PE-N_3) offers the possibility for the usage in an efficient [3+2]-*Huisgen* cycloaddition[148] (see chapter 3.2.2) and, on the other hand, can be easily transferred into an amine group. For the latter transformation, PE-N_3 was dissolved in dry toluene and reacted with a dispersion of $LiAlH_4$ in THF at 90 °C. After purification, the resulting amine terminated polyethylene (PE-NH_2) as well as PE-N_3 were characterized by ^{1}H-NMR to validate the successful conversion.

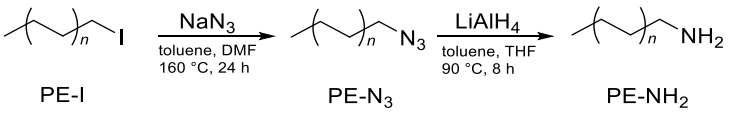

Scheme 3-2. Applied synthesis for the formation of PE-N_3 and PE-NH_2.

From the ^{1}H-NMR spectra the successful formation of PE-N_3 and PE-NH_2 was directly confirmed. In both cases the characteristic signal of the methyl end-group (δ = 0.88 ppm) was observed whereas the multiplet at δ = 1.1 – 1.4 ppm was assigned to the polymer backbone as described for PE-I.

For PE-N_3, the triplet at δ = 2.81 ppm corresponds to the methylene group adjacent to the nitrogen. A small broadening of the signal compared to PE-I was observed, which can be explained by the paramagnetic properties of the ^{14}N-isotop.[149] Compared to PE-I, The determined chemical shift of this signal is only slightly shifted downfield. This observation is in agreement with observations discussed in literature.[14]

In contrast to PE-N_3, the examination changed for PE-NH_2. The methylene-group bound to the nitrogen showed a drastic shift towards high-field compared to PE-N_3 and PE-I. The ~CH_2-NH_2 signal was shifted to δ = 2.52 ppm, whereas the triplet at δ = 2.81 ppm completely disappeared. This validated the successful conversion of PE-N_3 into PE-NH_2. In both cases the integrals between the methylene-group adjacent to the respective functional group and the methyl end-group are identically compared to the examination of PE-I.

From these results the successful and quantitative functionalization starting from PE-I to PE-N_3 to PE-NH_2 was confirmed. All three polymers were obtained with a high purity and a high degree of functionality (91 %) and therefore were applicable for the surface modification reactions described in chapter 3.2.2.

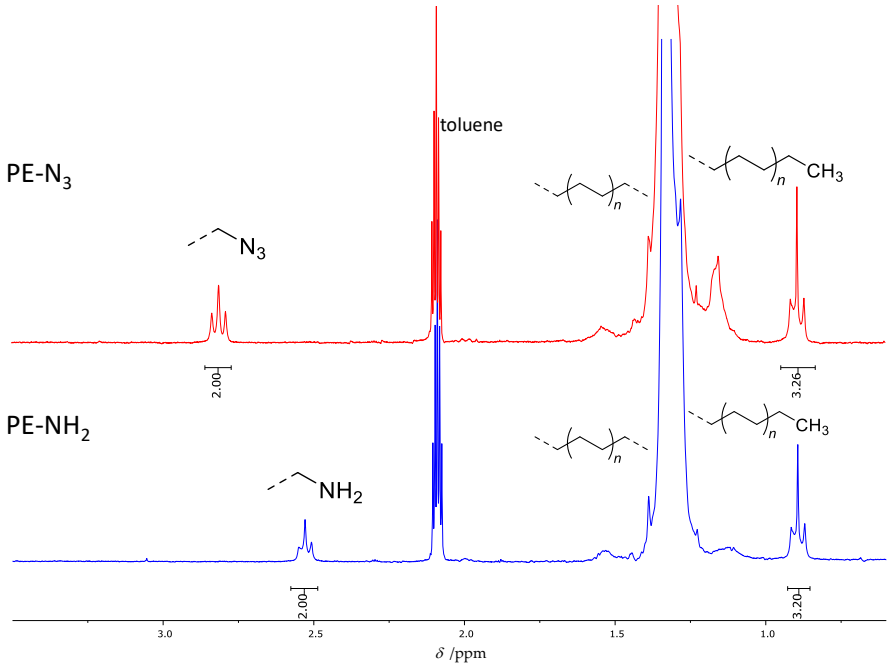

Figure 3-3. ^{1}H-NMR spectra of PE-N_3 and PE-NH_2. Both spectra were recorded in toluene-d8 at 80 °C.

Synthesis of Vinylic Terminated and Epoxide Terminated Polyethylene

In addition to the introduction of nitrogen-based functionalities, a second approach was applied in this work based on observations made in literature.[147,150] As described before, the major strategy was to use only one polymer species as a building platform. Therefore, two additional functional end-groups were introduced based on PE-I.

In the first reaction step, the iodo end-group was applied as leaving group comparable to the discussion made before. However, in this approach an elimination reaction was conducted. Iodo end-functionalized polyethylene was dissolved in toluene at 90 °C. After full dissolution was obtained, a dispersion of potassium *tert*-butoxide (^{t}BuOK) in THF was added. For the reaction it was required to use dry and degassed solvents (Scheme 3-3).[150] Due to the addition of a strong base, the iodide end-group

was eliminated resulting in a vinylic terminated polyethylene (PE_{vin}). Based on this species an additional functionalization was performed. PE_{vin} was implemented in a reaction with *meta*-chloroperoxybenzoic acid (*m*-CPBA).[147] In order to avoid possible side reactions under the harsh reaction conditions, *m*-CPBA was added dropwise and the reaction was quenched after 2.5 h with methanol. The resulting epoxide functional polyethylene (PE_{epo}) and PE_{vin} were characterized via ^{1}H-NMR.

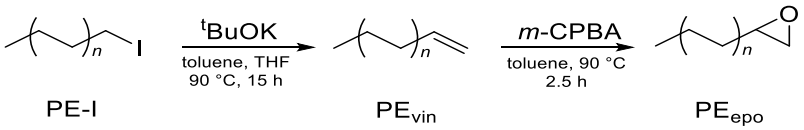

Scheme 3-3. Applied synthetic route for the formation of vinylic terminated and epoxide terminated polyethylene.

The ^{1}H-NMR spectrum of PE_{vin} showed a stringent change compared to the spectrum of PE-I. Besides the signals at $\delta = 1.1 - 1.4$ ppm and $\delta = 0.88$ ppm, corresponding to the saturated polymer backbone, two additional signal were detected (Figure 3-4). The two multiplet signals at $\delta = 5.0$ ppm and at $\delta = 5.7$ ppm could be clearly assigned to the formed vinylic end-group. In addition, the characteristic triplet of the ~CH_2-I-group at $\delta = 2.8$ ppm completely disappeared. Nevertheless, it had to be mentioned that the overall end-functionality decreased from 91 % to 72 % due to possible side-reactions. Nevertheless, based on this result, the formation of PE_{vin} was confirmed.

In the case of PE_{epo} a small amount of vinylic end-groups were observed indicating an incomplete conversion as well. However, in addition to the described signals, three additional peaks were detected at $\delta = 2.6$ ppm, $\delta = 2.38$ ppm and at $\delta = 2.15$ ppm overlapping with the toluene signal. Based on these observations, the transformation from PE-I to PE_{vin} and finally to PE_{epo} was validated although no quantitative conversion was achieved. Nevertheless, for surface modification, the polymer was used in an excess followed by purification and separation. Consequently, PE_{epo} is applicable for the designed strategy.

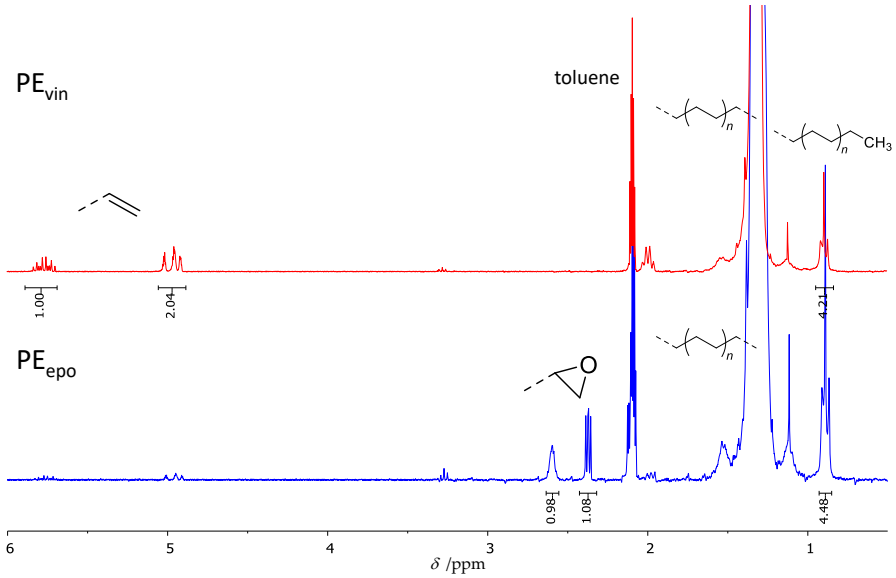

Figure 3-4. ^{1}H-NMR spectra of PE_{vin} and PE_{epo}. Both spectra were recorded in toluene-d8 at 80 °C.

To sum up, within this subchapter the successful synthesis of iodo end-functionalized polyethylene with an excellent end-group functionality and a narrow molar mass distribution was presented. Based on PE-I further functionalities such as azide (PE-N_3), amine (PE-NH_2), vinylic (PE_{vin}) and epoxide (PE_{epo}) moieties were introduced into polyethylene and confirmed by ^{1}H-NMR spectroscopy.

3.2.2 Synthesis of Polyethylene Modified Wood Surfaces

After the formation of variable presynthesized functional polyethylene, these polymers were applied in surface modification reactions. As mentioned in the beginning of this chapter, two strategies were designed. In order to ensure an adequate surface area, wood powder with a particle diameter of 70 – 150 µm was applied.

The first synthetic route is based on unfunctionalized wood particles by using the high amount of accessible hydroxyl groups inherent present on the surface. The wood surface was pretreated with an aqueous solution

of sodium hydroxide that enhances its nucleophilic character of the hydroxyl group for *Williamson*-type reactions (Scheme 3-4).[151] Afterwards, the pretreated wood particles were filtered, dried and stored under an argon atmosphere.

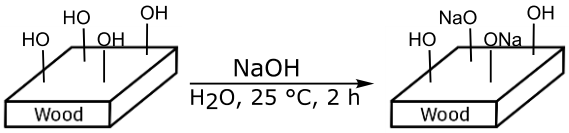

Scheme 3-4. Pretreatment of the wood particles with sodium hydroxide.

As mentioned before, the iodide end-group acts as a good leaving group. Consequently, a nucleophilic substitution between PE-I and the pretreated wood surface should be feasible. For that reason, polyethylene iodide was dissolved in toluene at 100 °C and mixed with the wood particles. DMF (50 vol%) was added to achieve dissolution of the polymer and to enhance the hydrophilicity of the solvent. This leads to a swelling of the wood particles which increased the accessibility of the hydroxyl groups that are commonly less reactive under hydrophobic conditions (Scheme 3-5, right-handed).

Furthermore, an additional synthetic pathway based on PE_{epo} was applied. Due to the high ring strain of the epoxy group, it was assumed that an efficient modification reaction should be applicable via a nucleophilic attack of the surface bound hydroxyl-groups. Two different reaction conditions were implemented. First, epoxide terminated polyethylene and pretreated wood particles were blended and heated up over the melting range of PE (150 °C, Scheme 3-5, left-handed A). The second reaction was carried out in solution at 100 °C using toluene and DMF (1 : 1) as solvents and trifluoroacetic acid (TFA) that acts as a lewis acid (Scheme 3-5, left-handed B).

It has to be mentioned that the designed reaction pathways were successful but did not provide sufficiently high grafting-densities of the wood surface. This might cause by the high amounts of side reactions under those harsh reaction conditions and the inefficiency of the coupling reaction. Therefore, it was assumed that prefunctionalization of the wood surface with highly reactive groups should overcome this limitation.

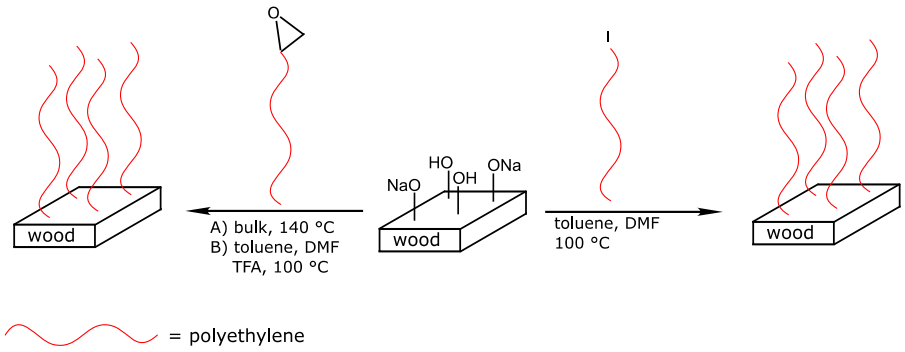

Scheme 3-5. Applied synthesis of the wood surface modification via PE-I (right-hand side) and PE_{epo} (left-hand side).

Considering the results discussed before, prefunctionalization of the wood surface into carboxyl-groups as described in literature was applied. For the reaction pretreated wood particles were reacted with succinic anhydride in DMF under the addition of an auxiliary base (pyridine).[152] Afterwards, the prefunctionalized wood particles ($wood_{carbo}$) were purified via a soxhlet extraction and dried. Presynthesized PE-NH_2 was subsequently reacted with these wood particles in an amide-coupling reaction using *N,N'*-dicyclohexylcarbodiimide (DCC) and 4-dimethylaminopyridine (DMAP). The reaction was carried out at 100 °C in a solvent mixture of DMF and toluene (1 : 1) for 72 h to achieve high conversion.

The functional polyethylene was applied in large excess and therefore, a special focus was kept on the purification of the polymer-modified wood surface to remove all non-bound polymer. Considering this, a Soxhlet extraction was performed using xylene with a high boiling temperature (144 °C) in combination with several dispersion–filtration steps using boiling toluene and DMF. The ^{1}H-NMR spectra of the filtrates validated a completely successful purification step. The resulting wood hybrid material as well as $wood_{carbo}$ were analyzed via attenuated total reflection Fourier-transform infrared spectroscopy (ATR-FTIR) that will be discussed in chapter 3.3.1.

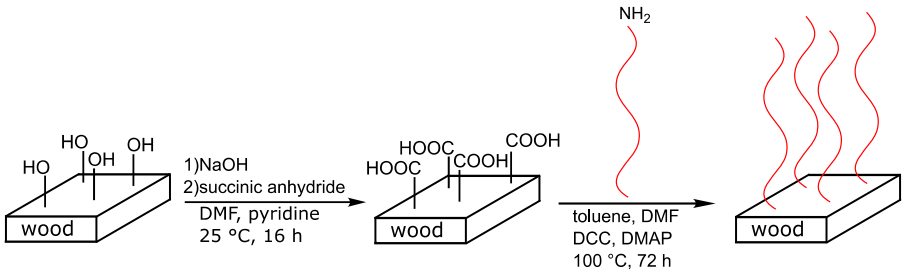

Scheme 3-6. Synthesis of polyethylene modified wood via an amide-coupling reaction.

In addition to the first modification strategy, an additional approach was investigated based on azide terminated polyethylene. The azide moiety can react efficiently and with excellent yields with alkyne moieties in a [3+2]-cycloaddition that is called *Huisgen*-reaction, one prominent example for a *click*-reaction.[148] Considering this, the first step was a prefunctionalization of the wood surface with an alkyne group. The reaction was performed on expertise made in literature for nanocellulose and transferred and optimized for the applied system.

Pretreated wood particles were reacted with a large excess of propargyl bromide in toluene (Scheme 3-7). The resulting particles ($wood_{alk}$) were subsequently purified and dried.[151] The obtained prefunctionalized wood particles were subsequently reacted with PE-N_3 under variable reaction conditions in order to optimize the synthesis. One reaction pathway was conducted using toluene and DMF in combination with $CuSO_4$ and sodium ascorbate that can reduce the copper (II) species *in situ*. The resulting copper(I)-species catalyzes the reaction that should provide excellent yields, especially in combination with a high reaction temperature (140 °C). A second reaction was performed using a copper(I)-species directly with PMDETA as a ligand resulting in a soluble complex. This reaction was carried out under an argon atmosphere at 110 °C for 72 h (Scheme 3-7). The obtained particles were applied for further characterization.

All obtained PE–wood particles were purified as described before and subsequently analyzed by different methods described in the next subchapter in detail. Compared to the synthesis based on PE-NH_2, the modification via PE-N_3 involved one reaction step less and thus, the major focus within this work was kept on the second approach.

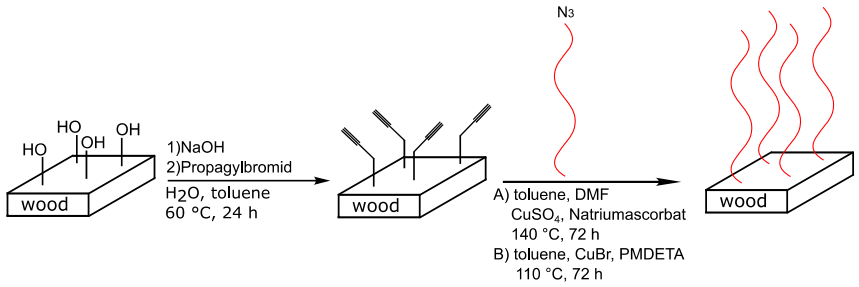

Scheme 3-7. Synthesis of polyethylene modified wood via a [3+2]-cycloaddition using PE-N_3.

3.3 Characterization of Polyethylene Modified Wood Surfaces

3.3.1 Characterization via ATR-FTIR

Attenuated total reflection Fourier-transform infrared spectroscopy (ATR-FTIR) is a powerful tool for surface characterization. For a detailed evaluation of the reaction, unfunctionalized wood, alkyne prefunctionalized wood ($wood_{alk}$), polyethylene modified wood (synthesized according to Scheme 3-7) and pure polyethylene as reference were measured by ATR-FTIR (Figure 3-5). In addition, the same characterization was performed for all substances applied according to Scheme 3-6 including $wood_{carbo}$ (for the ATR-FTIR spectrum see Appendix A).

The unfunctionalized wood surface was used as a reference. In this spectrum (Figure 3-5 D) two broad signals at 3300 cm^{-1} and at 2900 cm^{-1} were observed. Both characteristic signals can be assigned to O–H and C–H stretch vibrations corresponding to the basic structure of wood.[153] After prefunctionalization with an alkyne group, the spectrum of $wood_{alk}$ is comparable to the preliminary wood ones, but with one major difference (Figure 3-5 C). The signal at ~3300 cm^{-1} showed a shoulder compared to spectrum D. The occurrence of this additional peak can be assigned to the characteristic C–H stretching band of the alkyne group

indicating the successful surface transformation.[154] In case of carboxyl prefunctionalized wood surfaces an additional peak with high intensities at 1720 cm^{-1} could be detected that clearly corresponds to C=O bending vibrations (for the respective spectrum, see Appendix A).[154] Both observations validated the successful prefunctionalization of wood into $wood_{carbo}$ and $wood_{alk}$.

The analysis of polyethylene modified wood surfaces showed a drastic change in the ATR-FTIR spectrum independently of the applied coupling reaction. The spectra revealed a strong decrease of the signal's intensities of the stretch vibration corresponding to $wood_{alk}$ and $wood_{carbo}$. From the disappearance of the shoulder at 3300 cm^{-1} it can be concluded that the alkyne group was consumed during the reaction and is shielded by the formed polyethylene layer (Figure 3-5 B). Beside the decrease of this vibration band, the appearance of two additional signals at 2850 cm^{-1} and 2910 cm^{-1} was observed. These characteristic signals were detected for the reference sample containing only polyethylene (Figure 3-5 A). Considering this, both signals can be attributed to the C–H stretching vibration corresponding to the polymer backbone.[155]

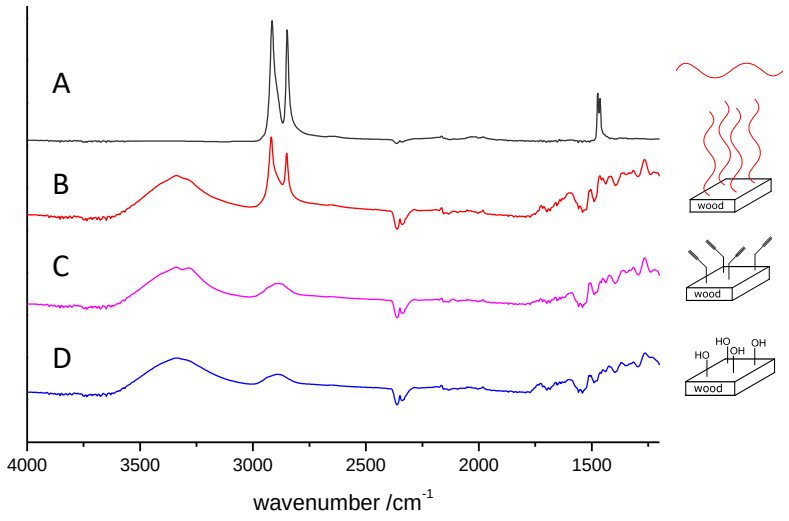

Figure 3-5. ATR-FTIR spectra of polyethylene (A), PE–wood synthesized via a [3+2]-cycloaddition (B), alkyne prefunctionalized wood (D) and unfunctionalized wood (D).

ATR-FTIR analysis confirmed the prefunctionalization of the wood surfaces either by an alkyne or by a carboxyl moiety. Furthermore, the analysis validated the successful fabrication of polyethylene modified wood particles based on both coupling reactions. Since the synthesis of PE–wood particles via a [3+2]-cycloaddition could be performed more efficiently, the focus was kept on this species. The surface properties of the modified wood surface will be characterized in detail in the next chapter.

3.3.2 Thermal Characterization of PE–wood Particles

In order to characterize the thermal properties of PE modified wood surfaces, thermogravimetric analysis (TGA) and differential scanning calorimetry (DSC) were conducted.

In case of TGA, PE–wood particles as well as unfunctionalized wood and polyethylene, both used as references, were analyzed. During the TGA measurement, a constant heating rate (10 K min^{-1}) from 25 °C to 1000 °C was applied (Figure 3-6). During the heating procedure, the unmodified wood particles decomposed at a temperature of about 350 °C resulting in a strong decrease of the relative mass in a small temperature range. A comparable curve behavior was observed for the TGA analysis of free polyethylene, but with a combustion temperature of ~450 °C.

Considering the analysis of the references, polyethylene modified wood surfaces showed a mixed behavior. At a temperature of about 350 °C the sample started to decompose comparable to unmodified particles. In addition, continuous heating the sample resulted in further decomposition over a wide range of temperature. This drastic change in the course of the curve can be explained by existing of polyethylene. Due to the wood's modification, the overall decomposition behavior is a combination of the characteristics of both particles as well as polyethylene. Still, decomposition occurred not at a distinct temperature as observed for both references, but over a broad temperature range that might be attributed to an inhomogeneous PE-coverage of the surface. This might have resulted in areas with high and areas with low grafting-densities as discussed in literature for other particles.[128]

These assumptions can cause a change of the combustion temperature of

surface-bound polyethylene chains resulting in a broadened curve shape. Considering this in combination with the decomposition of either polyethylene or unfunctionalized wood, a quantitative examination of the TGA analysis is not reasonable.
Nevertheless, from the comparison of PE–wood particles to both references, a change of the overall thermal decomposition caused by bound polyethylene was confirmed and might be interesting for further investigations.

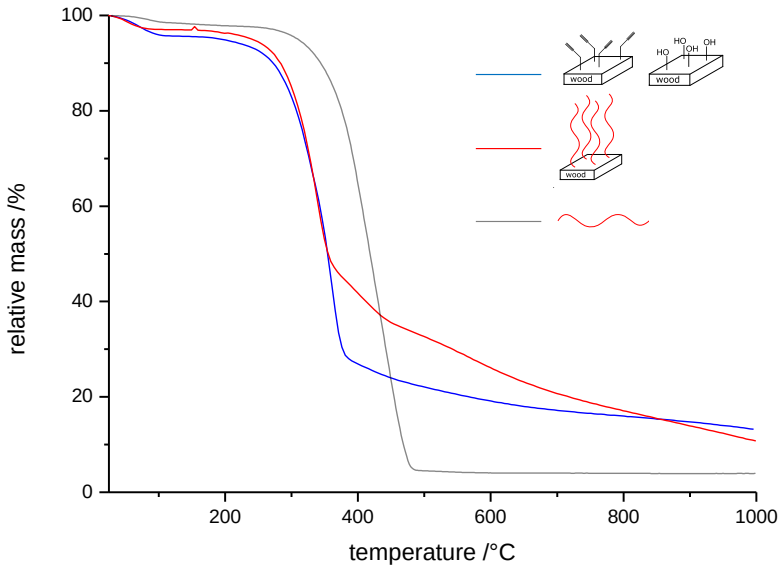

Figure 3-6. TGA analysis of unfunctionalized and alkyne prefunctionalized wood (blue), polyethylene (grey) and polyethylene modified wood (red).

Based on the observation obtained from TGA, DSC analysis was conducted in a heating mode below the determined decomposition temperatures (Figure 3-7). Comparable to prior discussions, polyethylene and unmodified wood particles were measured as reference samples. The unmodified wood particles showed no change in heat capacity in the measured temperature range resulting in a baseline curve. The DSC spectrum of polyethylene revealed a narrow melting range between

100 °C and 120 °C explainable by the homogeneity of the PE sample which was validated by HT-SEC (chapter 3.2.1).
The analysis of PE–wood particles revealed a completely different behavior. The DSC curve is entirely shifted to lower temperatures while a broadening of its shape is observed. From this observation a crystalline structure of the PE chains bound to the surface can be assumed resulting in a melting behavior of those. Additionally, the porosity of the particles might influence the melting behavior of the hybrid material as well.[25] In agreement with the results obtained from TGA, an inhomogeneous surface coverage is reasonable to assume. Based on this consideration, a broadening of the curve caused by variable surface-bound PE density occurred.
The most likely explanation for the temperature shift is that due to the prearrangement of the polyethylene chains on the surface, the crystallinity is reduced compared to unbound PE. This arrangement resulted in a decrease of the melting temperature and therefore caused the curve's shift. The DSC analysis further confirmed the formation of covalently bound PE on the wood's surface.

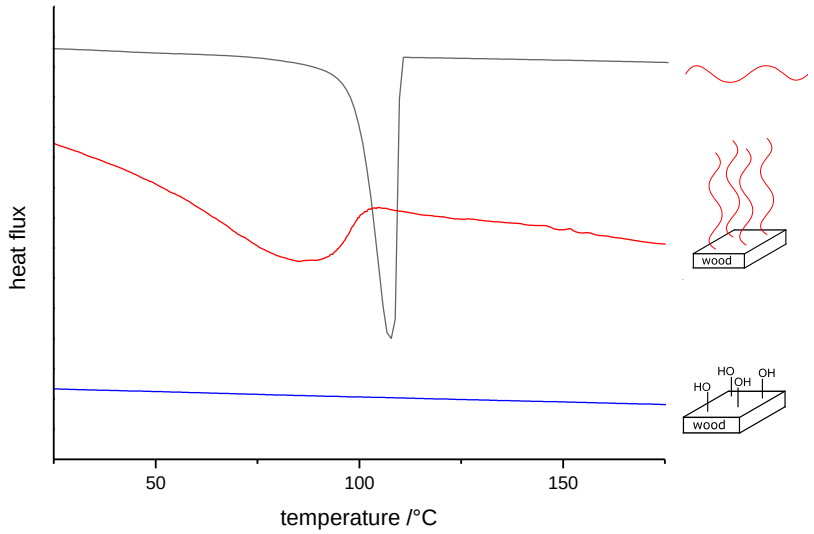

Figure 3-7. DSC measurement of PE-N_3 (black), unfunctionalized wood (blue) and polyethylene modified wood (red). For better visualization the curve of PE-wood was magnified.

To sum up, in this subchapter the thermal properties of PE modified wood surfaces were investigated. From both TGA and DSC characterization a polyethylene grafted surface was validated resulting in a change of the thermal behavior. On the one hand the decomposition property changed observed by TGA and on the other hand a crystallinic surface with a reduced melting temperature was achieved, both caused by a strong attachment of polyethylene.

3.3.3 Surface and Wetting Properties of Polyethylene Modified Wood Particles

In order to visualize the surface's structure, scanning electron microscopy (SEM) of unfunctionalized, alkyne prefunctionalized and polyethylene modified wood particles was performed. The SE micrographs of untreated wood showed fiber structures with a relatively smooth surface (Figure 3-8). After the subsequent prefunctionalization, the micrograph of $wood_{alk}$ revealed an identical surface structure. In contrast, the analysis of polyethylene modified wood particles showed an increase of the surface's roughness. This change of the surface topography might be assigned to the formation of a polymer layer indicating the transformation of the surface's structure due to the PE attachment.[156]

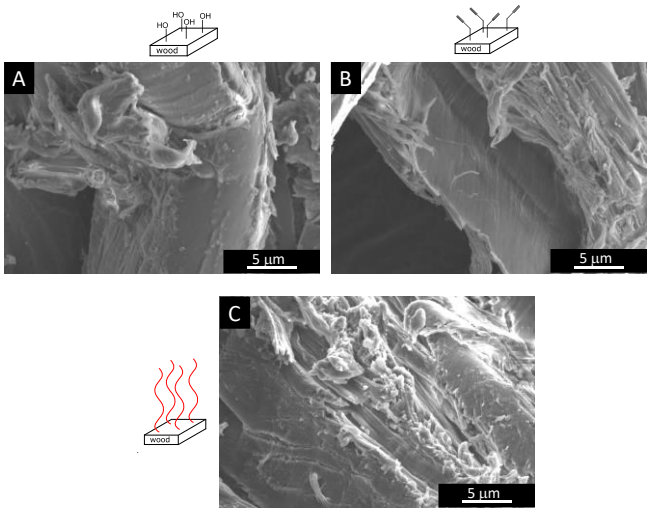

Figure 3-8. SE micrograph of unfunctionalized wood (A), alkyne prefunctionalized wood (B) and polyethylene modified wood (C) particles.

In order to further confirm the macroscopic change of the surface and to characterize its wetting properties, water contact angle (WCA) measurements and dynamic vapor sorption (DVS) analysis were conducted. For water contact angle measurements, the material was pressed into pellets, a water droplet was casted onto the surface and a photographic image was taken in the meantime with a high-speed camera. As references unmodified wood and $wood_{alk}$ were characterized as well. In both cases, the resulting water droplet was immediately absorbed by the wood surface (Figure 3-9). This strong absorption behavior can be assigned to the hydrophilicity of the material that is responsible for several limitations of its area of application (for further details see chapter 2.5 and 3.1).
The complete opposite was observed for PE modified wood particles. The casted water droplet remained entirely on the surface up to 10 min without being absorbed by the surface, comparable to unbound polyethylene. Due to the polyethylene layer bound to wood, a strong increase of the hydrophobicity was achieved resulting in a water-repellent surface. Water contact angle measurements validated the successful surface transformation from hydrophilic to hydrophobic. Based on the hydrophobization, an increased resistance against microorganisms as mentioned before might be achieved and should be further investigated.

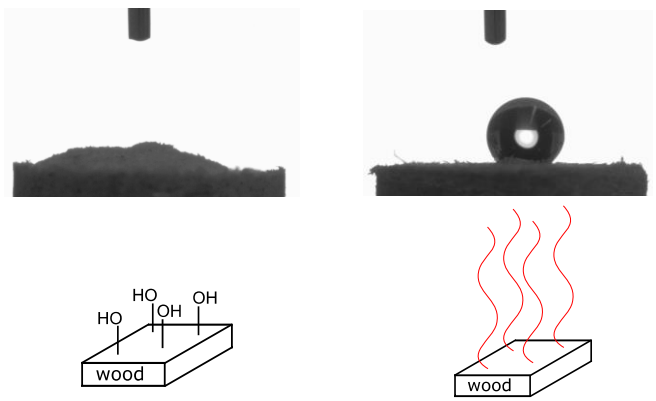

Figure 3-9. Water contact angle measurement of unfunctionalized wood and $wood_{alk}$ (left handed) and polyethylene modified wood particles (right handed).

For gaining deeper insights into the wetting properties, dynamic vapor sorption measurements of unmodified and PE–wood particles were performed. In DVS measurements, the sample is let to dry to 0 % and the relative humidity is changed stepwise while measuring the mass of the sample after a gravimetric equilibrium is reached. From the experiment the overall amount of an absorbed solvent by the sample can be determined. It is declared as equilibrium moisture content (EMC) and recorded as function of the relative humidity.

The sorption and desorption curves of unmodified and PE–wood particles are shown in Figure 3-10. For the purpose of clarity, $wood_{alk}$ is not presented in this figure. The curve was located in between the EMC values of wood and PE–wood. In case of unmodified wood, EMC increased from 0 % to 23 % at the maximum applied humidity. A hysteresis is observed for the desorption curve caused by differences of the sorption and desorption process.

For PE modified wood a comparable shape of the curve is observed but the maximum reached EMC is determined at 14 %. The decrease of the overall absorbed water of PE–wood compared to non-treated wood which can be explained by the hydrophobic polymer layer. Therefore, permanent attachment of polyethylene on the wood surface increased its overall hydrophobicity.

From the DVS a strong increase of the hydrophobicity of the material can be confirmed and is in complete agreement with the observations made by WCA measurements.

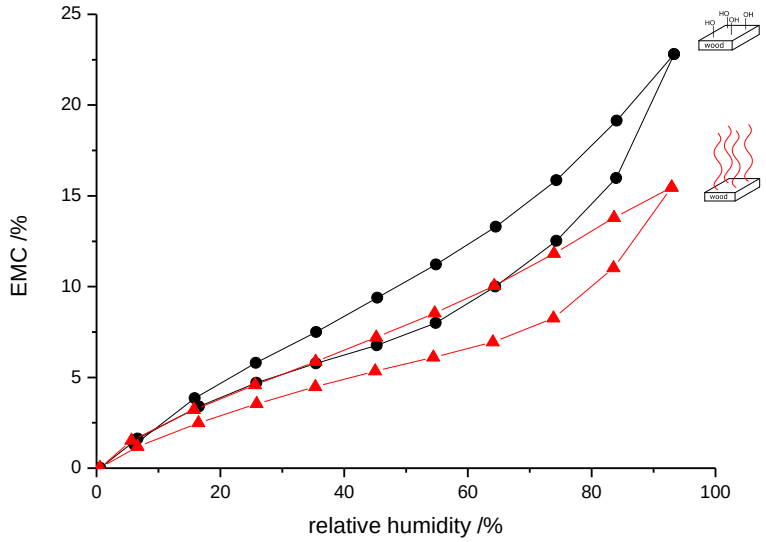

Figure 3-10. Dynamic vapor sorption measurement of unfunctionalized (black) and PE modified (red) wood particles.

In this chapter, the design and performance for the fabrication of polyethylene modified wood particles were presented. The successful introduction of a covalently bound polyethylene layer was confirmed by ATR-FTIR in combination with a thermal analysis of the hybrid material conducted by DSC and TGA. In addition, a strong hydrophobization of the particles was achieved confirmed by both WCA and DVS analysis.

3.4 Polyethylene Modified Silica Nanoparticles

3.4.1 Grafting-to Approach

After the successful modification of hydrophilic surfaces was confirmed exemplary for wood, the developed strategy should be transferable to other hydrophilic materials such as silica. For its surface modification different synthetic routes were developed, whereas the most efficient synthesis will be presented herein. The silica nanoparticles (SiNP) were synthesized in a typical *Stöber* process using a solvent mixture of methanol and ethanol (1 : 1) leading to an OH-functionalized surface.[157] Considering the results discussed in chapter 3.2.2, a strong nucleophilic anchor group was introduced onto the silica surface. For this purpose, freshly prepared SiNPs were subsequently reacted with 3-aminopropyl-trihydroxylsilane (Scheme 3-8). The amine modified silica particles were reacted in a nucleophilic substitution with iodo end-functional polyethylene. After purification of the modified particles, validated by ^{1}H-NMR analysis of the filtrate (comparable to chapter 3.2.2), the obtained PE–SiNPs were characterized via dynamic light scattering (DLS) and TGA.

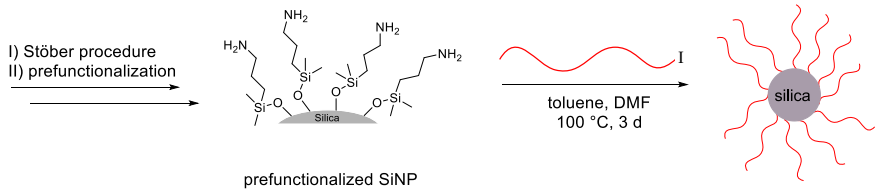

Scheme 3-8. Applied synthesis for the fabrication of polyethylene modified SiNPs.

In order to determine the hydrodynamic diameter of the respective particles, DLS analysis was performed on SiNPs and PE–SiNPs. To ensure comparable results, the respective particles were dispersed in ethanol at 25 °C via ultra-sonification and immediately analyzed. The DLS analysis of SiNPs revealed a size distribution with a maximum at ~43 nm (Figure 3-11). After modification with PE, the obtained distribution was entirely shifted to higher hydrodynamic diameters with an intensity maximum at 68 nm. The increase of the particle's diameter

can be assigned to the formation of a polyethylene shell around the Si-core. Under the assumption of stretched polymer chains bound to the surface a strong increase of the diameter was expected indicating the successful formation of PE brushes on the silica NPs.
The measurement was repeated after the samples were allowed to rest overnight. Remarkably, in case of unmodified SiNPs the measurement revealed the same distribution. In contrast to this, polyethylene modified SiNPs sedimented resulting in no measurable size distribution. By changing the solvent from ethanol to toluene at 80 °C, the complete opposite was observed. Unmodified SiNPs aggregated and entirely precipitated, whereas PE–SiNPs remained in dispersion. These observations can be attributed to the solvent's properties. Ethanol is a good solvent for hydrophilic silica particles, whereas toluene is an appropriate solvent for PE. This experiment was challenging to be performed and has to be optimized regarding to its reproducibility. Nevertheless, the results indicate that the formation of a polyethylene shell surrounding the Si-core has a strong influence on their dispersion behavior originating from the solution properties of PE. The observed solvent and temperature depending aggregation was further developed and transferred to other nanoparticles. A detailed discussion of this effect will be discussed in chapter 4.5.

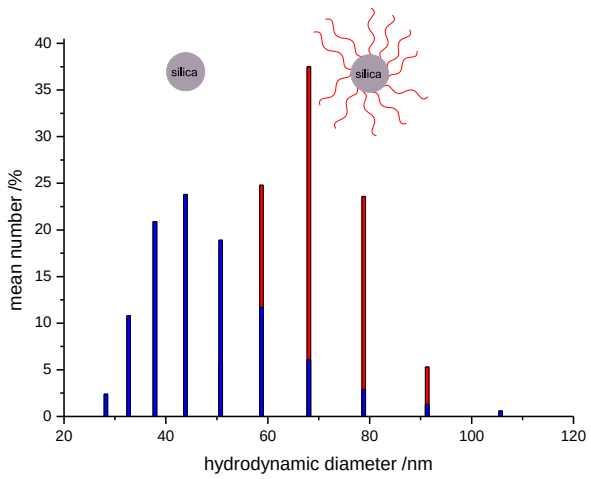

Figure 3-11. Dynamic light scattering analysis of SiNP (blue) and PE–SiNP (red) measured immediately after their dispersion in EtOH.

In addition to DLS measurements, thermogravimetric analysis of SiNPs, PE–SiNPs after removing the excess of polyethylene and the unpurified reaction mixture of PE–SiNPs and PE-I was performed (Figure 3-12). For the SiNPs, measured as reference, a relative loss of mass of about 10 % was determined. This can be attributed to the evaporation of absorbed solvent molecules during the heating process.
In contrast to this, the TGA curve of the reaction mixture containing PE-I and PE–SiNP showed a different behavior. Its analysis revealed two additional distinct steps in the relative mass. First, at temperatures of about 400 °C a relative loss of mass of ~15 % was observed corresponding to unbound PE-I. The determined decomposition temperature is in agreement with the TGA measurement of PE-I discussed in chapter 3.3.2 (Figure 3-6). After purification, the mass loss of PE-I completely disappeared validating a complete separation of free polymer and PE–SiNPs.
Additionally, a distinct step at 550 °C was observed for both the reaction mixture and purified PE–SiNP. In both cases, the decrease of the relative mass was determined to 3 % indicating a relatively low grafting density. Nevertheless, it can be assumed that due to the covalent attachment of polyethylene, its decomposition temperature increased compared to free polymer indicating the permanent attachment of PE. The analysis via TGA further confirmed the results obtained by dynamic light scattering.

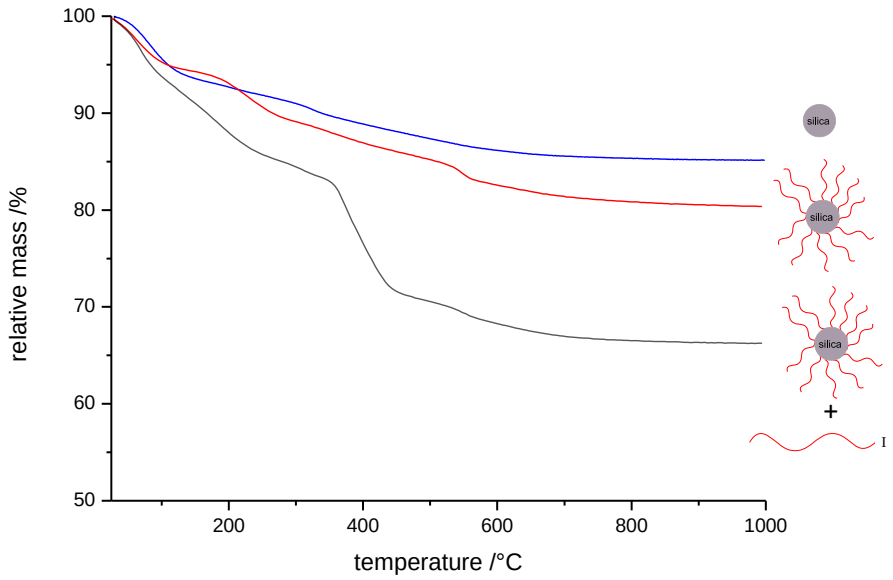

Figure 3-12. Thermogravimetric analysis of SiNP (red), PE–SiNP (blue) and blended PE-I and PE–SiNP (black).

In this subchapter the synthesis of polyethylene modified silica nanoparticles via an efficient nucleophilic substitution was presented and confirmed by DLS and TGA experiments. Nevertheless, optimization of the reaction conditions in order to achieve high grafting-densities as well as additional experiments are necessary to validate the assumptions discussed above. During the experimental work, a publication about PE modified SiNPs in a comparable approach was reported.[130] Considering this, the author's focus shifted to metal nanoparticles that will be presented in chapter 4.

3.4.2 Grafting-from Approach

In addition to a grafting-to approach discussed before, a synthetic strategy for the formation of polyethylene modified nanoparticles in a grafting-from approach was designed. For this approach a covalently bound chain transfer agent bearing an organo magnesium moiety is required.

The design of the synthesis included multiple reaction steps starting from fresh-prepared SiNP synthesized in a *Stöber* process.[157] The obtained nanoparticles were subsequently prefunctionalized with different halide moieties via a condensation reaction using hydroxyl silanes. In order to achieve high flexibility of the halide groups, variable linker lengths were applied, whereas a longest commercially available linker including 12 carbon atoms was the most promising starting material. Considering this and the high reactivity of iodine towards elemental magnesium forming *Grignard* analogous compounds, an iodine moiety was introduced (Scheme 3-9 A).[158]

However, after the prefunctionalization a large amount of hydroxyl-groups remained on the silica surface.[128] These polar groups were able to react with the targeted organomagnesium compounds inhibiting their formation. Therefore, the silica surface was protected by a silane protecting group using a large excess of dimethyldichlorosilane under an argon atmosphere. The obtained nanoparticles were immediately reacted with activated magnesium. Various activation methods were applied, whereas the reduction of dry $MgCl_2$ with lithium resulting in fine dispersed magnesium provided the most active magnesium (B). This species provide a large surface, is extremely pyrophoric and is known as *Rieke* magnesium. [159]

Afterwards, 1,4-dioxane was added to shift the Schlenk equilibrium towards the diorganomagnesium compound (C).[160] Titration experiments showed that only a small amount of these species were formed indicating the inefficiency of a reaction between magnesium and prefuntioncalized silica particles.

These modified particles were subsequently applied in a typical catalyzed chain growth polymerization as discussed before (chapter 3.2.1). As a reference sample, protected SiNPs and elemental magnesium were treated under the same conditions. Purification was performed as described in chapter 3.2.2 and 3.4.1 (D). In order to characterize the

surface bound polymer, the particles were dissolved using hydrofluoric acid.

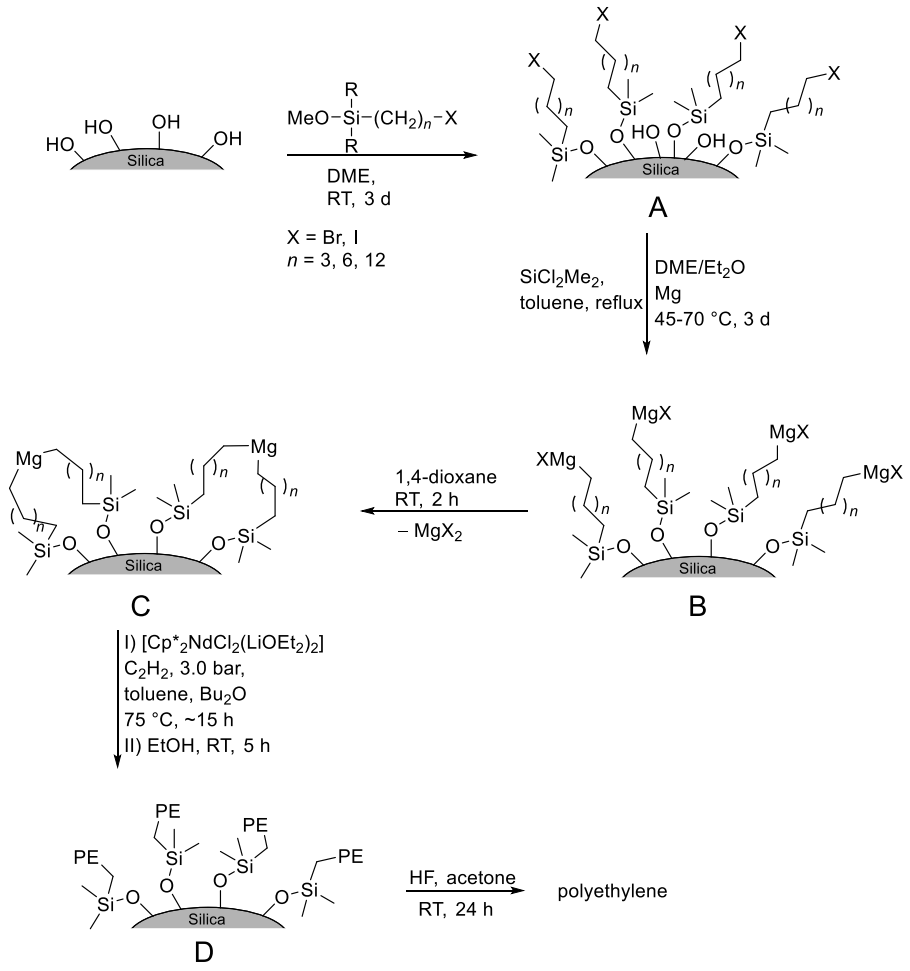

Scheme 3-9. Synthetic route for the formation of PE–SiNP in a grafting-from approach.

The obtained PE–SiNP before and after their purification, as well as the cleaved polyethylene, were characterized by ^{1}H-NMR spectroscopy (Figure 3-13). For the analysis, the NMR tube was filled with the respective nanoparticles, it was heated to 90 °C for 5 h and the supernatant was analyzed. The ^{1}H-NMR spectrum of the unpurified particles revealed the characteristic signals corresponding to the polyethylene backbone (δ = 1.1–1.3 ppm, Figure 3-13 A), whereas the reference sample showed no detectable signals.

From the latter analysis it can be concluded that the activation of the catalyst only took place for treated particles (Scheme 3-9 C), but was not observed for the reference sample. The formation of free polyethylene can be attributed to the occurrence of termination products. Considering the obtained observation and the mechanism discussed in chapter 2.3, it is reasonable to assume that the formation of an organomagnesium species was successful.

In the ^{1}H-NMR spectrum of the respective particles after purification no signal corresponding to the polymer backbone could be detected proving the complete separation of free polyethylene (Figure 3-13 B). After dissolving the particles using HF, the appearance of a broad multiplet at δ = 1.1–1.3 ppm was observed that can be attributed to polyethylene subsequently cleaved from the surface (Figure 3-13 C).

The obtained results might indicate that a covalent attachment of PE to the silica surface is achievable via the designed approach. Up to now, this is the first approach for the formation of PE brushes on a substrate using a grafting-from approach in a catalyzed chain growth procedure. Nevertheless, it has to be noted that an insufficient grafting-density was achieved hindering a full characterization of the particles.

For further investigation and enhancement of the grafting density, the developed system needs to be optimized and examined in detail. Based on the titration experiments, the formation of organomagnesium moieties on the surface is probably the limiting step in the system. To overcome this obstacle, highly efficient reaction pathways have to be developed and applied in the future. One possibility might be the usage of active halides on sp^2-hybridised carbons bound to the surface in combination with homogenous *Grignard* compounds in so-called *Knochel* type reactions. Due to the homogeneity, the requirement of a reaction between magnesium particles and SiNPs would be avoid.

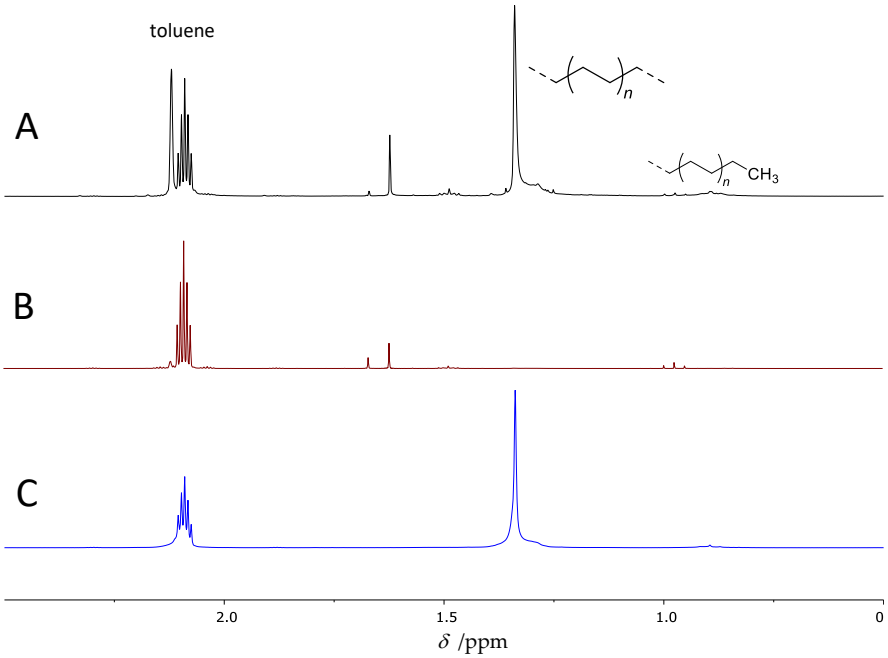

Figure 3-13. ^{1}H-NMR spectra of PE–SiNP after polymerization (A), after purification (B), after HF treatment (C). All spectra were recorded in toluene-d8 at 80 °C.

3.5 Conclusion

In this chapter, a route for the formation of well-defined polyethylene covalently attached to wood surfaces was presented for the first time. The synthetic route was based on either azide or amine prefunctionalized polyethylene synthesized via a catalyzed chain growth mechanism with an excellent end-group functionality. The surface modification was performed by a prefunctionalization with an anchor group onto wood followed by an efficient coupling reaction using end-functional polyethylene. ATR-FTIR analysis of the respective particles confirmed the successful introduction of an anchor group as well as the permanent attachment of polyethylene. Thermal analyses (DSC and TGA) of the obtained hybrid materials validated the formation of crystalline polymer brushes in combination with a decreased melting temperature.

SE micrographs indicated a modification of the surface's topography caused by polyethylene attached to wood. Due to the formation of polymer brushes on the surface, the hydrophobicity of wood was strongly enhanced validated by both water contact angle measurement and dynamic vapor sorption analysis. The transformation into water-repellent wood surfaces might reinforce its dimensional stability caused by moisture resistance against degradation caused by microorganisms.

In addition, the developed strategies were transferred to silica nanoparticles resulting in polyethylene–silica nanohybrids. The obtained PE–SiNP structures showed an increased hydrodynamic diameter compared to unmodified silica indicating the attachment of PE. From thermogravimetric analysis a loss of mass with an increased decomposition temperature was observed that can be attributed to surface-bound polyethylene which confirmed DLS analysis even further. Moreover, a synthetic strategy for the formation of PE–silica hybrids in a grafting-from approach was designed and investigated by ^{1}H-NMR indicating the formation of polyethylene brushes. Both strategies should be further optimized and studied in detail in order to enhance the grafting-density of PE on wood and expand its applications.

To sum up, a novel and efficient route for the surface modification of hydrophilic materials with well-defined polyethylene was developed and characterized in detail.

4 Polyethylene Grafted Noble Metal Nanoparticles

Note
The majority content of this chapter has already been published.[161] The permission to apply the content and figures has been granted from the journal and the authors.

4.1 Introduction and Motivation

Nanoscience and nanotechnology with the focus on polymer grafted metal nanoparticles is currently one of the most fast-growing fields in research.[137,138] To enable the fabrication of such hybrid materials an adequate interaction between the metal-core and the polymer-shell is required.[122] Due to the lack of polar moieties in polyethylene, the combination of PE and metal nanoparticles is almost undeveloped.[34]
To overcome this limitation and expand the field of polyethylene-based nanohybrid materials, the major goal of this project was the development of a procedure for the formation of polyethylene grafted gold and silver nanoparticles and their full characterization. Silver nanoparticles are of special interest due to their antibacterial properties[30] whereas gold nanoparticles exhibit a wide area of application ranging from consumer products[143] to catalysis[143] to biosensoring[31] caused by their unique optical properties.
Novel hybrid materials consisting of polyethylene and noble metal nanoparticles should exhibit a combination of the components' properties. For this purpose, the focus laid on the thermomorphic behavior of PE due to its critical solution temperature (detailed discussion in chapter 4.5). In addition, an investigation of the stabilization effect of capped nanoparticles as well as their dispersibility in a polyethylene matrix was explored which is commonly limited.[32]

Predesign and criteria of the applied system

The developed synthetic route for the formation of polyethylene modified gold and silver NPs was conducted via a grafting-to approach. The presynthesis of functional polyethylene provides the advantage of full predeterminability and characterizability of the polymer. Thus, well-defined PE with a suitable anchor group and high end-group functionality can be tailored. A well-established and appropriate end-group with a high affinity towards the respective metal surface was investigated among others in the group of *Vana* in detail.[139–141] It was demonstrated that a trithiocarbonate (TTC) moiety fulfills the criteria to form stable gold- or silver-core–polymer-shell particles.

Accordingly, the synthesis of a TTC terminated PE was aimed and conducted via a procedure assigned from literature.[97] In addition to the trithiocarbonate group, a thiol end-functional polyethylene was assorted to gain a polymer with a less reactive end-group against nucleophiles for special purposes. In addition to that, due to the requirement of fully dissolved polyethylene, the ligand-stabilized gold and silver nanoparticles should be dispersible in toluene. To achieve an efficient formation of core–shell particles, a ligand exchange procedure was designed.

4.2 Synthesis of Polyethylene Capped Gold and Silver Nanoparticles

4.2.1 Polymer Synthesis and Characterization

Based on the synthesis' predesign, the first step was the modification of polyethylene with a trithiocarbonate moiety. To incorporate this polar group into nonpolar PE a strategy reported in literature was adapted.[97] The synthesis of magnesium terminated polyethylene was conducted applying a typical CCG procedure based on butyloctylmagnesium and ((cp*)$_2$NdCl$_2$Li(OEt$_2$)) comparable to the synthesis described in chapter 3. To form a polymer-shell that fully stabilizes the particles, high molar masses in combination with an adequate end-group functionality were required. Therefore, the polymerization was conducted until precipitation was observed resulting in high molar mass PE. To ensure an

efficient end-group modification in-situ, to the polymer solution presynthezised bis(benzylsulfinyl thiocarbonyl)disulphide was added immediately after precipitation was observed (Scheme 4-1 I). The PE–Mg–PE intermediate can insert into the sulfur–sulfur-bond resulting in the desired TTC terminated PE (PE_{TTC}). PE_{TTC} was reacted in a typical aminoylsis protocol yielding a thiol terminated polyethylene (PE-SH) using hydrazine as nucleophile (Scheme 4-1 II). Hydrazine was applied to suppress the formation of disulfides and in addition, to ensure a complete conversion.[162] The reaction was carried out in toluene and DMF for 24 h. The conducting temperature was at least 80 °C in order to achieve a full dissolution of PE. After purification by simple filtration, both polymers were analyzed by ^{1}H-NMR and HT-SEC.

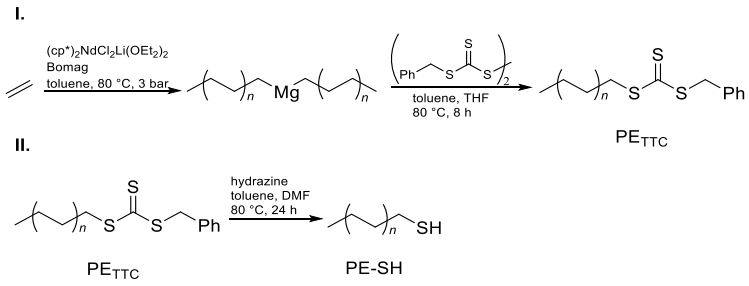

Scheme 4-1. Applied synthesis route to obtain PE_{TTC} (I.) and PE-SH (II.).

^{1}H-NMR and HT-SEC Characterization of PE_{TTC} and PE-SH

From the ^{1}H-NMR characterization the successful formation of PE_{TTC} and PE-SH can be extracted (Figure 4-1). In case of PE_{TTC} the characteristic singlet (δ = 4.4 ppm) of the methylene group connected to the trithiocarbonate group and the phenyl-group can be clearly observed. In addition, the triplet at δ = 3.2 ppm can be assigned to the methylene end-group of the polyethylene backbone adjacent to the TTC group. Besides these characteristic signals, typical peaks corresponding to the polyethylene backbone (δ = 1.1–1.4 ppm) and the methyl end-group (δ = 0.88 ppm) are detectable. The aromatic signals based on the phenyl end-group could not be evaluated rationally because the spectra were measured in toluene-d8 providing signals in the same range. By comparing the characteristic singlet of the methylene group (δ = 4.4 ppm)

with the methyl end-group, a functionalization degree of ~60 % could be assigned. It has to be noted that due to poor signal-to-noise ratios this value provides a rough tendency. This relatively low end-group functionalization can be explained with the inefficient reaction of PE–Mg–PE with the disulfide caused by possible termination and side reactions. Furthermore, as the polymerization is conducted up to high molar masses, termination products of PE are expected. The termination products either contain a vinylic group or a saturated methyl end-group (discussed in 2.2), that both have no influence on the attachment to a metal-surface. Therefore, a functionalization degree of ~60 % should be sufficient for this project.

After aminolysis, only one methylene group (δ = 2.6 ppm) could be observed. In combination with the disappearance of the methylene groups described before, it can be concluded that the formation of PE-SH was quantitively achieved without any change in the functionalization degree. The evaluation of the ^{1}H-NMR spectra of both polymer species validated the successful and efficient formation of PE$_{TTC}$ and PE-SH.

To obtain an overview of the molar mass distribution, HT-SEC analysis of PE$_{TTC}$ was performed (Figure 4-2). The chromatogram revealed a strong shoulder due to the different elution times of functionalized and unfunctionalized, terminated polyethylene. This observation can be assigned to the termination products observed in NMR spectroscopy. Therefore, an estimation of the molar masses was based on the peak maximum (M_P = 2500 g mol^{-1}). Nevertheless, from the HT-SEC characterization it can be extracted that the polymerization provided the forecasted molar masses, although a non-negligible proportion of unreactive termination products were formed.

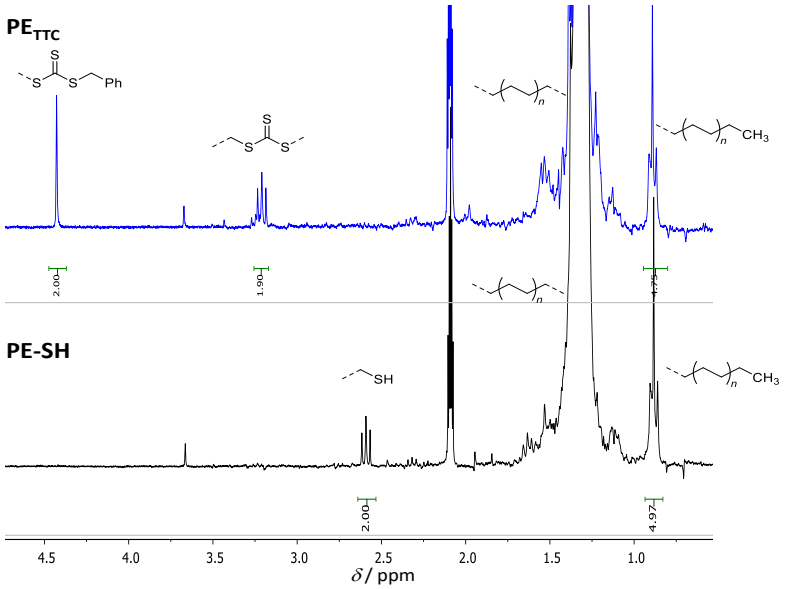

Figure 4-1. ^{1}H-NMR spectra of PE$_{TTC}$ and PE-SH. Both spectra were measured in toluene-d8 at 80 °C.

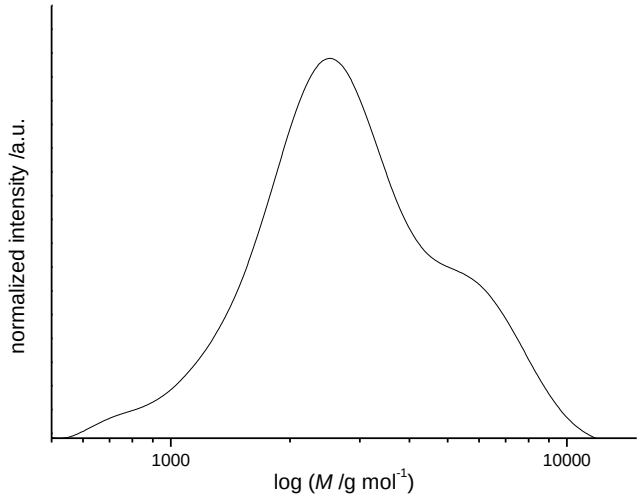

Figure 4-2. Size-exclusion chromatogram of PE$_{TTC}$ measured in TCB at 160 °C.

From both characterization methods it could be verified that the formation of PE$_{TTC}$ and PE-SH was successful and consequently both can be applied for the next step: the reaction with the nanoparticles-surfaces.

4.2.2 Synthesis of Gold- and Silver-Core–Polyethylene-Shell Nanoparticles

After the successful synthesis of the polymer was validated, the obtained end-group functional polyethylenes were implemented for the formation of core–shell-structures. Due to the low solubility and the small range of applicable solvents, all reactions had to be carried out in a non-polar solvent such as toluene at relatively high temperatures over 80 °C. Considering that, the silver nanoparticle (AgNP) and gold nanoparticle (AuNP) needed an adequate solubility in toluene. Based on this, tetraoctylammonium bromide (TOAB) capped gold particles resulting from the *Brust–Schiffrin* procedure[163] and oleylamine capped silver nanoparticles[164] were used. Both particle types synthesized via these methods are fully dispersible in toluene. The synthesis of the respective particles was performed by *Wentao Peng*. Both ligands are well-investigated and only exhibit a relatively low attachment to the respective surface.[139] In contrast to this, due to the high binding affinity of the thiol- and TTC-group to the highly active metal-surface, an efficient ligand exchange procedure can be performed.
The syntheses of polyethylene modified either silver or gold nanoparticles were performed in comparable routes: As mentioned above, to achieve a high flexibility of the polyethylene chains, the polymer was dissolved in toluene at 90 °C for 1 h in a vial. To ensure high grafting-densities and considering the degree of end functionality, an excess of the polymer was employed (50 wt% compared to the NPs). After full dissolution of the polymer, the purified nanoparticles dispersed in toluene were added to the respective polymer solution at 90 °C and mixed for 30 min (Scheme 4-2). In case of AgNPs the reaction was carried out under an argon atmosphere to avoid oxidation of the surface at high temperature. The obtained nanohybrids were directly subjected to characterizations and applications that will be discussed in the next subchapters.

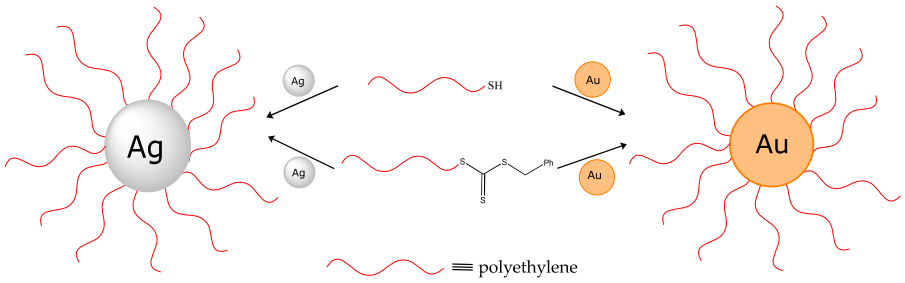

Scheme 4-2. Simplified reaction scheme for the synthesis of PE–AuNPs and PE–AgNPs.

4.3 Characterization of Gold- and Silver-Core–PE-Shell-Nanohybrids

A trithiocarbonate moiety was chosen because it can acts as chain transfer agent in a RAFT polymerization and therefore gives rise to block copolymers.[14] On the other hand the thiol-group can be used for further reactions e.g. via thiol-ene chemistry. Its reduced reactivity towards nucleophiles might be a criterium for several other applications.[165]
From primary DLS and transmission electron microscopy (TEM) analysis, the successful anchoring of both TTC and thiol functional polyethylene onto gold and silver surfaces was confirmed. Since the synthesis of TTC terminated polyethylene was more efficient, the focus in the next chapter is on PE$_{TTC}$. Due to the comparable affinities of AuNPs and AgNPs towards sulfur containing moieties, both types of particles will be discussed in one chapter.

4.3.1 Dynamic Light Scattering

In order to characterize the solution behavior, dynamic light scattering analysis of the respective AuNP, PE–AuNP, AgNP and PE–AgNP was performed. Using this method, a determination of the hydrodynamic radius of the particles is gained depending on e.g. the solvent and

therefore, all measurements were conducted under identical conditions. For the analysis, the capped and unfunctionalized nanoparticle dispersions were diluted with toluene and measured at a temperature of 90 °C to ensure a complete dissolution of the polymer-shell, respectively. In addition, the obtained dispersions were cooled down to 25 °C and measured again.

The analysis of unfunctionalized AuNPs showed a narrow size distribution while the intensity maximum could be determined at ~10 nm (Figure 4-3). The DLS analysis of the PE–gold-nanoparticles resulted in two major differences. At a temperature of 90 °C the entire distribution is shifted to higher hydrodynamic diameters with a maximum at ~22 nm in combination with a slightly broadened shape of the curve. The shift to higher diameters can be attributed to the formation of a swollen polymer-shell around the AuNPs resulting in an increased size. Furthermore, the distribution of the unfunctionalized particles completely disappeared. Consequently, from these data it can be extracted that a high surface loading of the respective nanoparticles with PE was achieved. In addition, it can be observed that the formed nanohybrids exhibit a strong stability even at high temperatures. This validated the assumption that sulfur containing polyethylene provides a strong interaction to the gold surface.

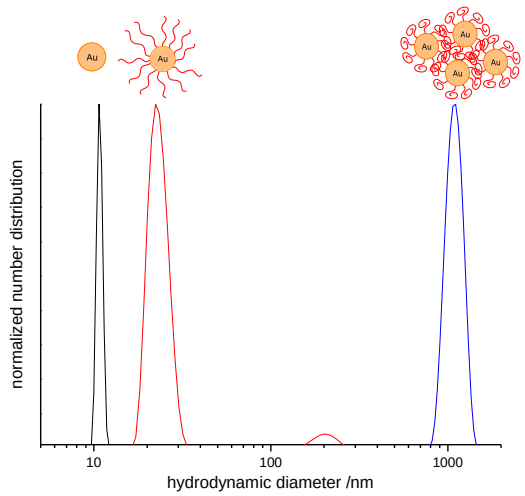

Figure 4-3. DLS measurement of AuNP at 90 °C/25 °C (black), PE–AuNP at 90 °C (red) and PE–AuNP at 25 °C (blue). All samples were measured in toluene and normalized to the maximum.

Furthermore, at a temperature of 25 °C the PE–AuNPs showed an interesting behavior compared to unfunctionalized AuNPs. The distribution of the hydrodynamic diameter of the ungrafted gold nanoparticles was independent on the applied measuring temperature. In contrast to this, after cooling to room temperature, the entire diameter-distribution of polyethylene capped AuNPs shifted to high values of about 1000 nm. This observation is assigned to aggregation of PE–AuNPs and indicates that the solution behavior of capped nanoparticles is entirely determined by the polyethylene-shell. Below the critical solution temperature, the PE-shell becomes insoluble resulting in a segregation of PE–AuNPs from the solvent and the formation of their agglomerates including non-bound polymer. Remarkably, after reheating the sample a decrease of the diameter is observed back to the primary distribution at maximum of ~22 nm. The reversibility of the aggregation/disaggregation process confirmed the presence of a stable PE-shell during the entire procedure and excluded the formation of unfunctionalized AuNP-aggregates.

The measurement of unfunctionalized and PE-grafted silver nanoparticles showed comparable results. The pure AgNPs exhibit a narrow hydrodynamic diameter distribution around 11 nm. The PE-AgNPs showed a strong increase of the measured diameter with a maximum at ~28 nm and a broadened shape of the curve that might be attributed to different grafting densities of the polyethylene shell. The results validated strong sulfur–silver-interaction and consequently a strong attachment of the polyethylene-shell even at harsh temperature conditions.

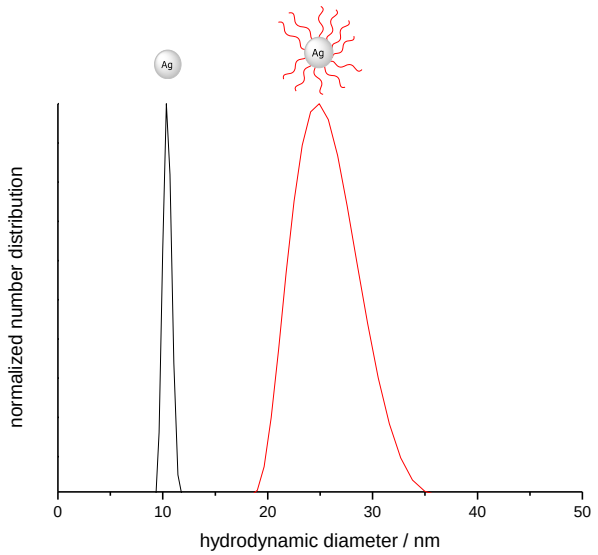

Figure 4-4. DLS measurement of AgNP (black) and PE–AgNP (red). All samples were measured in toluene at 90 °C.

From the DLS measurements of the respective unfunctionalized and PE-modified nanoparticles it could be extracted that the formation of polyethylene grafted gold and silver nanoparticles was successful. In addition, it was proven that an appropriate grafting density of the polymer-shell, a strong attachment to the surface and a high stability was achieved. Due to the observation it was validated that the dispersion behavior of PE–AgNP and PE–AuNP is entirely corresponding to the adhered polyethylene-shell.

4.3.2 Transmission Electron Microscopy

In order to validate the data obtained from DLS analysis and to visualize the behavior of the particles in the dried, solid state, transmission electron microscopy (TEM) was performed. Via an electron beam transmitted through a sample, a direct visualization of the particle's structure in vacuum is possible. From the TE micrographs the size distribution of the respective nanoparticles can be extracted (Figure 4-5). The average

diameter was determined to ~7 nm for AuNPs and to ~9 nm for AgNPs. In addition, it was observed that the silver nanoparticles exhibited a much narrower size-distribution compared to AuNPs. The data obtained from TEM analysis were in a good agreement with the size distribution obtained by DLS analysis (chapter 4.3.1), whereas the slight discrepancies can be attributed to the differences in the setup and measurement of the respective method.
From the congruence of DLS and TEM analysis it was confirmed that the increase of the hydrodynamic diameter discussed in chapter 4.3.1 is clearly corresponding to the attached polyethylene-shell.

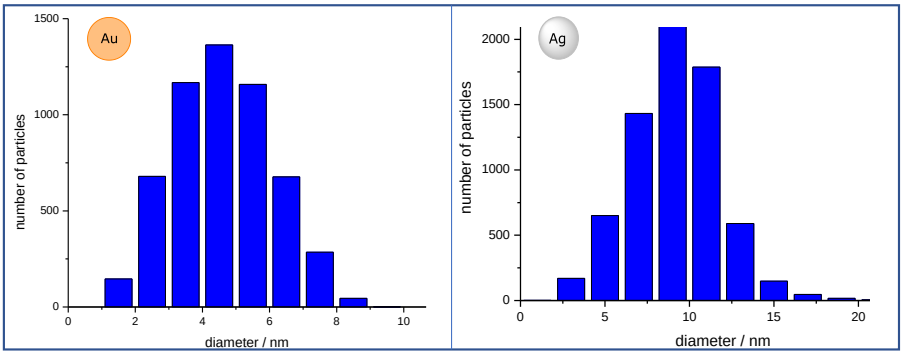

Figure 4-5. Size distribution of AuNPs (left) and AgNPs (right) obtained from TEM measurements.

Besides the determination of the respective diameter, further information within the TE micrographs could be extracted (Figure 4-6). Both unfunctionalized gold as well as silver nanoparticles showed a strong tendency to form aggregates. This aggregation arises from tending to reduce the surface area resulting in strong attractive particle–particle-interactions. In contrast to this, opposite observations were made for PE–AuNPs and PE–AgNPs. By comparing the TE micrograph of AuNPs with PE–AuNPs an increase of the inter-particles distance could be observed. In addition, a perfect separation without the formation of aggregates of the capped particles was monitored. Similar observations were made for AgNPs and PE–AgNPs. In case of modified silver nanoparticles a hexagonal arrangement was noticed in some areas as reported before for other nanohybrids.[141] This well-structured self-

assembly was not observed for capped gold particles, probably due to the homogenous size distribution of AgNPs.
Furthermore, the monitored interparticle distance of the respective PE capped nanoparticles was remarkable high compared to the relatively low molecular weight of the applied polymer. This might be explainable due to the usage of high crystalline polyethylene (~90 %) resulting in a stretched polymer-shell, especially assuming a high grafting-density. Another explanation could be found in the uncomplete end-group functionality (~60 %) resulting in free polyethylene that can swell the attached polyethylene-shell.
From the DLS and TEM analysis it can be concluded that to each distinct particle a polyethylene shell is attached. This validated the successful and effective synthesis of metal-core–PE-shell hybrids in the applied grafting-to approach.

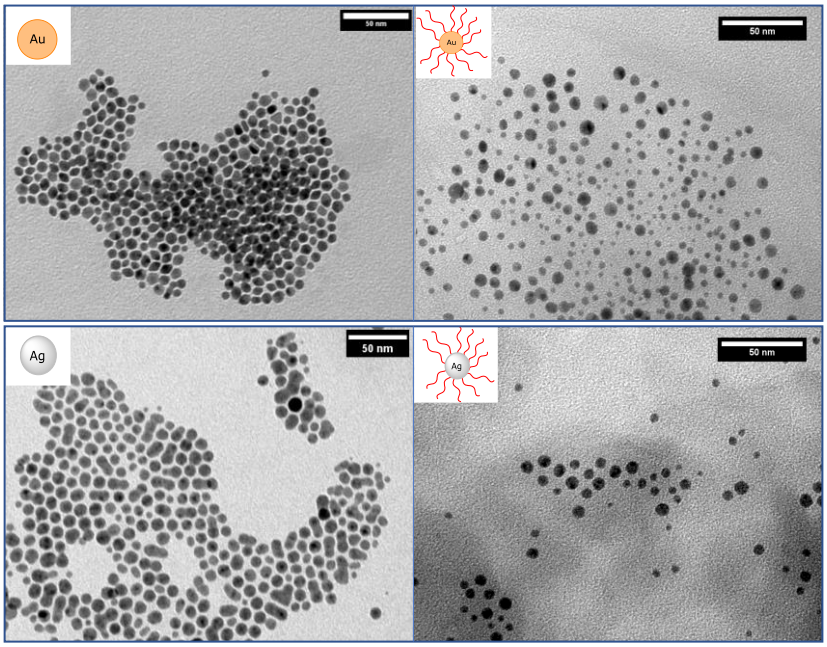

Figure 4-6. Exemplary TE micrographs of unfunctionalized as well as PE-capped gold (on top) and silver (bottom) nanoparticles.

4.4 Long-time Stability of PE Capped Nanoparticles and Fabrication of their Composites

4.4.1 UV-vis Characterization and Long-time Stability of PE–AuNPs

As described in chapter 2.5, based on the strong plasmonic resonance, UV-vis spectroscopy is a powerful tool for the characterization of gold nanoparticles.[144] The characteristic absorption depends on various factors e.g. the solvent, temperature and the size of the particles. Therefore, by keeping the measurement parameters constant, from the UV-vis analysis a direct characterization and comparison of the particle's size and environment is achievable. In order to validate that the formation of a polyethylene-shell did not influence the optical properties of the gold NPs that are required for various applications such as biosensoring[31], UV-vis analysis of fresh prepared pure AuNPs and capped PE–AuNPs were performed in toluene at 90 °C (Figure 4-7).
From the data it can be extracted that the capped gold particles exhibit the same optical properties independent on the polyethylene-shell compared to unfunctionalized AuNPs. The shape of both curves was identically and no shift of the characteristic absorption maximum (λ = 530 nm) was determined. This absorption band is responsible for the typical red color of the applied AuNP that was also observed for PE–AuNPs. Based on these examinations it can be concluded that the unique optical properties are also inherent in PE modified AuNPs and the formation of aggregates was excluded using UV-vis spectroscopy. The results are in good agreement with TEM and DLS characterizations and a high temperature stability of PE–AuNPs was further confirmed using UV-vis spectroscopy.

In addition, in order to approve that the polyethylene-shell provides a high stability of the particles also over a long time, AuNPs as well as PE–AuNPs were dried and stored for 2 months. In the solid state, the PE capped nanoparticles completely retained their red color. In contrast to this, the unfunctionalized gold nanoparticles changed their color during the time from red to blue to black indicating a strong tendency for

irreversible aggregation. Nevertheless, both types of particles were afterwards dispersed in toluene.
The core–shell-particles could be dispersed completely by simple reheating the sample to 90 °C resulting in a transparent red dispersion. In case of the unfunctionalized AuNPs, the majority of the sample could not be redispersed even via ultrasonication and furthermore, a blue dispersion was obtained. For verification, both samples were characterized via UV-vis spectroscopy (Figure 4-8). The analysis of the obtained spectra validated the observation made before. For the aged AuNPs a strong red-shift of the absorption maximum to $\lambda = 546$ nm occurred whereas the recorded spectra of PE–AuNPs is almost identically to the analysis of fresh prepared PE–AuNPs. Consequently, from this characterization it was validated that the polyethylene-shell provided an adequate stabilization of the particles due to steric shielding over a long period while keeping the optical properties underlining the advantage of polymer coated particles. In addition, the usage of polyethylene as protecting-shell of metal-nanoparticles might have further advantages over other polymers because of the high crystallinity and especially the predominant chemical, mechanical and thermal stability.

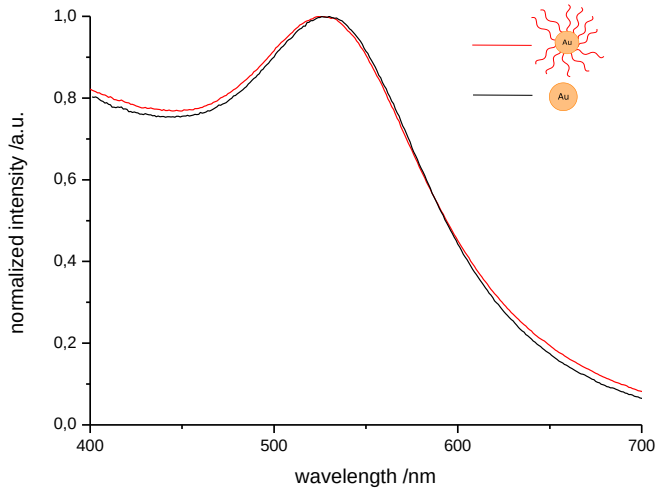

Figure 4-7. UV-vis spectra of fresh-prepared unfunctionalized (black) and PE-capped (red) AuNPs in toluene at 90 °C.

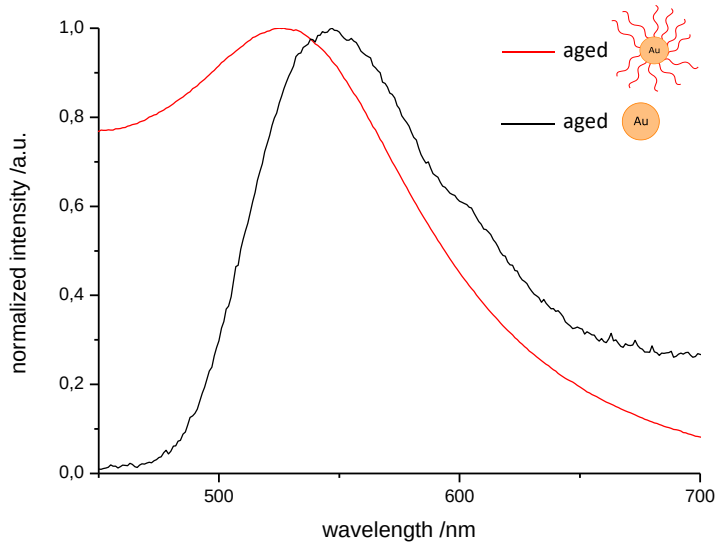

Figure 4-8. UV-vis spectra of aged AuNP and PE-AuNP after drying and redispersion in toluene at 90 °C.

4.4.2 Incorporation into a Polyethylene Matrix

To achieve a complete miscibility of a metal-nanoparticle in a polyethylene matrix, suitable surface properties of the particles are required to ensure a strong interaction of the interface with the matrix. For semi-crystalline polymers like PE commonly an inhomogeneous particle dispersion in the matrix occurs due to weak surface–PE interactions resulting in aggregation and migration of the NPs.[32,146] Briefly, only one strategy based on PE synthesized via CCG is reported by *D'Agosto* and coworkers for the formation of polyethylene brushes on iron oxide resulting in a fine dispersion of the capped iron-particles in a polyethylene matrix.[34] In order to expand this field to noble metal NPs and to demonstrate the advantage of the attached and stable PE-shell on gold- and silver-nanoparticles, an incorporation of those into an analogous commercial available polyethylene matrix was investigated. For proof of principle, a HDPE matrix polymer ($\bar{M}_w = 7.2 \cdot 10^3$ g mol^{-1}) was applied and dissolved in toluene at 90 °C. After complete dissolution, PE-capped AuNPs and AgNPs were blended with the matrix solution,

respectively. The composites were subsequently dried and analyzed via TEM (Figure 4-9). To get a full impression of the usability of the applied route, different particle dosages were incorporated. The analysis of the nanocomposites confirmed a complete fine dispersion of PE–AuNPs and PE–AgNPs within the matrix. This observations were valid for high (~15 wt% capped-particle content, Figure 4-9a+c) and a low (~4 wt% capped-particle content, Figure 4-9b+d) for both either gold or silver nanoparticles. In addition, from the TE micrographs it can be observed that the nanoparticles are exclusively dispersed in the matrix polymer (grey shadow in the micrograph) whereas the areas without polyethylene are completely particle-free validating the strong particle–matrix-interaction. The results proved that the incorporation of the PE-shell–metal-core was efficiently achievable even at high particle content demonstrating the advantage of PE-capped gold and silver nanoparticles. This successful and efficient route for the formation of stable composites might be transferred to a wide range of application such as the formation of antibacterial packaging materials and foils.[146]

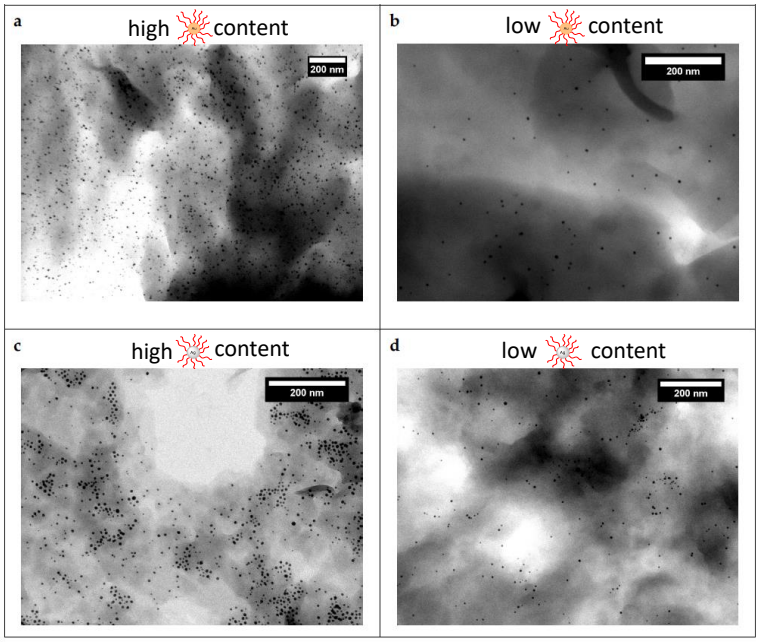

Figure 4-9. TE micrograph of PE–AuNP with a high (a) and low (b) as well as PE–AgNP with a high (c) and low (d) particle contend dispersed in a PE matrix.

To sum up, in this subchapter the successful synthesis of polyethylene grafted gold- and silver nanoparticles was presented and reported for the first time. The respective capped nanoparticles were fully characterized via DLS and TEM. Both analysis and the UV-vis measurements of unfunctionalized and PE grafted particles confirmed a strong attachment of the polymer-shell resulting in stable and long-living nanostructures. In addition, these particles were completely dispersible in a polyethylene matrix with different particle contents.

4.5 Temperature-Dependent Dispersibility of Capped Gold- and Silver-Nanoparticles

Within this subchapter the temperature depended solubility of nanoparticles was investigated in detail based on the primary observations obtained from DLS (chapter 4.3.1). During the analysis using dynamic light scattering, it was confirmed that the PE capped gold nanoparticles formed aggregates at temperatures below the critical solution temperature whereas these structures disaggregated completely and reversible by simple reheating the sample. After it was confirmed that the polyethylene-shell determines the solution behavior of the respective nanoparticles, it was assumed that the thermoresponsive properties of PE might be transferable to the field of nanomaterials that has not been reported before. In scientific research, responsive polymers like poly(*N*-isopropylacyrylamide), one of the most-established temperature-responsive polymers, is of an important interest, especially in nanomedicine.[166–168] As mentioned before, polyethylene exhibits a drastic change of the solution behavior in a small temperature range around 80 °C. This special feature of polyethylene was developed for applications mainly by the pioneer work of *Bergbreiter* and coworkers. Polyethylene either synthesized via anionic polymerization or by an oxidized commercially available PE was further functionalized and implemented as a ligand for different catalysts resulting in thermomorphic systems.[169–171] Furthermore, this approach was also applied for a polyethylene supported catalyst synthesized via CCG.[11] The advantage of this strategy is that below the critical solution temperature, the PE supported catalyst was inactive and completely precipitated,

whereas after heating the solution became homogenous and the reaction occurred. Afterwards, the catalyst could be easily recovered by cooling the sample followed by filtration. This approach for homogenous catalysis was adopted and further investigated in chapter 5.4.2. Nevertheless, after the successful synthesis of polyethylene capped nanoparticles, the major question of this project was if the properties of PE can be combined with noble metal-nanoparticles which would expand the field of responsive nanomaterials.

The first verification for the switchable aggregation/disaggregation of PE–AuNPs as well as PE–AgNPs was visible to the unaided eye: Both PE capped nanoparticles were filled in a vial and dissoluted with toluene. Afterwards, both dispersions were heated to 90 °C resulting in a well-dispersed homogenous sol. Within these mixtures no formation of aggregates was observed over a long time due to the strong attachment of the polyethylene-shell. As a reference, unfunctionalized AuNPs and AgNPs were mixed with unfunctionalized polyethylene and treated under the same conditions. The vials were subsequently cooled down to room temperature and stored without any movement overnight. In case of the blank samples no change of the mixture could be monitored meaning that the dispersion completely remained red colored (AuNP) or yellow colored (AgNP) (for the pictures see Appendix B). In contrast to this, the observations made for PE–AuNPs and PE–AgNPs were completely different. In both cases, a two-phase system consisting of aggregated, settled down particles and a colorless solvent phase was obtained (Scheme 4-3). The decolorization of the mixture indicates a quantitative separation of the particles from the solvent. These observations can be explained due to the polyethylene-shell. At lower temperature, PE became insoluble resulting in a segregation of the solvent and the formation of aggregated PE-capped nanoparticles which subsequently precipitated, validated also by DLS analysis (Figure 4.3.1). Based on the observations made for the blank samples it can be excluded that the particles are simple enclosed into insoluble PE, validating the requirement and advantage of a strong attached polymer-shell. Remarkably, after reheating the vials a quantitative and quick redispersion was achieved. To validate the observations and further

investigate and quantify the system, UV-vis spectroscopy of PE–AuNPs was performed.

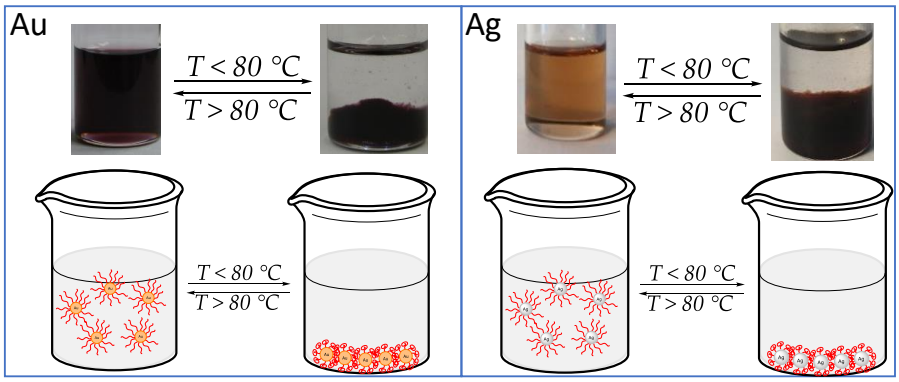

Scheme 4-3. Temperature-dependent dispersibility of PE–AuNP and PE–AgNP.

As described in chapter 4.4.1, UV-vis spectroscopy is an excellent and sensitive method for the characterization of gold nanoparticles. Based on the prior measurement of PE–AuNP, the absorption maximum at $\lambda = 530$ nm was tracked. The sample was heated to 90 °C and the measurement was conducted (Figure 4-10). Afterwards the sample was cooled down to 25 °C and measured again after 12 h of resting time. This procedure was repeated several times resulting in four cycles in order to demonstrate the full reversibility of (de-)aggregation. The measurements at 25 °C showed no appreciable absorption. Due to the sensitivity of UV-vis it was validated that a quantitative separation of the capped NPs from the solvent occurred.

In contrast to this, from the UV-vis analysis at 90 °C it can be extracted that a perfect reversal of the temperature-dependent solubility was achieved without any alteration of the absorption maximum. Based on these results it was confirmed that an efficient and completely reversible transfer between the sediment and dispersed state of grafted nanoparticles was facilitated without any destruction of the core–shell-structures underlining the advantage of the developed system.

In addition, the temperature-dependent solubility of PE–AuNPs was studied in detail. For the examination, a step-by-step heating procedure of the nanoparticles was performed in combination with UV-vis measurements (Figure 4-11). The temperature was altered from 25 °C up to 90 °C in 5 °C steps with a resting time of at least 2 h between each UV-vis measurement in order to achieve a full temperature and solubility equilibrium. Between 25 °C and 65 °C no increase of the absorption could be determined indicating the absence of PE–AuNPs within the light pathway. On the one hand this observation validated that the fine dispersion of the PE–AuNPs did not occur under a critical temperature and on the other hand it excluded that convection is responsible for the disaggregation.
By heating the sample over 70 °C a drastically increase of the absorption was detected which was constant even by further heating up to 90 °C. At 70 °C the attached polyethylene-shell reached its solution temperature and therefore a fine and quantitative dispersion was achieved resulting in a homogenous sol of the stabilized colloids. This temperature is slightly decreased compared to the observation made for the solubility of the pure polymer. This is explainable because of preorganization and inhomogeneity caused by the attachment on the surface that reduces the crystallinity of the polymer and therefore its solution temperature. This is comparable to the explanation made in chapter 3.1.2. Although at 70 °C the absolute absorption maximum was obtained, at least 2 h at 70 °C until the full maximum was required whereas at 90 °C after 5-10 min a completely homogenous dispersion was achieved.

The analysis and determination of a distinct temperature confirmed the usability of polyethylene as a temperature responsive polymer-shell and validated the strong attachment to the surface described before. Additionally, within this chapter it could be demonstrated that PE grafted nanoparticles exhibit a strong and completely reversible aggregation/disaggregation based on the thermoresponsive characteristics of polyethylene, expanding the field of responsive nanostructures.

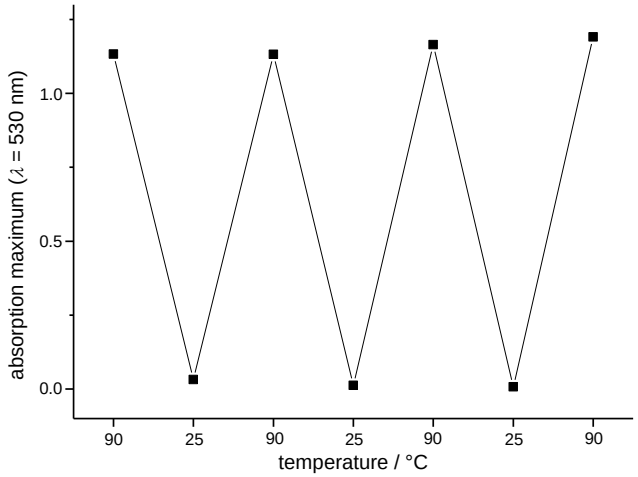

Figure 4-10. UV-vis measurement of the temperature-dependent aggregation in four cycles. The measurement was conducted in toluene at 25 °C or 90 °C.

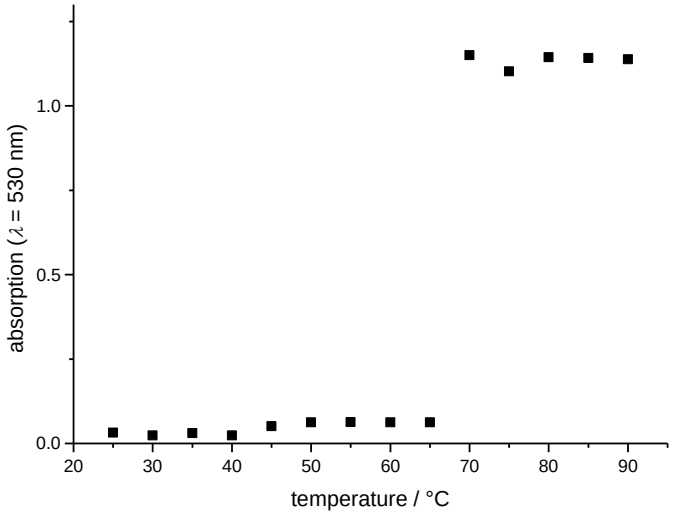

Figure 4-11. UV-vis measurement of PE–AuNPs in 5 °C steps in a temperature range of 25 °C to 90 °C.

4.6 Synthesis of Polyethylene Grafted Palladium Nanoparticles

The developed synthetic route for the formation of PE-shell–metal-core nanostructures was transferred to oleylamine capped palladium nanocrystals (PdNP) to prove the versatility of the system. The palladium nanoparticles dispersed in toluene were kindly provided by *Darius Rohleder*.[172] For the synthesis, PE$_{TTC}$ was dissolved in toluene at 90 °C and mixed with ligand-stabilized PdNPs for 30 min (Scheme 4-4). Afterwards the obtained dispersion was dried and analyzed by TEM. As a blank sample, ungrafted palladium nanoparticles were also analyzed under the same conditions. From the TE micrographs it can be extracted that in case of uncapped NPs a strong irreversible aggregation is observed. In contrast to this, PE–PdNPs are well dispersed and separated. Therefore, it can be concluded that the formation of a polyethylene shell was successful and due to the steric stabilization, the formation of aggregates can be suppressed. Nevertheless, it has to be mentioned that in case of PE–PdNPs in some areas also aggregation was observed, and the temperature depended solubility as well as the long-time stability as described for Au and Ag was not observed. These results on the one hand validate that the strategy can be transferred to other particle types, but on the other hand it demonstrated that further investigations for a strong attachment of polyethylene to palladium surfaces is required that was not part of this project.

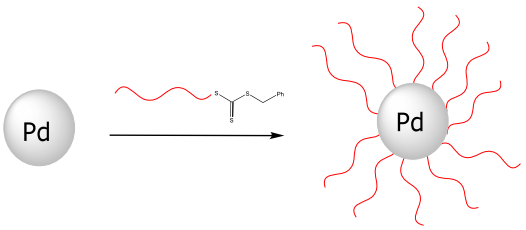

Scheme 4-4. Simplified synthesis of polyethylene grafted palladium nanoparticles. The reaction was carried out in toluene at 90 °C.

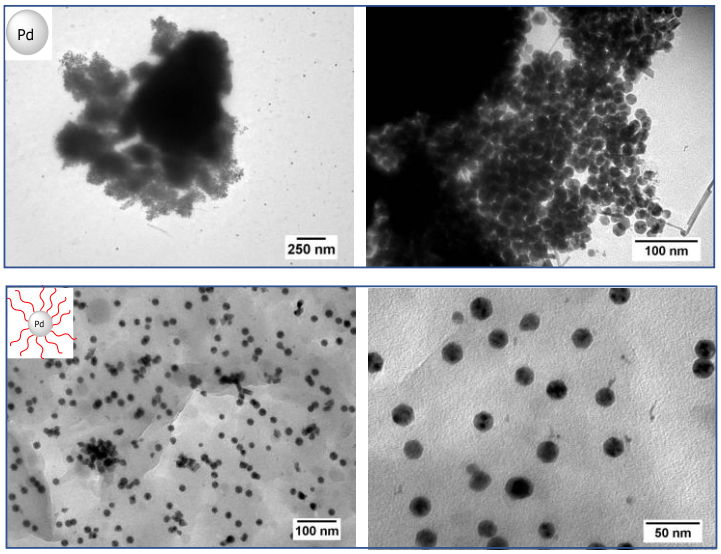

Figure 4-12. TE micrographs of PE grafted (on top) and unfunctionalized (bottom) palladium nanoparticles.

4.7 Conclusion

Within this chapter a straight-forward and effective synthesis for the formation of polyethylene capped gold- and silver nanoparticles was presented. By designing a well-defined trithiocarbonate (PE_{TTC}) or thiol (PE-SH) terminated polyethylene, a strong anchoring of the polymer onto the respective metal surface was achievable via an efficient ligand exchange procedure. The obtained nanohybrids were subsequently characterized by TEM, DLS and UV-vis analysis validating the successful surface modification.

The DLS analysis of the respective capped nanoparticles displayed a strong increase of the hydrodynamic diameter compared to unfunctionalized NPs due to the attached PE-shell. TEM analysis revealed a full separation of the PE–AuNPs and PE–AgNPs without the occurrence of aggregation. The UV-vis characterization of capped and unfunctionalized AuNPs confirmed that the unique optical properties could be maintained irrespective of the polymer-shell.

In addition, PE–AgNPs as well as PE–AuNPs were completely and fine dispersible into a polyethylene matrix at different particle contents without the observation of aggregates. The PE capped NPs have proven to exhibit an excellent stability at high temperatures and showed a long lifetime without the occurrence of any aging processes compared to unfunctionalized AuNPs, confirmed by UV-vis and TEM. Furthermore, the PE grafted nanoparticles exhibited a completely reversible aggregation/dis-aggregation based on the solubility of the polyethylene-shell. This observation was studied in detail via UV-vis spectroscopy. The temperature depending dispersibility enables a complete separation and regeneration of the respective nanoparticles in toluene at a distinct temperature. It could be shown that the applied concept is also applicable for other nanoparticles such as palladium.

All in all, a novel synthetic route for the formation of PE-capped noble metal nanoparticles was investigated leading to an expansion of the field of polyethylene-based nanostructures as well as including polyethylene as a responsive polymer-shell for nanohybrids.

5 Charged End-Functional Polyethylene

Note
Byron Helmut Staudt and this thesis' author contributed equitable to the content of this project. During the experiments, the focus of Byron Staudt was related to polymer characterizations, whereas the author's major focus was laid on the synthetic approach of this project. Nevertheless, the entire results will be presented in both theses comparably. Furthermore, the majority of the content has been already published with an equally contribution and the results were adapted with the permission of the journal and the authors.[173]

5.1 Introduction and Motivation

The defined modification for fine-tuning the properties of polyethylene by introducing functional end-groups is still in the focus of scientific research. By combining the unique characteristics of polyethylene with suitable functional groups new classes of materials and features are accessible.[11,14,17] Besides improved properties due to chemical modification, a full characterization of tailored polymers is required for applications and therefore of special interest. In this field, especially for end-group determination, mass spectrometry (MS) using soft ionization methods like ESI-MS and MALDI-MS is an established method for polymer characterization.[19,20,98] Nevertheless, due to the high hydrophobicity of polyethylene, mass spectrometric analysis of PE is still limited and requires suitable functional and strong polar groups within the polymer chain.[21,93,97]
In this chapter the efficient incorporation of permanent and temporary charged end-groups into PE synthesized in a catalyzed chain growth procedure was investigated. The basic intention was the introduction of a cationic group for two major tasks. First, due to the lack of polar binding sites in polyethylene, the characterization via mass spectrometry is

hindered. One major goal of this project was to expand the usability of MS in the field of PE characterization. Second, the focus was on the applicability of a permanent charged group for versatile applications, including phase transfer properties in combination with the strong thermomorphic behavior of PE. Additionally, the resulting cationic-modified polyethylene should be applicable for further functionalization reactions.

Predesign and Criteria of the Applied System

The main synthetic route for the formation of permanent and temporary charged polyethylene should comply several criteria. First, to make the modified PE suitable for large-scale application, its synthesis should possess a simple and variable reaction route. The second presumption is that PE should be prefunctionalized to provide a building platform for its variable modification to further enhance the field of applications.

Based on the experience described in chapter 3.2.1, iodo end-functionalized polyethylene (PE-I) synthesized via CCG was chosen as starting material due to the reaction's efficiency and its low cost. The functionalization based on PE-I was performed in combination with a nucleophilic substitution, because of easy accessibility of reagents and the negligible formation of side products. Therefore, nucleophilic, commercially available amines are promising starting materials. Additionally, the introduced charged end-group should be applicable for continuing transformations. Consequently, the amines should bear a second functional group. Hydroxyl groups were chosen because of their non-reactivity against PE-I and variable reaction pathways for further modifications.

5.2 Synthesis and Characterization of Permanent and Temporary Charged Polyethylene

5.2.1 Synthesis

As mentioned above, the first step of the designed synthetic route is the formation of iodo prefunctionalized polyethylene (PE-I) to create a building platform based on only one polymer species. The synthesis was conducted using the same procedure as discussed in chapter 3, however, with a fundamental difference of the reaction time. Briefly, PE-I was synthesized in a CCG procedure using butylocytylmagnesium (Bomag) and $(cp^*)_2NdCl_2Li(OEt_2)_2$ (ratio = 200 : 1) and the reaction was carried out in toluene at 80 °C. The main difference to the prior discussed procedure was that the polymerization was not conducted until precipitation was observed. This was required to ensure a high degree of end-group functionalization and to avoid high molecular polymer fractions (Scheme 5-1).

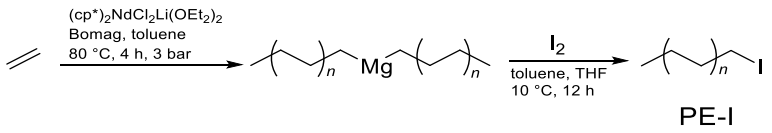

Scheme 5-1. Synthesis of polyethylene iodide.

The permanent attachment of an amine or ammonium bearing a hydroxyl-group was performed in an efficient and simple nucleophilic substitution. For comparison, two commercially available amines – one secondary amine and one tertiary amine – were utilized. The latter amine provides a permanent charged PE (PE-N^+), whereas the secondary amine resulted in an uncharged end-group (PE-N) declared as a temporary charged group due to subsequent protonation (Scheme 5-2). To ensure a complete dissolution and high flexibility of the polyethylene iodide, all reactions were carried out at temperatures above 80 °C using toluene as solvent. To achieve a quantitative conversion, variable amounts of the respective amine was applied to optimize the reaction conditions. It was proven that at least a triple excess of the respective amine was required. The resulting polymer was efficiently purified by simple filtration.

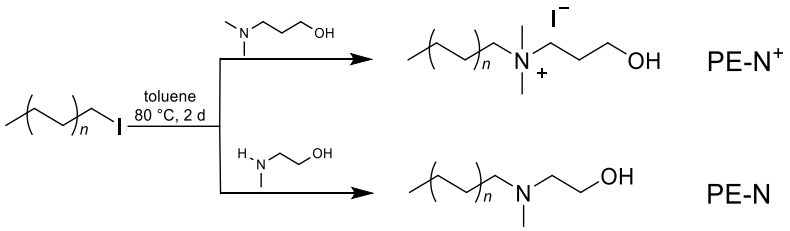

Scheme 5-2. Applied synthesis of PE-N and PE-N$^+$.

5.2.2 Size-Exclusion Chromatography of PE-I and PE-N$^+$

To prove that the polymerization proceeds under controlled conditions, PE-I was analyzed via high-temperature SEC (see Figure 5-1). To validate that SEC is a suitable technique for the characterization of permanent charged PE, also PE-N$^+$ was characterized via HT-SEC. Both chromatograms as well as their characteristic values such as $\bar{M}_n$ (650 g mol^{-1}), $\bar{M}_w$ (780 g mol^{-1}), M_P (850 g mol^{-1}) and the dispersity ($Đ$ = 1.19) were almost identical. The low dispersities of the samples indicated a successful control of the polymerization. The identical shape of the molecular weight distributions revealed that the charged end-functionalized polyethylene did not interact with the stationary phase of the HT-SEC and consequently HT-SEC is an adequate technique for its characterization. The differences in mass of PE-I and PE-N$^+$ (Δm = 23 g mol^{-1}) could not be determined via SEC due to the high error-proneness of this method especially at high temperatures in combination with the low discrepancy of the respective end-groups. Therefore, additional analytical methods had to be applied for the confirmation of a successful end-group transformation.

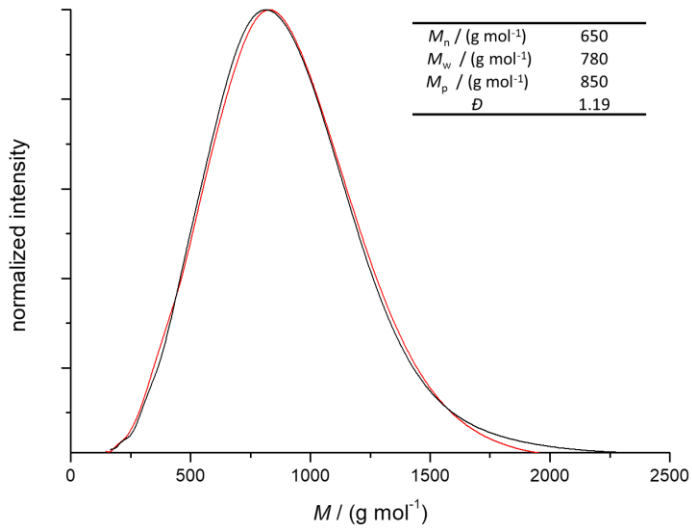

Figure 5-1. Molecular weight distribution obtained by HT-SEC of PE-I (black) and PE-N$^+$ (red).

5.2.3 Nuclear Magnetic Resonance Spectroscopy

One of the most appropriate and well-established techniques for the characterization of low molecular polyolefins and their end-groups is ^{1}H-NMR spectroscopy (demonstrated in chapter 3.2.1). The requirement is a homogenous solution and thus the analysis was carried out in deuterated toluene at 80 °C. The ^{1}H-NMR spectra of PE-I, PE-N and PE-N$^+$ could be measured with high intensities (Figure 5-2).

From the ^{1}H-NMR analysis of PE-I can be extracted that the iodo end-group functionality ~83 %. This determination was achieved by comparing the integrals of the methylene signal adjacent to the iodine (δ = 2.80 ppm, signal a) and the methyl end-group (δ = 0.88 ppm, signal c). The amount of vinylic end-groups due to β-H-elimination is negligible and cannot be determined by NMR spectroscopy. Other possible termination reactions based on impurities resulted in fully saturated polymer chains. Therefore, 83 % iodo end-group functionality is an approximation and might be even higher. The characteristic NMR signals of the methyl group (signal c) and the broad signal of the polymer backbone (δ = 1.1 – 1.5 ppm, signal b) of PE could be observed in all three

samples (PE-I, PE-N^+, PE-N).

The successful end-group transformation of PE-I into the respective amine was validated via NMR as well. Within the spectra of PE-N^+ and PE-N, the characteristic methylene signal adjacent to iodine completely disappeared, indicating a quantitative conversion for both reactions. In case of PE-N (Figure 5-2, center) all specific signals could be assigned: The singlet (δ = 2.05 ppm, signal f) corresponds to the methyl-group bound directly to the nitrogen. The methylene groups next to the nitrogen (δ = 2.20 – 2.30 ppm, signals e) resulted in two triplets, whereas the methylene group adjacent to the oxygen (δ = 3.42 ppm, signal d) is shifted towards downfield. In contrast to PE-N, in case of PE-N^+ the two signals of the methyl-groups directly bounded to the positive charged nitrogen (δ = 3.36 ppm, signal k) are strongly shifted to downfield due to the strong electron-withdrawing properties of the ammonium cation. The two methylene groups adjacent to the nitrogen (δ = 3.80 – 4.00 ppm, signal h, i) are also strongly shifted due to the charged ammonium-group as well. The methylene group bound to the oxygen (δ = 3.49 ppm, signal j) is only slightly influenced by the positive charge due to its distance and therefore is in the same range compared to PE-N. In addition, the methylene groups in β-position to the nitrogen (δ = 1.71 ppm, signal m, δ = 2.24 ppm, signal l) were shifted downfield compared to PE-N due to the strong electron-withdrawing behavior and therefore detectable. Beside the assigned signals, no additional peaks were observed, validating the successful and quantitative end-group modification via the applied synthetic route.

One major focus of this project was the characterization of charged polyethylene via mass spectrometry. MS is a powerful method for end-group analysis and will be discussed in detail in the next chapter.

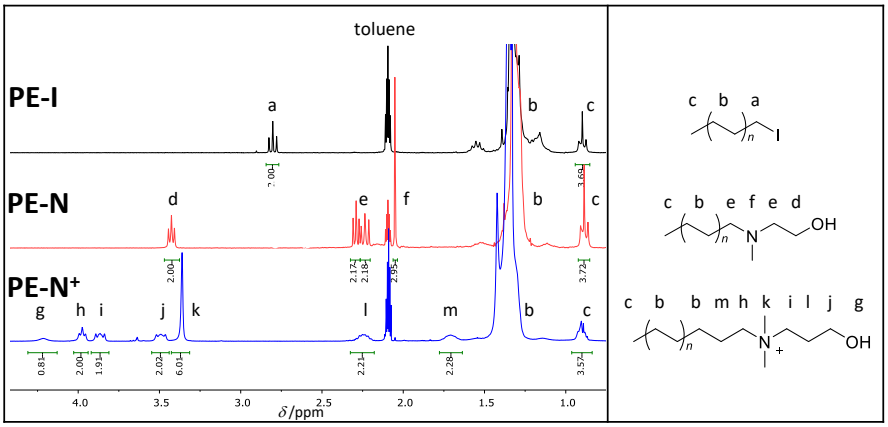

Figure 5-2. ^{1}H-NMR spectra of PE-I, PE-N and PE-N^{+}, carried out in deuterated toluene at 80 °C.

To sum up, an efficient and scalable synthesis for the formation of charged functional polyethylene was presented. The successful control of the polymerization was confirmed by HT-SEC, whereas the quantitative end-group transformation was validated by ^{1}H-NMR characterization.

5.3 Mass Spectrometry of Charged End-Functional Polyethylene

5.3.1 MALDI-TOF-MS

Typically, an accurate characterization of polyethylene via mass spectrometry is strongly restricted due to the lack of polar binding sites, as discussed in chapter 2.4.[21] This limitation can be overcome by the introduction of a charged group enabling the direct analysis of PE without the requirement of metal adducts. The quality of MALDI mass spectra are fundamentally influenced by the sample preparation and the usage of a suitable matrix.[19] Therefore, various matrices were employed whereby trans-2-[3-(4-tert-butylphenyl)-2-methyl-2-propenylidene] (DC TB) and 2-(4-hydroxylphenyl-azo)benzoic acid (HABA) were most suitable for the applied system. To achieve an appropriate incorporation

of PE into the matrix, the polymer was dissolved in toluene at 90 °C, followed by cooling of the solution resulting in a fine dispersion. This dispersion was immediately mixed with a matrix solution in an optimized concentration (matrix in THF: c = 40 mg mL^{-1}, charged PE in toluene: c = 5 mg mL^{-1}). In case of PE-N acetic acid was added to ensure a protonation of the amine functionality yielding a temporary charged polymer (PE-NH$^+$).

As a reference sample, PE-I was measured with and without the addition of a silver salt. Due to the lack of vinylic or coordinative groups signals were detected at all since no interaction with Ag$^+$ took place underlining the advantage of charged functional polymers. In case of the permanent charged PE-N$^+$, intensive signals with an excellent signal-to-noise ratio were obtained (Figure 5-3, top left). The measurement of PE-NH$^+$ also provided a distinct spectrum with a worse signal-to-noise ratio (Figure 5-3, bottom). Additionally, for PE-NH$^+$ on the one hand the formation of background signals was observed and on the other hand the obtained mass distribution exhibited a lower number of detected chains, especially at higher molar masses. One explanation could be that the protonation resulted in a less stable charged group which is susceptible for impurities and fragmentations.

These results showed that a permanently-charged polyethylene is superior for the analysis via mass spectrometry. Nevertheless, in both cases no auxiliary metal salts were required. Furthermore, the isotopic pattern was completely resolved for both polymer species. All signals are distinctly separated by a distance of 28 g mol^{-1} corresponding to one monomer unit. Each signal can be assigned to either end-group functionalized PE-N$^+$ or PE-NH$^+$ validating the suitability of mass spectrometry for these polymers. The calculated and experimental isotopic patterns are shown in Figure 5-3 and are in a good agreement with each other.

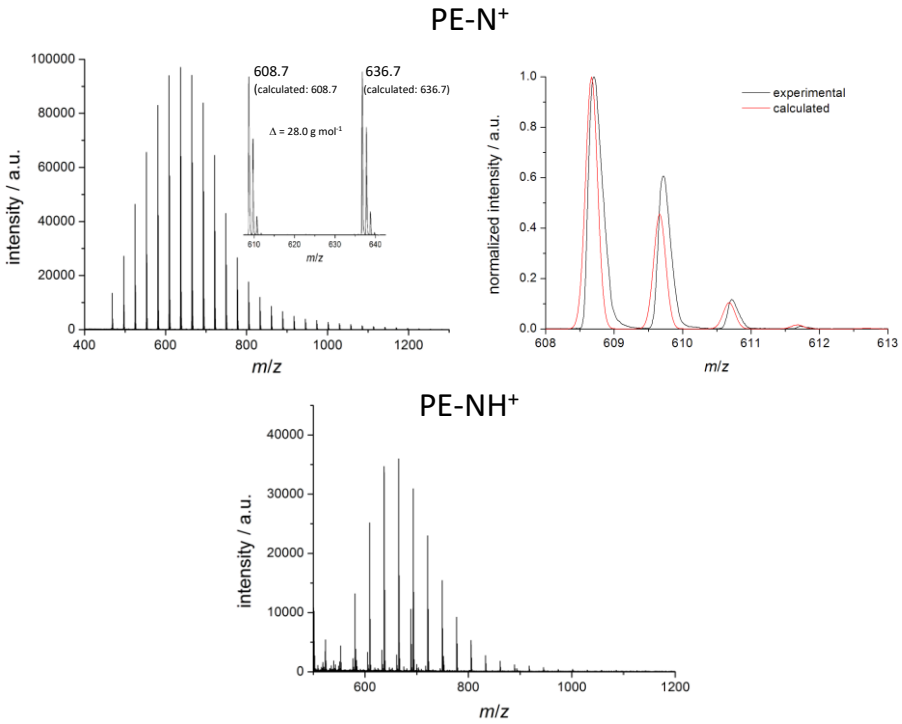

Figure 5-3. MALDI spectra of PE-N$^+$ and the respective calculated isotopic pattern (on top) and PE-NH$^+$ (bottom).

By comparison of the obtained molecular weight distributions based on the MALDI analysis with the ones obtained by HT-SEC (Figure 5-1) some discrepancies were observed. The overall molecular weight distribution is shifted to lower masses in case of MALDI characterization. For instance, the peak maximum (M_P) obtained from HT-SEC was determined to 850 g mol^{-1}, whereas MALDI-MS provided a M_P of 637 g mol^{-1}. For this discrepancy several explanations have to be taken into account. First, high-temperature SEC is a relative method based on calibration using PE-standards. These commercially available standards are synthesized in a conventional way and are partially highly dispersed. The applied standards are completely saturated whereas PE-I and PE-N$^+$ exhibit functional groups. These end-groups, especially due to the relatively low molecular weight of the polymer, can be considered as a

defect and might have a strong impact on the hydrodynamic volume and therefore to the detected masses. In addition, the overall end-group functionality was ~85 %. Termination products of high molecular weight cannot be detected by MALDI, but by SEC. This effect can also cause a difference in the respective molar mass distribution. The most likely explanation is attributed to the MALDI-MS technique. On the one hand, the sample preparation and the choice of the matrix influences the spectra quality, which causes errors although MALDI-MS is an absolute method for mass determination. On the other hand, the transfer of polymer chains into the gas phase is dependent on the molecular weight of the distinct chains. The evaporation of polymers with higher masses is much more limited and the transport efficiency in the applied TOF-analyzer is reduced as well. These effects are known as mass discrimination and are reported in literature (see also chapter 2.4).[174]
In summary, by using MALDI-MS it was demonstrated that a good assessment of the molecular weight distribution of charged polyethylene is achievable and a detailed end-group characterization can be performed.

5.3.2 ESI-TOF-MS

Whereas in MALDI-MS one major challenge was to receive appropriate matrices and sample preparation, the situation in ESI-MS is more complicated. Nevertheless, commonly more reproducible results are obtained by ESI-MS, and the analysis can be conducted more efficiently. One requirement of ESI-MS is the need of homogenous solutions with an appropriate solvent: Due to the solubility of PE commonly non-polar solvents like toluene above the critical solution temperature are required. Contradictory to this criteria, solvents of low polarity like toluene are not suitable for ESI-MS because the electric conductivity of these solvents is insufficient and no charged analytes can be generated due to the lack of dipole(solvent)–ion(analyte) stabilization.[99] Therefore, by applying pure toluene as solvent no ESI-MS spectra were detectable.
Based on observations made in literature, the following sample preparation was adopted, further developed and optimized for the investigated system.[116] One appropriate solvent that was applied in this project is dichloroethane (DCE) with a high relative permittivity

compared to toluene. PE-N^+ could be dissolved in DCE at temperatures above 95 °C and the obtained solution was cooled down resulting in a fine dispersion that was afterwards filtered yielding a saturated homogenous solution. It had to be considered that no spectra were obtained without any additional solvent due to the insufficient polarity of DCE for ESI-MS. Therefore, to enhance the polarity of the sample, the highly polar acetonitrile (MeCN) was added. Samples with varying amounts of MeCN and DCE (80 : 20, 50 : 50, 30 : 70) were examined.
The results showed that the spectra with the highest intensity was obtained by using a 50 : 50 mixture of DCE and MeCN (Figure 5-4 C). In contrast, a solvent mixture with a ratio of 80 : 20 (DCE : MeCN) created much lower intensities which can be explained by the low polarity of the solution (Figure 5-4 A). By further increasing the amount of MeCN (DCE : MeCN = 30 : 70) the intensity compared to an equally ratio decreased again (Figure 5-4 B), probably due to dilution of saturated analyte solution.
With the optimized solvent mixture, also ESI-MS analysis of PE-NH^+ (protonated by acetic acid) was conducted. In this case the intensity maximum was only half compared to PE-N^+ (Figure 5-4 D). From this observation it can be concluded that the permanently charged PE-N^+ is more suitable for ESI-MS. This is in good agreement with the results obtained from MALDI-MS. Compared to MALDI, the overall number of detected chains are quite low and the high molecular weight fraction could not be detected. One likely explanation is that during filtration higher masses are separated favorably compared to lower molar masses. In addition, the mass discrimination effects are possibly more prominent in ESI-MS.
Nevertheless, for PE-N^+ and PE-NH^+ clear ESI spectra were successfully obtained. The resulting signals are separated distinctly by a mass difference of 28 g mol^{-1} according to one monomer unit. Furthermore, the isotopic patterns were fine resolved and are in a good agreement to the calculated ones (Figure 5-4 E). The peak maximum of PE-N^+ (608 g mol^{-1}) compared to PE-NH^+ (580 g mol^{-1}) is shifted by a mass difference of 28 g mol^{-1} corresponding to the mass difference of the respective end-group. The latter observation demonstrated the difference to MALDI-MS and is attributed to the high reproducibility of ESI-MS.

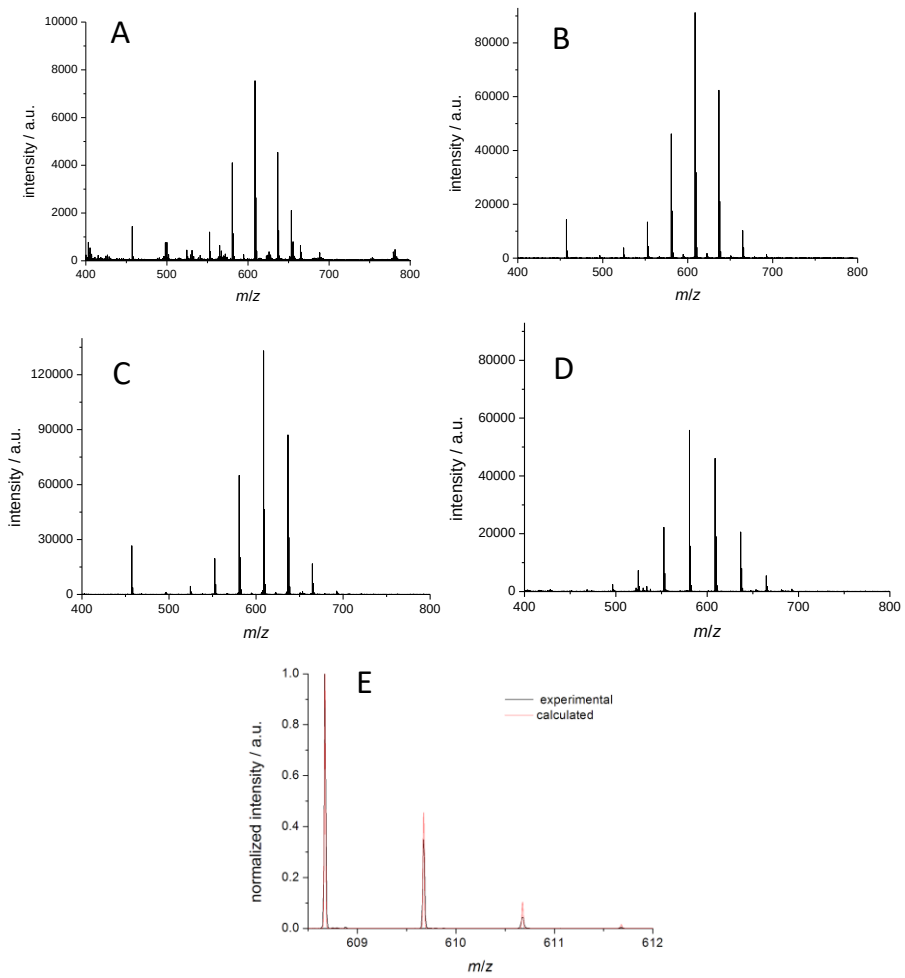

Figure 5-4. ESI mass spectra of PE-N^+ using DCE and MeCN in ratio of 80:20 (A), 70:30 (B) and 50:50 (C) with the corresponding isotopic pattern (E) and ESI-MS spectrum of PE-NH^+ (D).

In Table 1 the experimental determined and calculated molecular masses obtained from MALDI and ESI-MS are summarized together with the corresponding chemical formula.

Table 1. Summarized results of PE-N^+ and PE-NH^+ measured by MALDI-MS and ESI-MS.

method	**polymer**	**formula**	***m/z* experimental**	***m/z* calculated**
MALDI	PE-N^+	$C_{39}H_{82}NO^+$	636.7	636.7
	PE-NH^+	$C_{45}H_{94}NO^+$	665.9	665.7
ESI	PE-N^+	$C_{41}H_{86}NO^+$	608.669	608.670
	PE-NH^+	$C_{39}H_{82}NO^+$	580.644	580.639

In conclusion, it could be demonstrated that MALDI-MS as well as ESI-MS are suitable techniques for the analysis of charged functional polyethylene. It was shown that the sample preparation had to be optimized carefully for MALDI-MS and ESI-MS resulting in spectra with an excellent signal-to-noise ratio. Based on these results, the field of mass spectrometry was successfully expanded towards the characterization of polyethylene, especially for its end-group analysis. In addition, the data confirmed that a stable charged end-group (PE-N^+) is superior to simple protonation of an amine end-group (PE-NH^+) concerning the detection in MS.

5.4 Phase Transfer Properties of Charged Functional Polyethylene

In this chapter the versatility of charged functional polyethylene for applications beside the analysis via MS will be demonstrated, mainly based on two approaches. Both are connected to phase transfer properties of polyethylene due to the positive charge in combination with its thermoresponsive behavior.

5.4.1 Ionic Interactions of Charged End-Functional Polyethylene

In the first approach, a literature described strategy for charged polymers was adopted, refined and transferred to polyethylene. The group of *Cavicchi* and coworkers synthesized a charged RAFT-agent and applied it in a controlled polymerization. The authors observed an interaction of the charged polymer with an anionic compound and its transfer from an aqueous to an organic phase via an ion-exchange reaction.[175,176]

To prove that the system developed in this work also exhibits transfer properties, the anionic dye methyl orange (MO) was used in a model system. For the examination, two vials were filled with a diluted aqueous solution of MO yielding a strong orange-colored solution. Toluene was added carefully to one of the vials, which was used as a blank sample, and heated to 90 °C resulting in a two-phase system. PE-N^+ was dissolved in hot toluene and the solution was added to the second vial. The mixture was heated to 90 °C to ensure a full dissolution of PE. In both cases, MO remained completely in the aqueous (lower) phase due to good solubility of the ionic compound in water. Afterwards, both vials were agitated (Figure 5-5). In case of the blank sample, MO completely remained in the aqueous phase and the organic phase persisted colorless. The complete opposite was observed for the PE-N^+ containing mixture. After mixing the two phase-system, the entire anionic dye was transferred into the organic phase resulting in an orange-colored organic and a colorless aqueous phase. Most likely, a severe ion exchange is attributed to the strong solvation of sodium iodide (I^- = counter anion of PE-N^+) in water combined with favored hydrophobic interaction of the polymer backbone with the aromatic system of MO (Scheme 5-3).

The entire procedure was repeated using the protonated amine

terminated polyethylene. Remarkably, by using PE-NH$^+$, no phase transfer could be observed demonstrating the requirement of a permanently and stable charged end-group.

Figure 5-5. Resulting two-phase system of PE-N$^+$ in toluene, MO and water (left) and toluene, MO and water (right) after mixing at 90 °C.

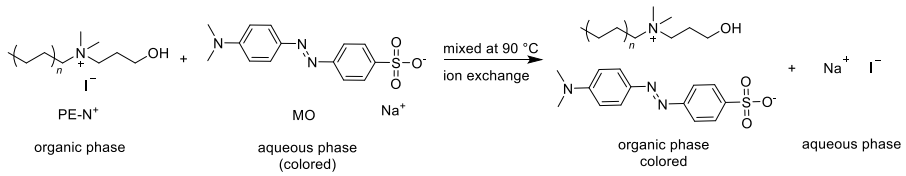

Scheme 5-3. Ion exchange reaction of PE-N$^+$ and MO in toluene/water.

Based on the results it was assumed that a strong ion–ion-interaction of PE-N$^+$ and MO occurred. The observations made for solutions were afterwards transferred to solid polyethylene, because of applicable areas of applications and additionally, in order to further investigate the PE-N$^+$–MO interaction. Considering the assumption, the following procedure was performed.

The PE-N$^+$/MO solution, which was obtained from the procedure described in the last paragraphs, was pipetted carefully. The mixture was subsequently dried under reduced pressure yielding a strong orange colored polymer (PE-N$^+$–MO) (Figure 5-6 A). In addition, commercially available polyethylene and MO were mixed and used as a blank sample. Tetrabutylammonium bromide, a well-established phase transfer agent,

was added to this mixture to ensure a miscibility of MO and the organic phase. Afterwards, the obtained colored solution could be dried as described for PE-N^+–MO under reduced pressure, yielding orange dyed PE (MO@PE) as well (Figure 5-6 B).
To demonstrate the advantage of the charged PE, both composites (PE-N^+–MO and MO@PE) were treated with various solvents such as ethanol or THF (Figure 5-6 C+D). PE-N^+–MO exhibited an excellent stability against organic solvent, meaning that the orange color remained completely. In case of MO@PE the colored polymer bleached out immediately. From this comparative experiment can be excluded that the anionic dye was only enclosed in the polyethylene backbone but interacts strongly with the charged end-group.

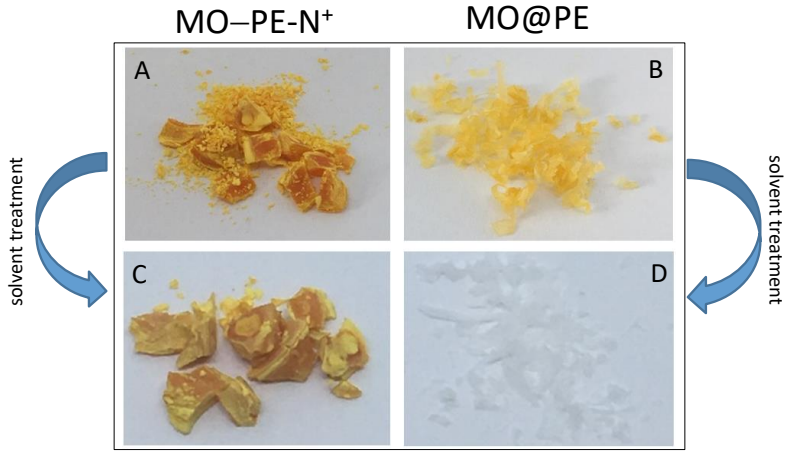

Figure 5-6. PE-N^+–MO before (A) and after (C) and MO@PE before (B) and after (D) solvent treatment.

The observations made for the applied model system (PE-N^+–MO) demonstrated the magnitude of the strong anionic–PE-N^+ interaction. The major advantage of the developed system is that anionic components can be incorporated into a hydrophobic polyethylene matrix. This can be reached without any additives via an efficient and simple procedure resulting in a solvent resistant and stable material. This approach might be transferable to other anionic compounds such as antibacterial materials for food packaging or anionic plasticizer and flame retardants.[177,178]

5.4.2 Charged End-Functional Polyethylene in Phase Transfer Catalysis

Based on the strong phase transfer properties discussed in the last paragraph, the application of PE-N^+ as a phase transfer catalyst (PTC) was a logical consequence. As described in chapter 4.5, *Bergbreiter* and coworkers performed pioneer work about the versatile application of functional PE. For instance, *Bergbreiter* et al. synthesized charged end-functional polyethylene via an anionic polymerization and applied this new species in phase transfer catalysis.[170,179] This approach was adapted and applied in this work with the focus on a systematical comparison to well-established phase transfer catalysts. To get a detailed impression of the phase transfer catalysis using PE-N^+, a simple reaction of sodium cyanide (NaCN) in water and 1-bromodecane in octane, a naturally non-miscible two-phase system, was applied (Scheme 5-4).

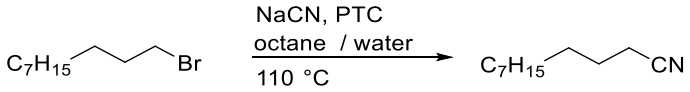

Scheme 5-4. Applied model reaction for phase transfer catalysis.

In order to ensure high flexibility of polyethylene end-groups and a full comparability to the employed PTCs, all reactions were carried out at 110 °C under the same conditions (concentrations of PTCs and reagents). The concentrations of the respective phase transfer catalysts were set to 2 mol%. In case of PE-N^+ the molecular weight was determined by HT-SEC. Beside PE-N^+ and a reference without any PTC, tetraphenylphosphonium bromide (TPPB), tetrabutylammonium bromide (TBAB), tetrabutylammonium iodide (TBAI) and tetraoctylammonium bromide (TOAB) were employed (Figure 5-7). For all examined reactions the conversion was determined via ^{1}H-NMR by comparing the integrals of the signals of the methylene groups adjacent to –Br (δ = 3.38 ppm) and –CN (δ = 2.31 ppm). The respective NMR spectra are listed in Appendix C.

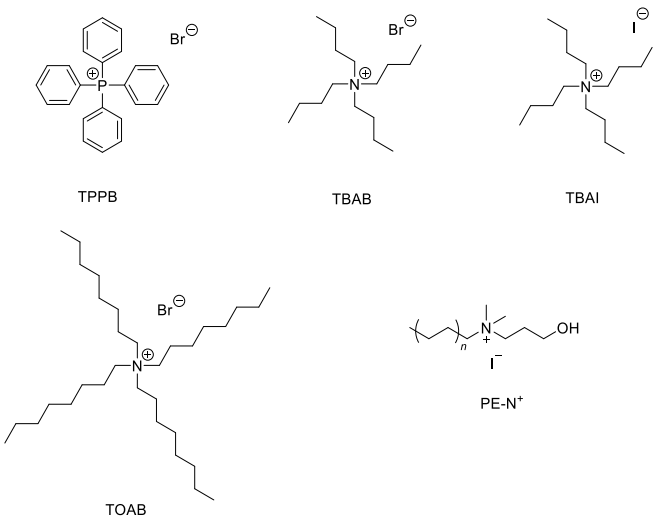

Figure 5-7. Applied phase transfer catalysts for the reaction of NaCN with 1-bromodecane.

To compile preliminary results and in order to prove that PE-N^+ is a suitable candidate for phase transfer catalysis, the reaction was carried out for a short time (4 h) using TPPB, PE-N^+ and a blank sample. As expected, for the blank sample no conversion of 1-bromodecane was achieved. Remarkably, by employing TPPB no conversion was observed either. In contrast, PE-N^+ used as phase transfer catalyst provided about 20 % conversion within the same reaction time. Two conclusions could be drawn based on these results. First, the usage of PE-N^+ as PTC was successful and second, TPPB is unsuitable for the applied reaction. This might be related to a) its relatively high polarity due to the electron distribution within the aromatic side groups and b) the side groups' steric hinderances.

Therefore, PE-N^+ and three additional amine-based PTCs bearing less sterically aliphatic side groups were applied. TBAB was chosen because it is a well-established and active phase transfer catalyst. Nevertheless, by using TBAB no notable conversion could be achieved even after 18 h. Within the same reaction time a conversion of over 80 % was determined by implementing PE-N^+, confirming the excellent PTC properties of this compound. To exclude an influence of the counter ion, TBAI was also tested. The requirement of this examination is regarded to the well-

investigated knowledge that iodide is able to act as a nucleophile as well as a leaving group and therefore may catalyze the reaction. Nonetheless, no conversion could be observed using TBAI. Consequently, it can be assumed that the counter ion has no influence on the reaction.
By considering this result, the most likely explanation is the polarity of the side groups bounded to the quaternary nitrogen. Indeed, by varying the side group from butyl to octyl (by using TOAB) a conversion of over 90 % was achieved. The yield of TOAB was higher than the achieved yield (80 %) using PE-N^+. It had to be taken into account, that the calculation of the PE-N^+ concentration was conducted on the results obtained from SEC, because of more practical handling. Therefore, it was not considered that only ~85 % active end-groups were introduced into PE. Consequently, the overall activity of participle PE-N^+ is comparable to the well-established TOAB. From these results it can be concluded that a high non-polar phase transfer catalyst is required for the applied model reaction. Polyethylene is extremely hydrophobic, but the charged end-group can interact with the phase interface and therefore catalyze the reaction.
To enhance the possible areas of application, further investigations about PE-N^+'s carrier properties e.g. in the field of micelles-building would be reasonable.

Table 2. Resulting conversions of the applied model reaction using various phase transfer catalysts (PTC).

PTC	*t* / h	conversion / %
blank	4, 18	0
TPPB	4	0
PE-N^+	4	20
TBAB	18	<2
TBAI	18	<2
TOAB	18	~92
PE-N^+	18	80

The major advantage of using PE-N^+ as a phase transfer catalyst is the strong thermoresponsive behavior of polyethylene based on its critical solution temperature. Due to its good solubility at high temperature and

its insolubility at ambient temperature, a complete precipitation of the PE-based catalyst occurs. The ^{1}H-NMR analysis of PE-N^{+} after the catalyzed reaction showed no significant change in the characteristic signals validating the efficiency and usability of the developed system (for the NMR spectrum see Appendix D). Therefore, the novel developed PE-N^{+} is completely recoverable by simple filtration.

It can be summarized that charged functional polyethylene is superior to many PTCs especially for hydrophobic environments because it combines easy handling, high activity and complete recoverability within one compound. In addition, it was demonstrated that PE-N^{+} can be easily and efficiently loaded with an anionic compound underlining the versatility of the phase transfer properties.

5.5 Further Functionalization Reactions

As described in the beginning of the chapter, the applied charged functional polyethylene is capable of undergoing further functionalization reactions. Two different synthetic routes were assayed. One is based on an additional RAFT end-group and the second one included an ATRP moiety. These types of end-groups had been chosen, because both enable block copolymerization using a PE-based macroinitiator.

5.5.1 RAFT-based End-Group Functionalization

The formation of a RAFT-bearing charged PE was conducted in two different approaches. The first route starts from PE-I, whereas the second one uses PE-N^{+} as a building block.

Nucleophilic Substitution based on PE-I

Comparable to the successful synthesis of PE-N^{+} and PE-N, PE-I was applied in a nucleophilic substitution. The first step was the synthesis of a RAFT-agent bearing a tertiary amine end-group. This compound was implemented with PE-I (Scheme 5-5). To optimize the reaction conditions, the temperature, the conducted reaction time and the solvent were

varied. The solvents tested ranged from pure toluene to diverse toluene/DMF mixtures to enhance the polarity due to its influence on the efficiency of a nucleophilic substitution. To guarantee a homogeneous solution of both reagents, the reaction temperature had to be adjusted for the respective conditions.

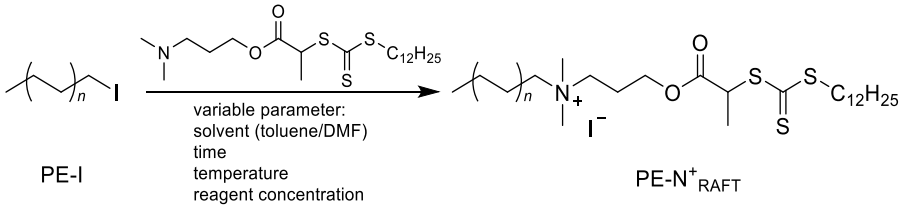

Scheme 5-5. Synthesis of PE-N^{+}$_{RAFT}$ via a nucleophilic substitution.

The resulting product was analysed by ^{1}H-NMR spectroscopy and mass spectrometry. Within this work, only the reaction of best results is discussed. After purification of the obtained polymer, a slightly yellow colour was observed that indicated the presence of a trithiocarbonyl-group. This assumption was confirmed by MALDI-TOF mass spectrometry, showing the successful formation of the desired PE-N^{+}$_{RAFT}$ (Figure 5-8). The experimental determined *m*/*z* values are in good agreement with the calculated ones (experimental determined M_P = 968.9 g mol^{-1}, calculated M_P = 968.8 g mol^{-1}). Within the mass spectrum a distinct separation of 28 g mol^{-1} between the peaks is observed corresponding to the polyethylene backbone. Furthermore, the resolved isotopic pattern underlined the successful formation of PE-N^{+}$_{RAFT}$. Nevertheless, mass spectrometry cannot be considered as a quantitative analysis, because the resulted side-products as well as PE-I cannot be detected as explained in chapter 5.3. Therefore, ^{1}H-NMR spectroscopy was performed to confirm the successful end-group transformation.

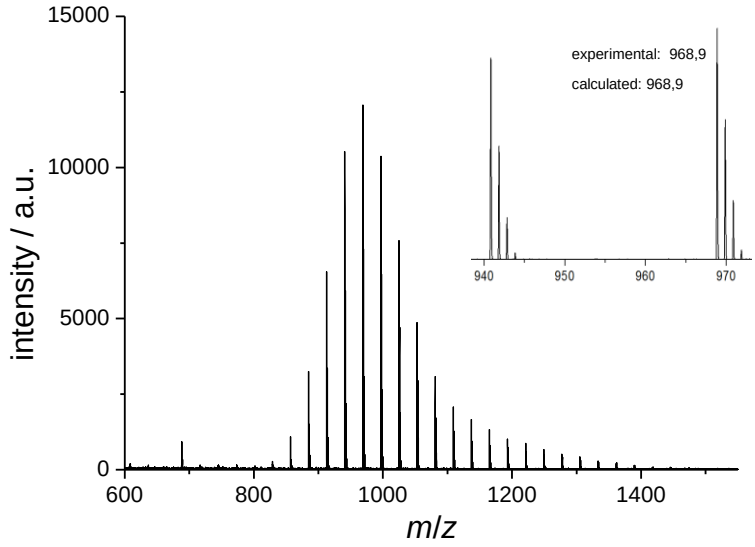

Figure 5-8. MALDI mass spectrum of PE-N^{+}_{RAFT}.

From the ^{1}H-NMR spectrum can be extracted that PE-I was completely consumed due to the missing characteristic signal corresponding to the methylene adjacent to the iodide (δ = 2.80 ppm) (Figure 5-9). Comparable to the analysis of PE-N^{+}, the formation of an ammonium terminated polyethylene can be directly detected by the observation of signals corresponding to the methyl-groups connected to the quaternary nitrogen (δ = 3.36 ppm). This characteristic signal corroborated the successful conversion of PE-I to PE-N^{+}_{RAFT}. This is in accordance with the MALDI mass spectrum. Nevertheless, by comparing the integrals of the Me_2N~ singlet to the signal of the methyl end-group -CH_3 (δ = 0.88 ppm) an insufficient conversion (~20 %) was determined. In addition, the ^{1}H-NMR spectrum contained several additional peaks that might corresponded to appeared side reactions. Due to the diversity of the signals corresponding to side products, an evaluation was not possible.

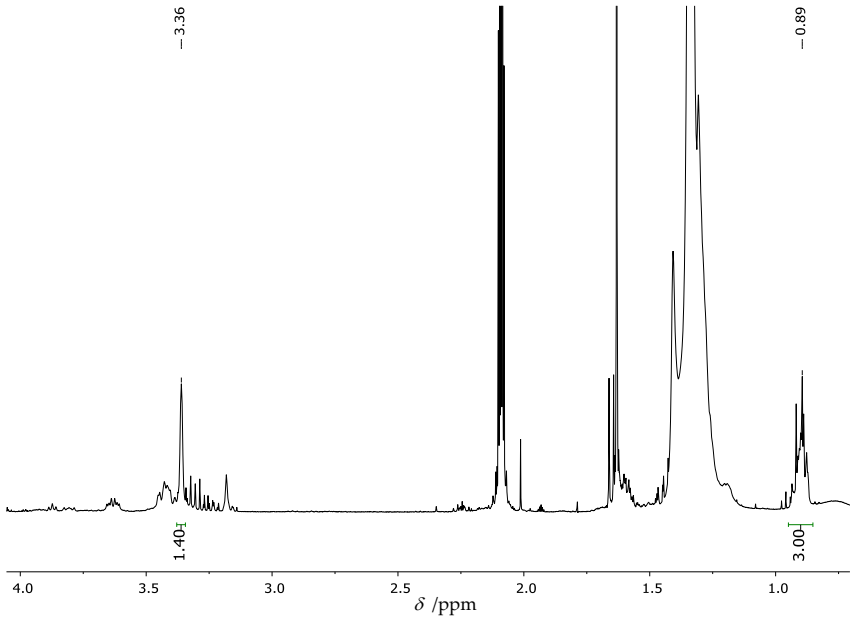

Figure 5-9. ^{1}H-NMR spectrum of PE-N^{+}$_{RAFT}$ synthesized in a nucleophilic substitution.

To sum up, the nucleophilic substitution on PE-I using a presynthesized amine-bearing RAFT-agent was achieved, but with an unsatisfactory conversion. The synthesis required further investigation that was not part of this project. For this reason and because the pursued strategy was the usage of PE-N^{+} as a reaction platform, the project's focus shifted to reactions on the hydroxyl group.

Further Modification based on PE-N^{+}

The synthetic route for the formation of PE-N^{+}$_{RAFT}$ based on PE-N^{+} was conducted via an esterification reaction. The applied RAFT-reagent contained a carboxylic group. To achieve a reaction between the carboxylic group and the hydroxyl group of PE-N^{+}, two acid activation methods were examined. The first major route consisted of the activation by converting the carboxyl-group into an acid halide. This can be achieved by the reaction of the RAFT-agent with thionyl chloride or oxalyl chloride. During the activation reaction, a turning of the colour from yellow to black was observed, commonly indicating the occurrence

of side reactions. Nevertheless, this activated species was directly implemented with PE-N^+ (Scheme 5-6).
The second synthetic route was the reaction of PE-N^+ with the unactivated RAFT-agent under the addition of DCC and DMAP. This reaction is known as *Steglich* esterification.[180] The reaction conditions were adjusted individually for each acid-activation method.

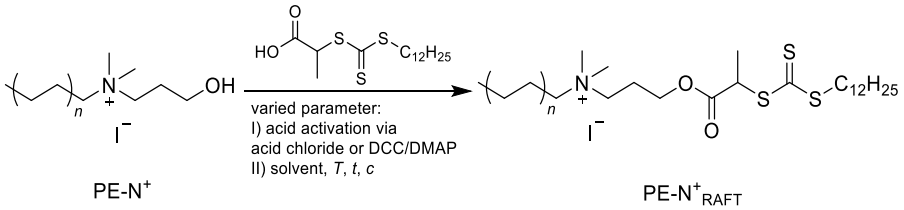

Scheme 5-6. Synthesis of PE-N^+_{RAFT} via an esterification reaction.

All the examined reaction conditions resulted in no or negligible conversion. Consequently, the desired product could not be detected via mass spectrometry. Furthermore, the typical ^{1}H-NMR spectrum exhibited a variety of different signals indicating the occurrence of numerous side-reactions (Figure 5-10). Remarkably, the characteristic methyl signal (ME_2N^+~) completely disappeared. From these observations it can be concluded that PE-N^+ degraded during the reaction. Two possible reasons were assumed.
First, the small distance between the positive ammonium- and the hydroxyl-group might cause possible interactions and hinderances with the activated carboxyl group. Second, the high number of functional groups – especially the reactive TTC group – is responsible for the occurrence of side reactions under the harsh conditions. To verify the first assumption, the linker's length between the nitrogen and the oxygen was increased by using a new amine as starting material.

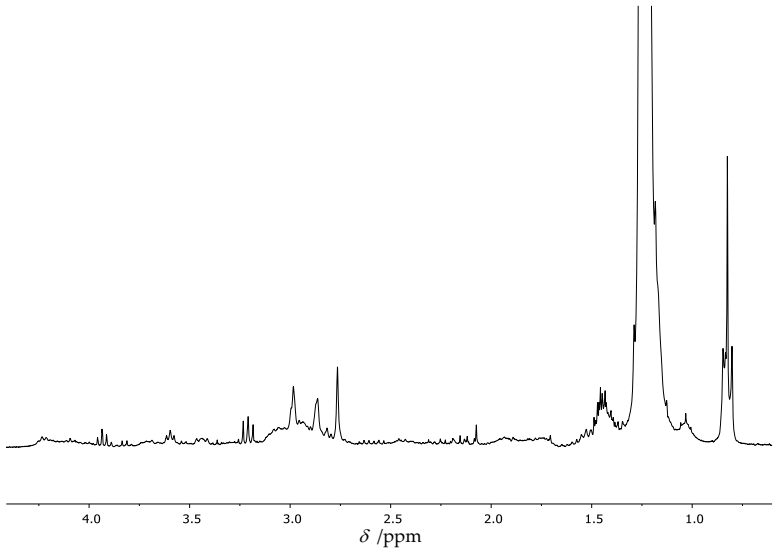

Figure 5-10. Exemplary ^{1}H-NMR spectrum of the esterification reaction based on PE-N^{+}. The spectrum was recorded in benzene-d6 and tetrachlorethane-d2 (1:2).

Variation of the Linker Length

To increase the length of the linker between the charged ammonium group and the potentially active hydroxyl-group, dimethylaminohexanol was employed in a nucleophilic substitution reaction. Based on the optimized reaction conditions for the formation of PE-N^{+} (see chapter 5.2), the amine was added in triple excess to PE-I in toluene at 90 °C for 2 d (Scheme 5-7).

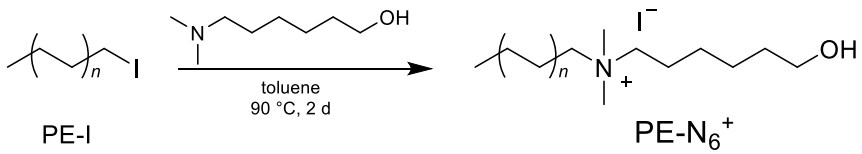

Scheme 5-7. Synthesis of PE-N$_6^{+}$.

The resulted product was subsequently analyzed by MALDI mass spectrometry (Figure 5-11). The discussion is equivalent to PE-N^{+} and therefore kept short. The spectrum indicated that the formation of the desired PE-N$_6^{+}$ was successful. The observed signals were separated by

28 g mol^{-1} corresponding to the polymer backbone and an adequate signal-to-noise ratio was achieved. In addition, the experimental determined molecular masses are in good accordance with the calculated ones validating the formation of PE-N_6^+.

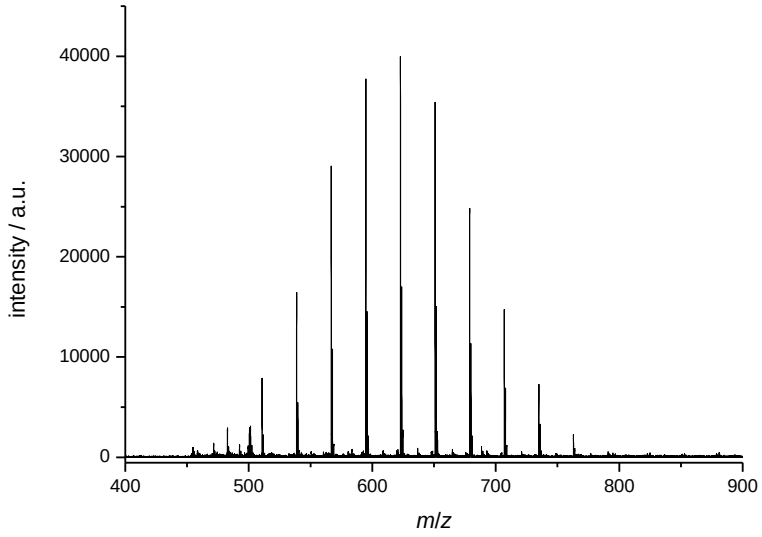

Figure 5-11. MALDI mass spectrum of PE-N^+_6.

In order to verify the quantitative formation of PE-N_6^+, ^{1}H-NMR analysis was conducted. All recorded signals can be assigned to the expected peaks from PE-N_6^+. The characteristic methyl signals corresponding to Me_2N^+~ (δ = 3.37 ppm) as well as the adjacent methylene groups (δ = 3.63, 3.80 ppm) were observed. Furthermore, the methylene-group bounded to the hydroxyl-group (δ = 3.50 ppm) was clearly detected as well as the characteristic signals corresponding to the polymer backbone (δ = 1.2-1.4 ppm) and the methyl end-group (δ = 0.88 ppm).

From both characterization methods can be concluded that the conversion of PE-I to PE-N_6^+ was achieved successfully and quantitatively. Therefore, PE-N_6^+ was employed for the esterification reaction described before without any notable conversion (for an examplaric ^{1}H-NMR spectrum see Appendix D). Accordingly, it can be

excluded that a variation of the amine had an influence on the reaction with a carboxylgroup.
One reasonable explanation might be that the RAFT-agent caused the incomplete reaction due its high reactive functionality. Based on this assumption, acid halides bearing less active groups were employed in order to simplify the reaction system.

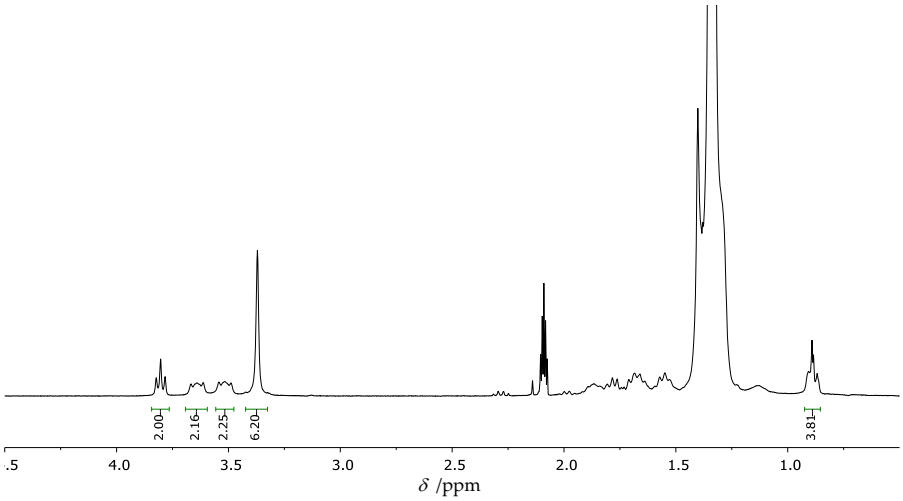

Figure 5-12. ^{1}H-NMR spectrum of PE-N$^{+}_{6}$ recorded in toluene-d8 at 80 °C.

5.5.2 ATRP-based Functionalization of PE-N^{+}

Although the further functionalization of PE-N^{+} was conducted as a proof of principle in order to show the versatility of the developed system, an additional group was implemented that can be used for further block copolymerizations. For the synthesis of a charged ATRP- or macroinitator(MA)-functionalized PE, a stategy adapted from the literature was applied.[16] A reaction of PE-N^{+} with either 2-bromopropionyl bromide or methacryloyl chloride was performed. These commercial available acid halides were chosen because of their generally efficient and highly yielded reactions.[181] To ensure a complete dissolution of PE-N^{+}, the reaction was carried out in toluene at 80 °C with the addition of an auxiliary base (NEt$_3$) (Scheme 5-8). Based on the

description in literature and on the experimental experience discussed in subchapter 5.5.1, the reaction time was set to 2 h to avoid time-dependent side reactions under those harsh conditions.

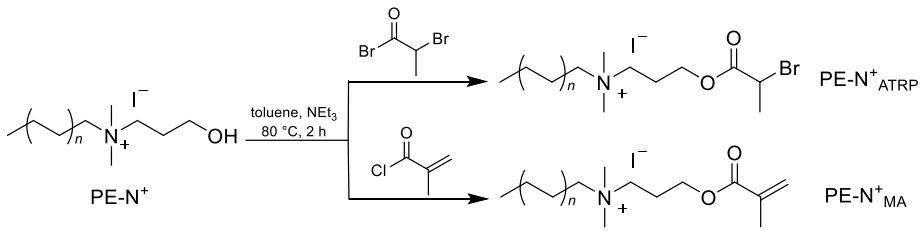

Scheme 5-8. Reaction scheme for the synthesis of PE-N$^+$$_{ATRP}$ and PE-N$^+$$_{MA}$.

The resulting PE-N$^+$$_{ATRP}$ and PE-N$^+$$_{MA}$ were characterized by MALDI mass spectrometry. The analysis of the respective spectra confirmed the successful functionalization based on PE-N$^+$ (Figure 5-13). The spectrum of PE-N$^+$$_{ATRP}$ exhibited a relatively low signal-to-noise ratio and indicated that a small amount of side products were formed. Also, in case of PE-N$^+$$_{MA}$, a second distribution shifted with a mass difference of 8 g mol^{-1} was detected. These signals could not be assigned to any reasonable structure, but are probably connected to formed side products or fragmentation reactions. Nevertheless, in both cases the main signals possesed high intensities and were attributed to the desired products. The observed peaks with the highest intensity are in a good accordance with the calculated structures (Figure 5-13 bottom).

Furthermore, the bromo isotopic pattern was observed in all cases validating the formation of the desired product. In order to prove the results obtained from the MALDI-MS, ^{1}H-NMR spectroscopy was performed. This characterization confirmed the successful synthesis of PE-N$^+$$_{ATRP}$ and PE-N$^+$$_{MA}$ (Figure 5-14). For both polymers the characteristic signal of the methylgroups adjecent to the nitrogen (δ = 3.40 ppm) was detected. In case of PE-N$^+$$_{ATRP}$, the appearance of the doublet at δ = 1.8 ppm may correspond directly to methylgroup adjacent to the ~CHBr-group. A quartet at δ = 4.7 ppm was assigned to the latter. The methylene groups next to the nitrogen and oxygen atoms are shifted towards low field and one of these signals overlaped with the Me$_2$N$^+$~

signal. Therefore, the respective integral is higher than the expected value.
For PE-N^+_{MA} the characteristic signals of the unsaturated vinylic end-group were observered at δ = 5.40 ppm and δ = 6.30 ppm. The methylgroup adjacent to the vinylic end-group could be observed as well (δ = 1.90 ppm). It has to be mentioned that in both spectra the analyzed integrals did not exactly correlated to the expected values. This observation underlined the assumption of undesired side products.

Nevertheless, from the analysis via ^{1}H-NMR in combination with MALDI-MS the sucessful formation of PE-N^+_{ATRP} and PE-N^+_{MA} in satisfying yields could be determined.

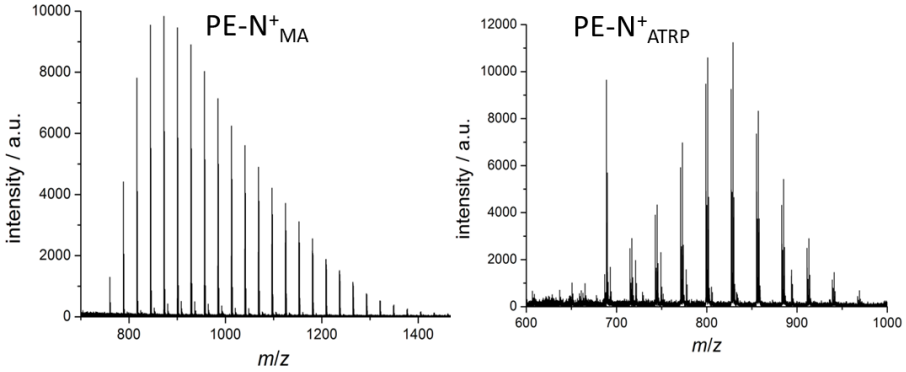

product	formula	*m/z* experiment	*m/z* calculated
PE-N^+_{ATRP}	$C_{50}H_{101}NO_2Br^+$	828.9	828.7
PE-N^+_{MA}	$C_{59}H_{118}NO_2^+$	872.4	872.9

Figure 5-13. Characterization of PE-N^+_{ATRP} and PE-N^+_{MA} via MALDI-MS.

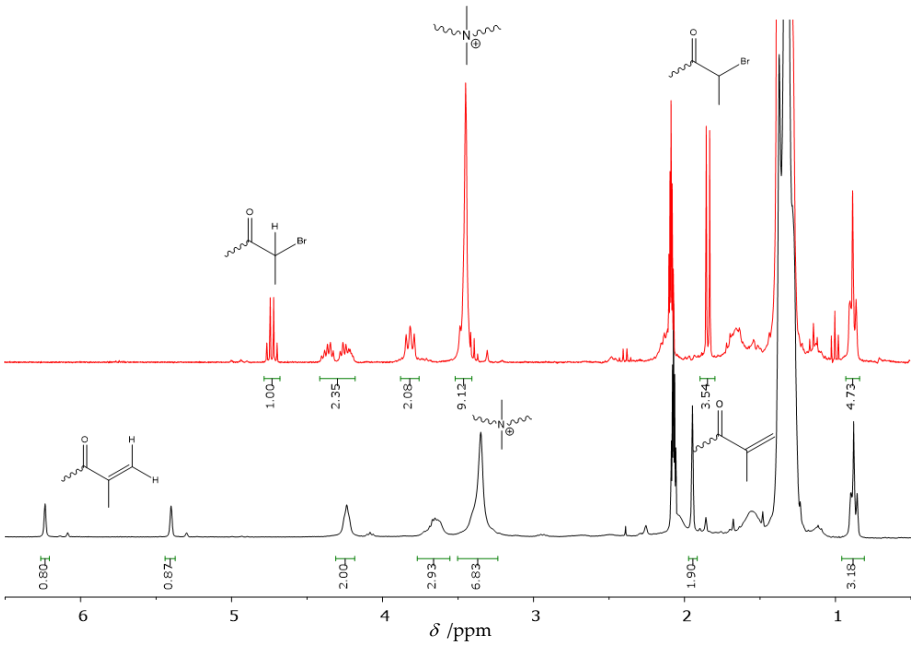

Figure 5-14. ^{1}H-NMR spectra of PE-N$^{+}_{ATRP}$ and PE-N$^{+}_{MA}$.

Block Copolymerization based on PE-N$^{+}_{ATRP}$

As described above, the functionalization of PE-N^{+} should provide an additional group that allows to conduct further block copolymerization. The ATRP functional charged polyethylene was applied in a controlled atom transfer radical polymerization (ATRP). Briefly, ATRP is a technique that is based on an atom transfer and consists of an ATRP-initiator and usually a copper (I) halide in combination with a ligand. In the first step of an ATRP-polymerization, the alkyl halide initiator reacts with the Cu(I)Br resulting in a copper (II) species and a radical that can propagate with a monomer unit. Due to the fast halide transfer between the active radical species and the dormant polymer-halide, a controlled radical polymerization is accessible.[182] Therefore, PE-N$^{+}_{ATRP}$ was employed as a macroinitiator in an ATRP-polymerization (Scheme 5-9). Beside the initiator, *n*-butylacrylate was applied as monomer and CuBr as transition metal catalyst in combination with the ligand PMDETA was employed. PMDETA is required to achieve a dissolution of the respective

copper complex. To ensure high solubility of all reagents, the polymerization was conducted at 100 °C in toluene in combination with anisole for tuning the polarity. After the polymerization, several filtration-redispersion cycles using THF were performed. Afterwards, an adhesive polymer was obtained. The occurrence of the stickiness can be assigned to poly(butyl acrylate) indicating the successful block copolymerization (PE-*b*-PBA). PE-N^+ was used under the same reaction conditions as a blank sample. In this case no change of the polymer's haptic was observed and no change of the respective molecular weight distribution was obtained.

In contrast to the reference, the SEC analysis exhibited a bimodal distribution (Figure 5-15) after the block copolymerization. The peak at lower molecular weight can be assigned to unreacted PE-N^+_{ATRP} indicating an incomplete reaction. Beside this peak, an additional well-defined distribution at higher molecular masses (~5000 g mol^{-1}, $Đ$ = ~1.2) was observed. From the appearance and shape of this signal in combination with the analysis of the blank sample and a change in the haptic of the polymer, it can be concluded that the block copolymerization was successful, although no MALDI-MS spectra could be detected. Further optimization and investigation of the block copolymerization as well as the polymer's purification are required for further applications but was not performed in this project due to lack of time.

To sum up, the primary results discussed in this subchapter demonstrated the versatility of charged functional polyethylene for further functionalization reactions and applications.

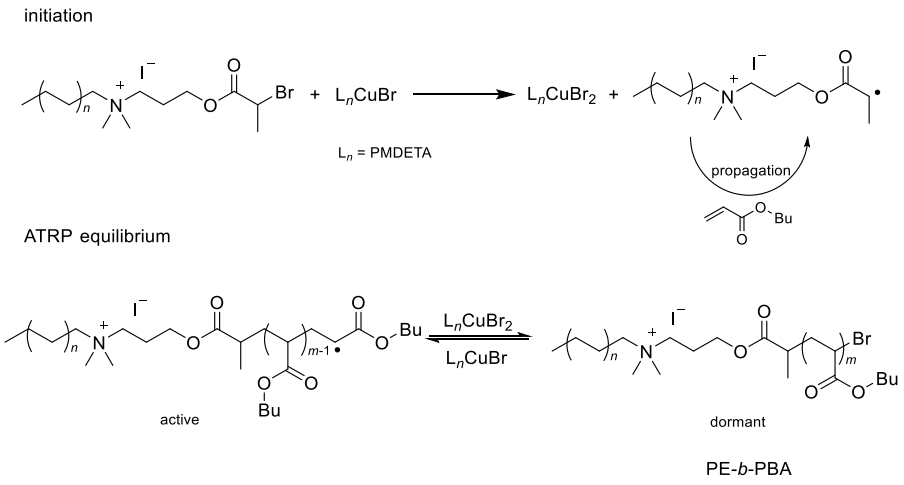

Scheme 5-9. Simplified mechanism of the ATRP copolymerization based on PE-N^{+}_{ATRP} and *n*-butylacrylate.

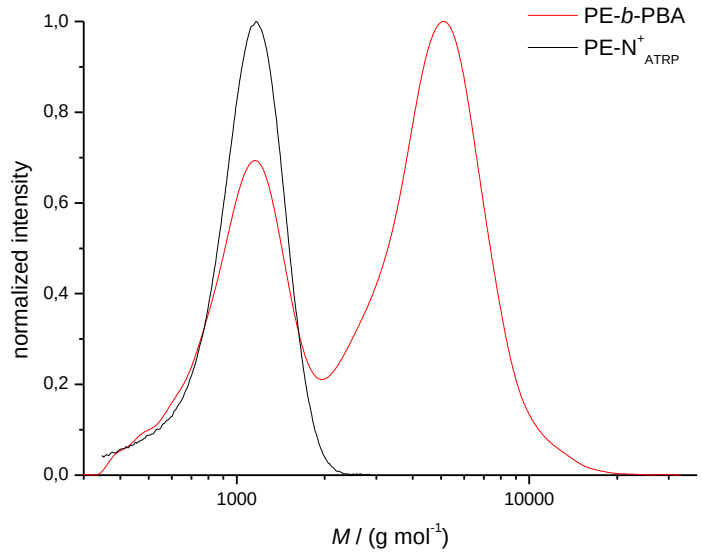

Figure 5-15. HT-SEC analysis of the block copolymerization based on PE-N^{+}_{ATRP}.

5.6 Conclusion

In this chapter, the development and performance of a novel synthetic route for the formation of cationic end functional polyethylene was described. The synthesis of a prefunctional polyethylene was performed in a typical catalyzed chain growth procedure, yielding an iodo end-functionalized polymer (PE-I) with a high degree of functionality as well as low dispersity. This well-defined prepolymer was reacted subsequently with various amines in an efficient and simple nucleophilic substitution. The resulting permanent charged (PE-N^+, PE-N^+_6) or temporary charged (PE-NH^+) end functional polymers were fully characterized by NMR-spectroscopy and HT-SEC. By the incorporation of a cationic group, the analysis via mass spectrometry was feasible. This approach provided an easy access to MS and thus expanded the field of MALDI-MS and even ESI-MS for the end-group characterization of polyethylene synthesized via CCG. The obtained spectra exhibited excellent signal-to-noise ratios and were measurable without the addition of any auxiliary metal salt. In addition to full characterization via mass spectrometry, the developed charged polyethylene showed excellent phase transfer properties validated by two different approaches. Strong ion–ion-interactions between PE-N^+ and an anionic dye enabled an efficient colorization of polyethylene in solution as well as in solid state. Due to the severe fixation, the colored solid polyethylene exhibited excellent resistance against various solvents without the observation of migration of the incorporated compound. Furthermore, due to the strong phase transfer properties, the charged functional polyethylene was applied as phase transfer catalyst. PE-N^+ showed higher or comparable phase transfer activities compared to well-established PTCs. Moreover, it was demonstrated that PE-N^+ is superior because its full recovery was achieved by simple filtration based on the solubility of polyethylene. Due to the introduction of an additional functional group into PE-N^+ further modification reactions were performed. This allowed e.g. the formation of a charged ATRP-macroinitiator that was fully characterizable via NMR spectroscopy and mass spectrometry. Based on this developed species a block copolymerization via ATRP was conducted. All the herein presented results confirmed the versatility of charged end-functional polyethylene for a wide range of applications.

6 Concluding Remarks and Future Perspectives

Within this work the versatility of various end-functionalized polyethylene for different purposes was demonstrated. Herein, a synthetic route for the formation of polyethylene modified wood and silica surfaces was developed (chapter 3). Additionally, the field of nanohybrid materials was extended by investigation and detailed studies of polyethylene grafted noble metal nanoparticles (chapter 4). Furthermore, the introduction of a permanent charged end-group into polyethylene and its characterization via mass spectrometry as well as its application was reported (chapter 5).

In the first project of this thesis the synthesis of various end-functionalized polyethylene via a catalyzed chain growth polymerization was described. Based on the obtained end-functional polyethylene, a novel synthetic route for the surface modification of wood particles was developed, resulting in covalently attached polyethylene onto pretreated wood surfaces. From ATR-FTIR analysis the successful premodification of wood as well as the anchoring of polyethylene was confirmed. Thermal analysis via DSC and TGA revealed the formation of a crystalline polyethylene layer bound to wood with a decreased melting and broadened decomposition temperature. Water contact angle measurement and dynamic vapor sorption analysis validated a strongly enhanced hydrophobicity of the modified wood surface. The developed strategies were transferred to silica nanoparticles. Preliminary DLS and TGA analysis confirmed the formation of polyethylene–silica nanohybrids in a grafting-to approach. Moreover, a strategy for the formation of such hybrid materials via a grafting-from approach was designed and investigated by ^{1}H-NMR spectroscopy.
For future applications, the resistance of PE–wood hybrids against degradation caused by weather or microorganisms should be investigated more thoroughly in a long-time experiment. In this context, the dimensional stability due to moisture-dependent shrinking and

swelling should be examined as well. Additionally, composites consisting of PE–wood particles and a polyethylene matrix should be fabricated and their influence on the overall mechanical properties examined. For PE–silica nanohybrids, an enhancement of the grafting density for both described approaches is required, as discussed in detail in chapter 3.4. It is reasonable to examine the observed temperature-dependent dispersibility of PE–SiNPs in detail. In addition, it could be promising to apply the modified particles as reinforcing material and investigate their impact on mechanical properties.

In the second project of this thesis the successful fabrication of polyethylene grafted noble metal nanoparticles was presented. By the introduction of sulfur-containing moieties into polyethylene an attachment to gold and silver nanoparticles via an efficient ligand-exchange procedure was performed. The permanent attachment of polyethylene brushes and their stability over a wide range of temperature was confirmed by dynamic light scattering. TEM and UV-vis characterization revealed a long-time stability of the respective nanohybrids without any observable aggregation and alteration. Furthermore, polyethylene capped AgNPs and AuNPs were excellently dispersible in a polyethylene matrix even at high particle dosages. A completely reversible aggregation/disaggregation of capped nanoparticles was observed and validated by UV-vis, demonstrating the outstanding thermoresponsive behaviour of PE and including polyethylene into the field of responsive polymer–nanohybrids. In preliminary experiments, it was proven that the developed synthetic route was transferable to palladium nanocrystals further confirming the versatility of the investigated system.
For future perspectives, it might be promising to incorporate the particles into materials like foils and to investigate e.g. their antibacterial behaviour and stability against migration. The described approaches should be further transferred to other metal nanoparticles for an even wider range of application. Based on the temperature-dependent aggregation, a full separation of capped nanoparticles from solvents or reagents would be feasible. Therefore, these hybrid materials might be applicable as efficiently recoverable components e.g. in catalysis.

In the third project the synthesis of permanent and temporary charged polyethylene was performed. Due to the introduction of a cationic moiety, MALDI-MS as well as ESI-MS analysis of PE without the requirement of auxiliary salts was achieved resulting in highly resolved spectra, giving new insights into the field of end-group analysis and further expanding it. The developed charged polyethylene exhibited excellent phase transfer properties. It was demonstrated that an anionic dye could be easily attached and incorporated into polyethylene both in solution and in the solid-state. The latter material showed excellent stability against various solvents without observing migration of the attached dye. Additionally, charged end-functional polyethylene was applied as a phase transfer catalyst in a model reaction. This species showed similar or even superior activities compared to well-established PTCs. Furthermore, complete recovery of the catalyst could be achieved by simple filtration caused by the thermomorphic behaviour of PE without any alteration of the compound. Due to the introduction of an additional functional group, further transformations of PE were performed resulting in e.g. a charged ATRP macroinitiator which was subsequently applied in a block copolymerization.
The synthesis of block copolymers and further modification reactions based on charged polyethylene have to be optimized in the future. Moreover, the incorporation of variable anionic compounds such as anionic plasticizers and flame retardants into charged PE might be promising. Due to strong ion–ion interactions, the phase transfer properties might be transferable to the formation of micelles in order to encapsulate anionic compounds in solution.

In this thesis, versatile and novel synthetic routes for both charged end-functional polyethylene and polyethylene modified hydrophilic as well as noble metal particles were developed resulting in highly improved and tunable surface properties based on the characteristics of PE.

7 Experimental Section

7.1 Commercially Acquired Substances

Ethylene (99.9%) and argon (99.999%) were purchased from Linde AG. Toluene (HPLC grade) was bought from Sigma-Aldrich Chemie GmbH, degassed and stored over a molecular sieve (3 Å). Butyloctylmagnesium (20 wt% in heptane) was purchased from Chemtura Europe GmbH. $AgNO_3$ (Fluka, 98%), $NdCl_3$ (99.9%) were used as received. Tetrahydrofuran (Sigma-Aldrich) was distilled over CaH_2 and stored over molecular sieve (3 Å). Phenylmethanethiol, lithium pentamethylcyclopentadienide (>98%) *N*,*N*-dimethylformamide (DMF) (p.A.), sodium citrate tribasic dihydrate (99%), methanol (99.8%), sodium borohydride (96%), dimethyldimethoxysilane, 3-aminopropyldimethylethoxysilane, dimethoxyethane, magnesium, sodium azide, lithium aluminium hydride, *meta*-chloroperbenzoic acid, potassium *tert*-butoxide, chloroform (p.A.), potassium hydroxide, aliquat 336, tosyl chloride (>98%), and hydrazine monohydrate (98%) were purchased from Sigma-Aldrich and used as received. 3-dimethylamino-1-propanol, 1-methylamino-2-ethanol, iodine (doubly sublimated), 2-bromopropionyl bromide, pyridine, tetraphenylphosphonium bromide (TPPB), n-butylacrylate, tetrabutylammonium bromide (TBAB), tetrabutylammoni um iodide (TBAI), anisole, tetraoctylammonium bromide (TOAB), octane, sodium cyanide, *N*,*N*,*N*′,*N*″,*N*″-pentamethyldiethylenetriamine (PMDETA), acetonitrile, trans-2-[3-(4-tert-butylphenyl)-2-methyl-2-propenylidene] malononitrile (DCTB), 1-bromodecane, dichloroethane (DCE), 2-(4-hydroxylphenyl-azo)benzoic acid (HABA), CuBr and methacryloyl chloride were purchased from Sigma-Aldrich and, if not stated otherwise, used without further purification. Silver and gold nanoparticles were synthesized by Wentao Peng. Palladium nanoparticles were provided by Darius Rohleder. Wood powder (70 – 150 µm) was applied after Soxhlet extraction using acetone and dichloromethane followed by drying under reduced pressure. All not mentioned chemicals and solvents were used without further purification.

7.2 Instrumentation

High-temperature size-exclusion chromatography (HT-SEC)

HT-SEC characterizations were performed using an Agilent G1888 network headspace autosampler, an Agilent 1260 pump, an Agilent 1322A degasser and a PSS 246 interface. The system contained a polefin 10 μm precolumn and three polefin separation columns (10^3 Å, 10^5 Å, 10^6 Å). The measurements were conducted at 150 °C using 1,2,4-trichlorobenzene as eluent. A two channel Q 4 IR detector for CH_2- and CH_3-signals was applied. The set up was calibrated using polyethylene references with a molecular weight between 340 g mol^{-1} and 126000 g mol^{-1}. Prior to the analysis, all samples were dissolved in 1,2,4-trichlorobenzene (3 mg/mL) at 160 °C for 1 h.

Mass spectrometry (MS)

ESI-MS-TOF analysis was conducted using a Synapt G2 HDMS (Waters Corporation) mass spectrometer either in the sensitivity or in the resolution mode. The calibration of the mass spectrometer was performed using sodium iodide in methanol (100 mg mL^{-1}). For the samples preparation of the respective PE analyte, the polymer was dissolved in dichloroethane (5 mg mL^{-1}) at 90 °C followed by cooling down the solution resulting in precipitation. The suspension was filtrated afterwards through syringe filter (0.45 μm) to obtain a saturated, homogenous solution. To this solution acetonitrile with varying volume-ratios (80 : 20; 50 : 50; 30 : 70) was added. In case of PE-N, 0.1 wt% of acetic acid was added. The respective mixture was sprayed into the mass spectrometer. The following parameters were applied: the source temperature was set to 120 °C, the capillary voltage was 5.0 kV with a offset voltage = 80 V and a cone voltage = 40 V. A desolvation temperature of 150 °C was used and the scan time was set to 0.5 s. Each discussed spectrum is the sum of 120 scans.
MALDI-MS-TOF measurements were carried out on an autoflex speed mass spectrometer in the reflection mode. The applied matrices were DCTB and HABA. The sample preparations were performed by mixing a solution of the respective matrix in THF (40 mg mL^{-1}) and a dispersion of polyethylene in toluene (5 mg mL^{-1}) (ratio = 4 : 1). PE-N was pretreated

with 0.5 wt% of acetic acid. The obtained mixtures (1 µL) were spotted on a stainless-steel target plate. The calibration of the MALDI mass spectrometer was performed using poly(methyl methacrylate) (PMMA) with a determined molecular mass and detected as a sodium adduct-species. The laser energy was adjusted for each sample individually. Each presented spectrum is the sum of 500 laser shots without any editing of the obtained date.

Nuclear magnetic resonance (NMR) spectroscopy

^{1}H-NMR spectra were recorded using a Varian Unity 300 spectrometer (300 MHz). The measurements were conducted at 80 °C using toluene-d8 as solvent. The determined chemical shifts (δ /ppm) were referenced to an internal standard corresponded to the residual of the solvent signal.

Scanning electron microscopy (SEM)

The measurement was conducted by Volker Radisch. Scanning electron microscopy (SEM) was performed on a Typ FEI Nova NanoSEM 650 microscope at an operating voltage of 2 kV. Prior the measurement, the samples were coated with nanocarbon film.

Thermogravimetric analysis (TGA)

Thermogravimetric analyses (TGA) were conducted using a Netzsch TG 209 F3 Tarsus. The measurements were performed in a temperature range from 25 °C to 1000 °C with a heating rate of 10 K min^{-1} under a constant nitrogen flow (10 mL min^{-1}).

Water contact angle (WCA)

The water contact angle analysis was performed with an OCA 15EC (OCA Measuring Instruments) using a TBO Video-based system (Dataphysics). The sample was treated with a water drop (2 µL) at variable spots on the respective surface. The wood particles were pressed into a pellet to achieve a flat surface.

Dynamic light scattering (DLS)

Dynamic light scattering was conducted on a Malvern Zetasizer NanoS set up, equipped with a He–Ne laser with a wavelength of λ = 633 nm. All samples were diluted in toluene, measured in a quart cuvette (10 mm) at 25 °C or heated to 90 °C and rested for at least 1 h prior to the analysis. A scattering angle of 173° was applied and the intensity distributions were recorded with 12 runs with duration time of 20 s per measurement.

Differential scanning calorimetry (DSC)

Differential scanning calorimetry was conducted using a DS-calorimeter Mettler Toledo DSC820 set up in combination with a cryostat (Lauda Ultra-Kryomat® RUK 90). All measurements were performed in an aluminum pan with a heating rate of 10 K min^{-1} in a temperature range between 25 °C and 200 °C under a constant nitrogen flow. The analysis was performed based on the second heating process.

Attenuated total reflection-FTIR (ATR-FTIR)

ATR-FTIR measurements were performed using a Bruker IFS88 spectrometer in combination with a Harrick MVP 2 StarTM ATR set up. In addition, the system contains a halogen lamp, a KBr beam splitter and a mercury cadmium telluride detector. The discussed spectra are an average of 32 scans in the range of 750 to 4000 cm^{-1}.

Dynamic vapor sorption (DVS)

The sorption/desorption analysis of unfunctionalized and PE-modified wood was kindly conducted by Lukas Emmerich under isothermic conditions at 20 °C using a surface measurement system. The relative humidity was increased stepwise starting from 0 % to 5 up to 95 % in 10 % steps. Afterwards the relative humidity was decreased from 95 % to 0 % in the same procedure. Between each datapoint the sample was rested until a constant weight was achieved.

Transmission electron microscopy (TEM)

The TEM analysis was conducted on a Philips CM 12 transmission electron microscope equipped with an Olympus CCD-camera (1376 × 1032 pixel). An acceleration voltage of 120 kV was applied. A 50 µm aperture in the condenser lens was used, while scattered electrons were blocked with a 20 µm aperture. The sample preparation was performed by drop-casting (90 °C in toluene) on a Plano 200 mesh copper grid holding an amorphous carbon film. To ensure a slow evaporation of the solvent, the grid was immediately covered with a glass cup.

Ultraviolet-visible spectroscopy (UV-vis)

For UV-vis analysis, a Cary 300 scan photospectrometer was employed. The spectra were recorded with a scan rate of 150 nm min^{-1} in a range of $\lambda = 250 - 800$ nm. The measurements were conducted in Hellma quartz cuvettes (path length: 10 mm) with varying temperatures (25 to 90 °C). The baseline correction was performed by subtraction of the pure dispersant spectrum.

7.3 Synthesis

Synthesis of $(C_5Me_5)_2NdCl_2Li(OEt)_2$

The precatalyst was synthesized in comparison to literature.[183] Briefly, a dispersion of $NdCl_3$ (1 eq.) and lithium pentamethylcyclopentadiende (2 eq.) in dry and degassed THF was refluxed for 12 h under an argon atmosphere. The solvent was removed in vacuum and the residual was extracted with dry and degassed diethyl ether. Removing of the diethyl ether under reduced pressure yielded the product as blue crystals.

Synthesis of bis(benzylsulfinyl thiocarbonyl)-disulfide

The synthesis was performed comparably as reported in literature.[184] A solution of phenylmethanethiol (1 eq.), potassium hydroxide (1.3 eq.), aliquat 336 (0.1 eq.), and carbon disulphide (1 eq.) in water was added dropwise at −5 °C to tosyl chloride (0,5 eq.), aliquat 336 (0.1 eq.) in

dichloromethane. The reaction mixture was stirred for 1 h and extracted subsequently with dichloromethane. The obtained yellow organic phase was washed with an aqueous solution of $NaHCO_3$ followed by water. After removing the solvent under reduced pressure, the residual was recrystalized from acetone yielding bis(benzylsulfinyl thiocarbonyl)-disulfide as yellow crystals. The product was immediately used for further reactions.

Activation of magnesium

Magnesium was activated in four different methods. All reactions were performed under an argon atmosphere using dry and degassed reagents.

a) In a typical experiment, magnesium pellets were heated under reduced pressure under vigorous stirring while heating using a hot-air blower for 4 h.
b) Magnesium pellets were treated carefully with diluted hydrochloride acid, filtered and immediately transferred into a schlenk flask followed by heating the pellets under reduced pressure as described in procedure a.
c) A small amount of dibromoethane was added to the pretreated magnesium pellets as described in procedure a.
d) Another method is the synthesis of fine-dispersed magnesium in a method reported by *Rieke* et al.[159] Dry magnesium(II)bromide was reacted with lithium in dry THF for 24 h under stirring. The fine dispersed black magnesium particles were immediately used for further reactions and had to be with special care due to its pyrophoric behaviour.

Synthesis of PE-N^+–MO

PE-N^+ (100 mg) was dissolved in toluene at 90 °C for 1 h. A diluted aqueous solution of methyl orange was added carefully, and the resulted two-phase system was heated to 90 °C. The obtained orange coloured organic phase was carefully pipetted and dried under reduced pressure. As a blank sample, this procedure was performed using unfunctionalized polyethylene in combination with tetraphenylphosphonium bromide and treated under the same conditions.

Synthesis of 1-cyanodecane via phase transfer catalysis

In a typical experiment, 1-bromodecane (1.0 eq.) in octane (~0.7 M) was mixed with fresh-prepared solution of sodium cyanide (4.0 eq.) in water (~2.7 M). The respective phase transfer catalyst (for details see chapter 5.4.2) was added and the solution was heated to 110 °C. After cooling the solution to room temperature, the organic phase was separated and dried under reduced pressure. For ^{1}H-NMR spectra of the respective product see Appendix C.

7.3.1 Polymer Synthesis

Synthesis of iodo end-functionalized polyethylene (PE-I)

The synthesis of iodo end-functionalized polyethylene was conducted in a typical CCG procedure in comparison to literature.[15] The polymerization of ethylene was carried out in a *Büchi* glass reactor (500 mL) connected to an ethylene feedstock at 80 °C. The reactor was filled with 400 mL dry toluene, degassed using a vacuum pump. Afterwards the solution was immediately saturated by the addition of gaseous ethylene with a constant pressure of 2.5 bar. Butyloctylmagnesium (Bomag) and the neodymium catalyst in toluene ([Mg] : [Nd] = 200 : 1) were added and the polymerization was conducted for 4 h or until precipitation was observed at 80 °C. The ethylene gas-phase was substituted with argon and iodine in THF (10 wt%, 5 eq. per [Mg]) was added directly by parallelly cooling down the mixture to 10 °C. The obtained yellow to brown solution was stirred for 12 h. The resulting polymer was precipitated in methanol, filtered and washed several times with methanol until the excess of iodine was removed. The collected polymer was dried under reduced pressure at 70 °C for 18 h. The iodo end-group functionality was determined by ^{1}H-NMR. For detailed discussions, ^{1}H-NMR spectra and HT-SEC analyses see chapter 3.2.1 and 5.2.

Synthesis of azide terminated PE (PE-N_3)

In a typical experiment,[15] a mixture of PE-I (1.0 eq.) and sodium azide (5 eq.) in water and DMF (1:1) was heated to 150 °C. The solution was stirred for 18 h. After cooling to room temperature, ethanol was added, the polymer was filtered and washed at least three times with ethanol. Afterwards, the polymer was dried under reduced pressure for 24 h at 60 °C.

Synthesis of amine terminated PE (PE-NH_2)

In variation to literature, PE-N_3 (1 eq.) was dissolved in dry toluene at 90 °C for 1 h.[15]A suspension of $LiAlH_4$ (10 eq.) in dry THF was added and the mixture was heated to 90 °C and stirred for 4 h. Afterwards, the reaction was cooled down to room temperature and the excess of $LiAlH_4$ was carefully quenched by the dropwise addition of methanol. The polymer was purified as described above.

Synthesis of vinylic terminated PE (PE_{vin})

A solution of PE-I (1 eq.) in dry and degassed toluene (2.5 wt%) was mixed with a suspension of ^{t}BuOK (10 eq.) in dry and degassed THF (1 M). The mixture was heated to 90 °C and stirred for 15 h. The solution was cooled to room temperature, methanol was added, and the precipitated polymer was filtered. After washing with methanol (three times), the recovered polymer was dried under reduced pressure.[150]

Synthesis of epoxide terminated PE (PE_{epo})

In accordance to literature, a solution of vinyl terminated PE (1 eq.) was dissolved in toluene (5 wt%) at 80 °C for 1 h. *m*-CPBA (8 eq.) was added dropwise and the solution was stirred for 2.5 h. The obtained solution was precipitated in methanol, filtered and washed five times with methanol. Drying under reduced pressure yielded epoxide terminated PE.[147]

Synthesis of trithiocarbonate terminated PE (PE_{TTC})

In adaption to a procedure described for PE-I and in literature for comparable compounds,[97] the polymerization of ethylene was performed in a 500 mL glass reactor at 80 °C. The reactor was filled with 400 mL dry toluene, degassed by a vacuum pump and saturated with ethylene with a constant pressure (2.5 bar). Bomag and $[(cp^*)_2NdCl_2Li(OEt_2)_2]$ in toluene ([Mg] : [Nd] = 200 : 1) were added and the polymerization was conducted until precipitation occurred. Afterwards, ethylene was removed and bis(benzylsulfinyl thiocarbonyl)disulfide (10 eq. per [Mg]) in dry THF was added immediately. After 8 h at 80 °C, the reaction mixture was cooled to room temperature and the polymer was precipitated, filtered and washed several times with methanol. The collected polymer was dried under reduced pressure at 60 °C for 18 h.

Synthesis of polyethylenethiol (PE-SH)

PE_{TTC} (1 eq.) and hydrazine monohydrate (20 eq.) were dissolved in toluene and DMF (1:1) at 100 °C. The reaction was stirred for 20 h followed by cooling down to room temperature. The polymer was precipitated in methanol, filtered, washed several times with methanol and dried under reduced pressure at 60 °C for 16 h.

Synthesis of ammonium and tertiary amine functionalized polyethylene ($PE\text{-}N^+$, PE-N, $PE\text{-}N_6^+$)

In a typical experiment, polyethylene iodide (1.0 eq.) was dissolved in toluene (10 wt%) at 90 °C. An excess (> 3.0 eq.) of the respective amine (3-dimethylamino-1-propanol, 1-methylamino-2-ethanol or 1-dimethyl-aminohexanol) was added and the solution was stirred for 72 h at 90 °C. The solution was cooled down to room temperature, filtered and the polymer was washed 5 times with methanol. The polymer was dried under reduced pressure at 70 °C for 18 h. For detailed discussion and analysis and see chapter 5.2.

Synthesis of PE-N^+_{RAFT}

The synthesis of PE-N^+_{RAFT} was conducted in two approaches. For a detailed discussion and analysis see chapter 5.5.1.

a) PE-I was dissolved in toluene and DMF (1 eq., 10 wt%) at 90 °C. To the solution the amine bearing RAFT agent (see chapter 5.5.1) was added (8 eq.) and the mixture was stirred for 48 h. The mixture was cooled down, methanol was added and filtered. The collected polymer was washed with methanol and acetone and dried under reduced pressure for 16 h at 60 °C.
b) PE-N^+ (1 eq.), DCC (5 eq.), 4-DMAP (0.1 eq.) and the carboxyl bearing RAFT-agent (5 eq., for structure see chapter 5.5.1) were dissolved in toluene and DMF (1 : 1) at 90 °C. The solution was stirred for 48 h followed by purification described in procedure a.

Synthesis of PE-N^+_{ATRP} and PE-N^+_{MA}

In a typical experiment, the PE-N^+ was dissolved in dry and degassed toluene (1.0 eq., 10 wt%) at 80 °C followed by the addition of either triethylamine or pyridine (1.5 eq., dry and degassed). Afterwards, 2-bromopropionyl bromide (for PE-N^+_{ATRP}) or methacryloyl chloride (for PE-N^+_{MA}) (at least 5.0 eq.) was added dropwise over a period of 30 min. The reaction was stirred at 90 °C for 2 h, cooled down and carefully quenched with methanol. The precipitated polymer was filtered, washed several times with methanol and dried under reduced pressure at 70 °C for 18 h. For detailed discussions and analyses see chapter 5.5.2.

ATRP block copolymerization using PE-N^+_{ATRP} and *n*-BA

PE-N^+_{ATRP} (1.0 eq.) was dissolved in dry toluene (10 wt% of the macroinitiator), dry anisole (1.0 eq.) and PMDETA (1.0 eq.) as well as CuBr (1.0 eq.) was added. The resulting mixture was degassed with argon followed by the addition of dry and degassed *n*-butylacrylate (100 eq.). The solution was heated to 100 °C in a heating block under vigorous shaking. After 4 h, the solution was cooled down, precipitated in methanol and filtered. The precipitate was redissolved in toluene at 90 °C, precipitated again in cold methanol, filtered and washed several times with methanol and diluted hydrochloric acid. The resulted adhesive

polymer was dried under reduced pressure at 70 °C for 18 h. For a detailed description and HT-SEC analysis see chapter 5.5.2.

7.3.2 Prefunctionalization and Polyethylene Modification of Surfaces

Wood pretreatment

Wood particles were extracted using DCM and toluene in a Soxhlet procedure for 18 h. Afterwards the particles were dried under reduced pressure. In an additional step, the particles dispersed in an aqueous solution of sodium hydride for 2 h followed by filtration and dying under reduced pressure.

Alkyne prefunctionalized wood

A procedure described in literature for comparable substrates was transferred to the applied system and varied.[151] Wood particles (1 g) were dispersed in an aqueous sodium hydroxide solution (1.5 wt % NaOH) for 2 h at 25 °C. Afterwards the dispersion was heating slowly to 60 °C followed by the addition of propargyl bromide (10 g, 80 wt% in toluene). The resulting mixture was stirred for 24 h at 60 °C. The reaction solution was cooled to room temperature, filtered and the wood particles were washed three times with IPA, water : IPA (1 : 1) and H_2O subsequently and dried under reduced pressure at 60 °C for 24 h.

Carboxyl prefunctionalized wood

Pretreated wood particles were dispersed in DMF (20 mL) followed by the addition of succinic anhydride (2 g) and pyridine (1 mL) and the mixture was stirred for 16 h at room temperature. The particles were filtered, washed with acetone and methanol and dried under reduced pressure at 70 °C.

PE modified wood particles via click-chemistry

In a typical experiment, alkyne functionalized wood particles (0.5 g), PE-N_3 (1 g, 1 eq.), CuBr (0.06 g, 0.6 eq.) and PMDETA (0.08 g, 0.6 eq.) were mixed in a glove box. Dry and degassed toluene (40 mL) and DMF (20 mL) were added and the mixture was heated to 120 °C for 3 d. After hot filtration the particles were redispersed in boiling toluene and filtered again. This procedure was repeated 10 times. Otherwise or in combination, the particles were extracted using a Soxhlet apparatus with boiling xylene. After the excess of PE was removed (confirmed by ^{1}H-NMR of the filtrate), the particles were washed with diluted hydrochloric acid followed by H_2O and methanol subsequently. The particles were dried under reduced pressure at 80 °C. For a detailed discussion see chapter 3.2.2 and 3.3.

PE modified wood particles via esterification

In a typical esterification reaction, carboxyl functionalized wood particles (0.5 g), PE-NH_2 (1 g), DCC (0.3 g), DMAP (0.05 g) were mixed in toluene and DMF (1 : 1, 20 mL) and stirred for 3 d at 100 °C. The purification was performed as described for the synthetic route via click-chemistry.

PE modified wood particles via nucleophilic substitution or ring opening reactions

The pretreated wood particles (1 g) and either PE-I or PE_{epo} (1 g) were mixed in toluene and DMF (1 : 1, 20 mL), followed by heating to 100 °C and stirring for 3 d. The work-up was performed as described before.

Synthesis of silica nanoparticles

SiNPs were synthesized in a typical *Stöber*-process.[157] A mixture of methanol (400 mL), ethanol (400 mL), aqueous ammonia (30%, 22.4 mL), water (20.2 mL) and tetraorthosilicate (25.2 mL) was stirred for 24 h at room temperature. After removing the solvent under reduced pressure, the obtained silica NPs were directly used for further reactions.

Polyethylene modified SiNPs in grafting-from approach

The applied synthesis is described in detail in chapter 3.4.2. The applied grafting-from approach is a multiple step reaction.

1) The respective silanol bearing anchor-group (linker length = 3 or 12) (0.8 g) was dissolved in THF followed by the addition of fresh-prepared SiNPs (1 g) and refluxed for 18 h. The mixture was diluted with hexane and centrifugated followed by three additional centrifugation/redispersion cycles using acetone.
2) The particles were dispersed in dry and degassed toluene under an argon atmosphere and dichlorodimethylsilane was added. The mixture was refluxed for 12 h before the solvents were removed under reduced pressure using a *Schlenk* apparatus. The flask was filled using argon and immediately used for the next reaction step.
3) Dry and degassed dimethoxyethane and diethyl ether were added carefully. Afterwards a suspension of fresh activated magnesium in diethyl ether was added. The resulting mixture was heated subsequently to reflux and stirred for varying reaction times (1 h to 3 d)
4) The cooled dispersion was treated with 1,4-dioxane (0.1 mL) and the dispersion was stirred for 2 h. Afterwards, the excess of magnesium was allowed to settle down, and the resulting SiNP dispersion was transferred under an argon atmosphere into the next step.
5) The suspension was transferred into the *Büchi* reactor, followed by the addition of toluene (250 mL) and a typical polymerization procedure was conducted as described for PE-I. Afterwards the reaction was quenched with EtOH and the particles were purified by centrifugation/redispersion cycles. In additional purification step, the particles were washed with boiling toluene.
6) To separate the particles from covalently bounded PE, the particles were dissolved in a solution of HF and acetone for 2 d followed by evaporation of the solvent.

PE modified SiNPs in a grafting-to approach

The respective silanol bearing anchor group (end-group = methacrylate, iodine, carboxylate, 0.3 g) was dissolved in dry THF (10 mL), added to silica particles (1 g) in dry THF (10 mL) and stirred over-night under slightly reflux conditions under an argon atmosphere. Afterwards the reaction mixture was diluted with hexane (100 mL) and centrifugated. After three centrifugation/redispersion (using acetone) cycles, the modified particles were reacted with the functionalized PE:

a) The acrylate modified silica (0.25 g) and PE-SH (0.04 g) were dried and dispersed in toluene and DMF (1 : 1, 5 mL) under argon atmosphere. Octadecylamine (0.05 g) was added and the reaction was stirred for three days at 90 °C. The reaction mixture was dissoluted with toluene at 90 °C and the particles were allowed to settle down. The solvent was removed carefully from the particles using a pipette to remove the excess of the polymer. This procedure was repeated at least ten times until all polymer was separated (confirmed by ^{1}H-NMR analysis of the filtrate).
b) The amine functionalized silica NPs (0.25 g) and PE-I (0.05 g) were dispersed in toluene and DMF (1 : 1, 5 mL). The mixture was stirred at reflux for 3 d followed by a work-up as described for a.
c) Carboxyl prefunctionalized SiNPs (0.25 g) and PE-NH_2 (0.05 g) were dispersed in toluene and DMF (1 : 1, 5 mL). DCC (0.05 g) and 4-DMAP (0.01 g) were added and the reaction was refluxed for 3 d followed by purification as described before.

Preparation of polyethylene grafted AuNPs, PdNPs or AgNPs

For detailed discussion see chapter 4.2.2. Briefly, either PE$_{TTC}$ or PE-SH (2 mg) were dissolved in toluene (1 mL) at 90 °C for 1 h. To this solution, a dispersion of silver-, palladium- or gold-nanoparticles in toluene (2 mL, c = 2 mg/mL) at 90 °C was added, respectively. The mixture was stirred for 30 min at 90 °C. The resulting dispersion was used without special purification for analysis and further experiments.

8 Appendices

Appendix A

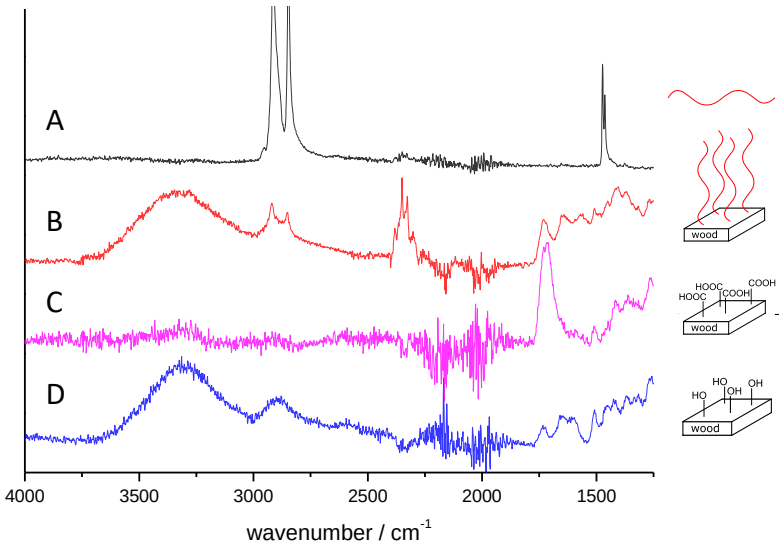

ATR-IR characterization of polyethylene (A), PE⊚wood synthesized via an amide-coupling reaction (B), carboxyl prefunctionalized wood (D) and unfunctionalized wood (D).

Appendix B

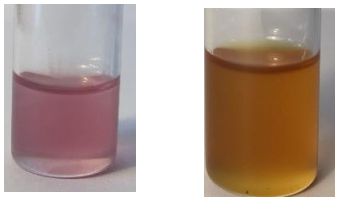

AuNP@PE and AgNP@PE after dissolution at 90 °C and cooling down to room-temperature.

Appendix C

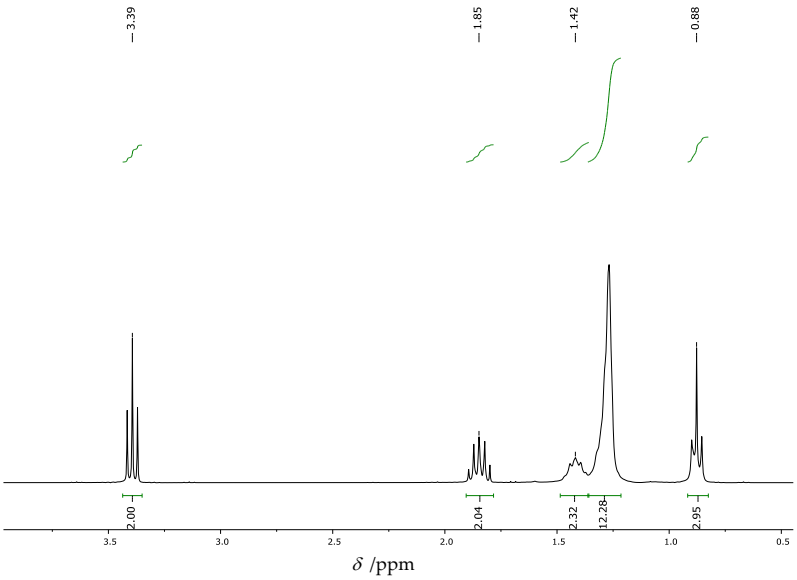

^{1}H-NMR spectrum of the conversion of bromodecane with sodium cyanide without any PTC (blank sample).

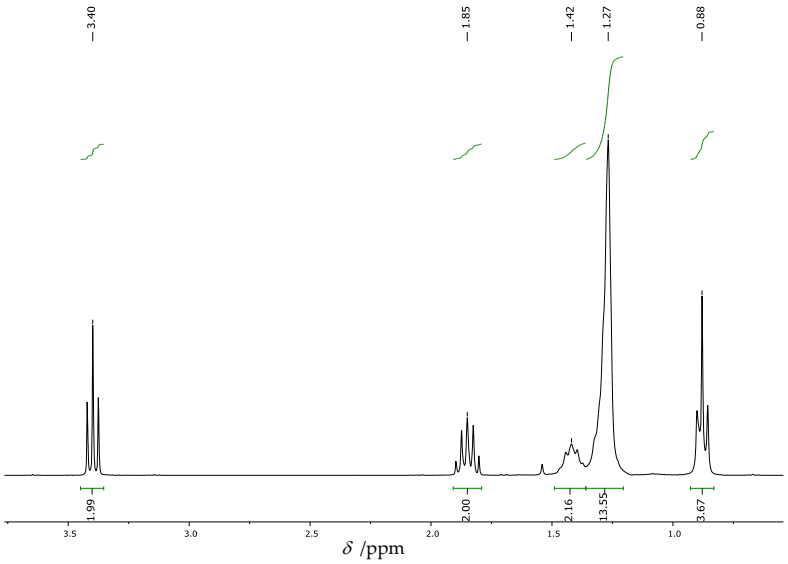

^{1}H-NMR spectrum of the conversion of bromodecane with sodium cyanide using TPPB.

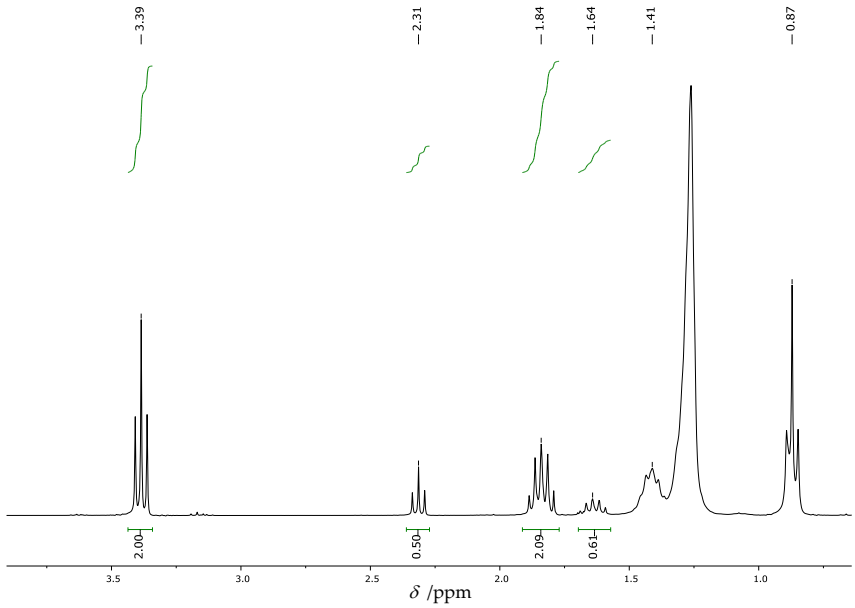

^{1}H-NMR spectrum of the conversion of bromodecane with sodium cyanide using PE-N^{+} after 4 h.

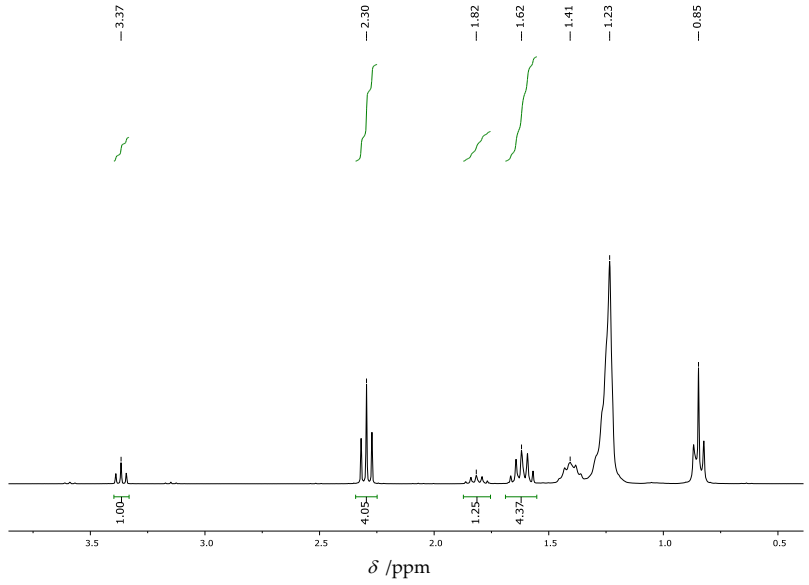

^{1}H-NMR spectrum of the conversion of bromodecane with sodium cyanide using PE-N^{+} after 18 h.

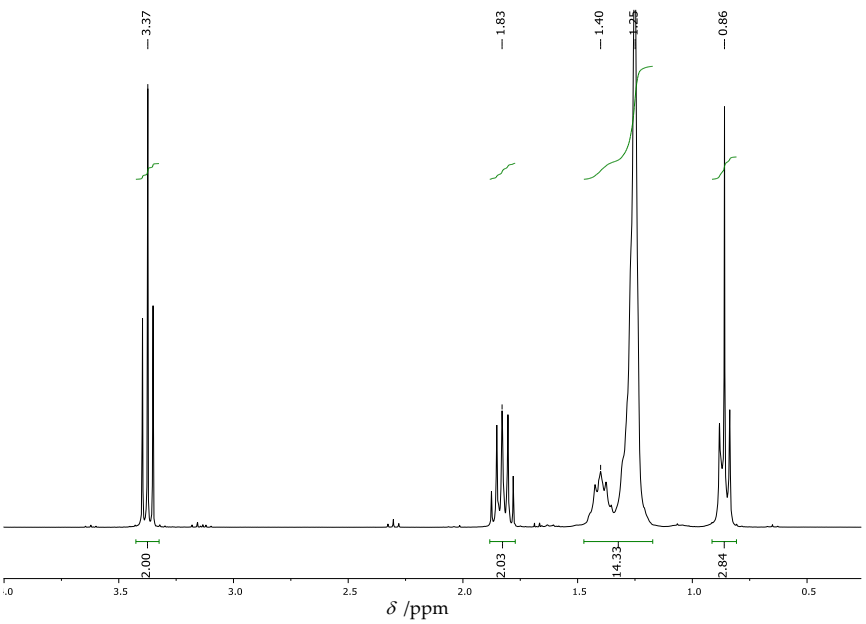

^{1}H-NMR spectrum of the conversion of bromodecane with sodium cyanide using TBAB.

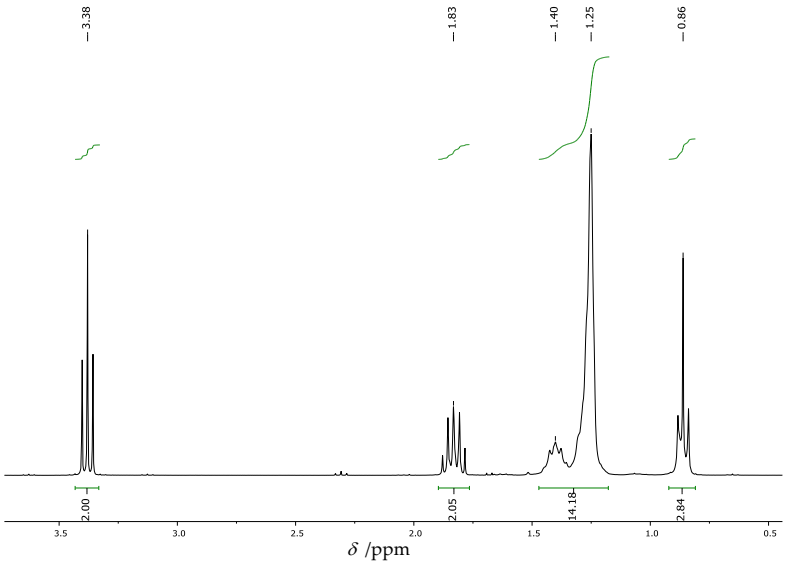

^{1}H-NMR spectrum of the conversion of bromodecane with sodium cyanide using TBAI.

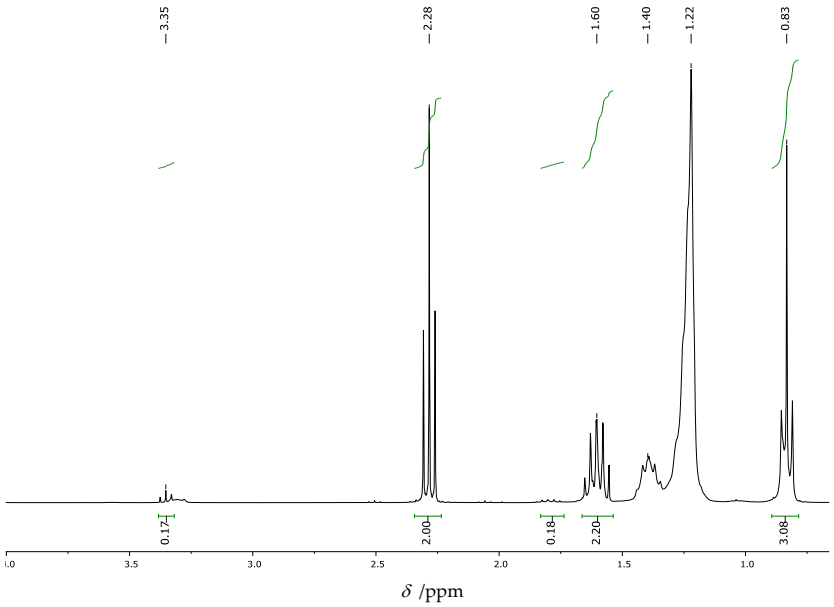

^{1}H-NMR spectrum of the conversion of bromodecane with sodium cyanide using TOAB.

Appendix D

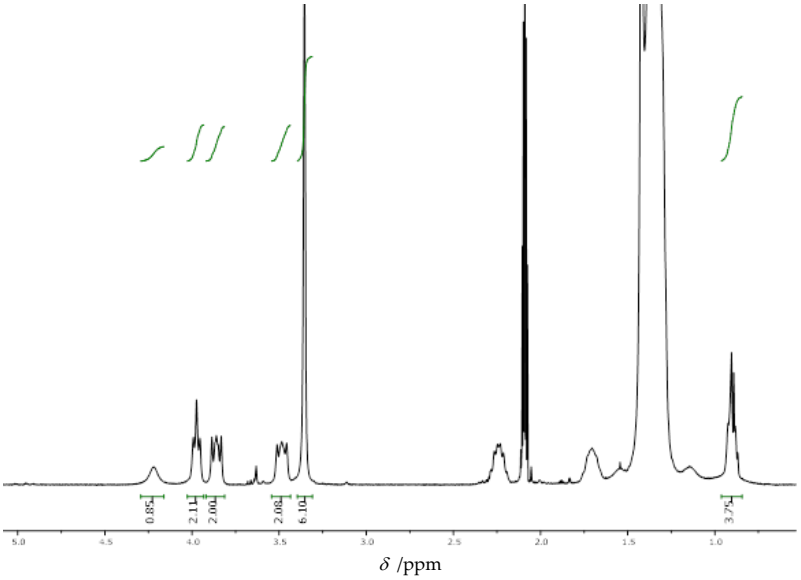

^{1}H-NMR spectrum of PE-N$^+$ after the model nucleophilic-substitution reaction.

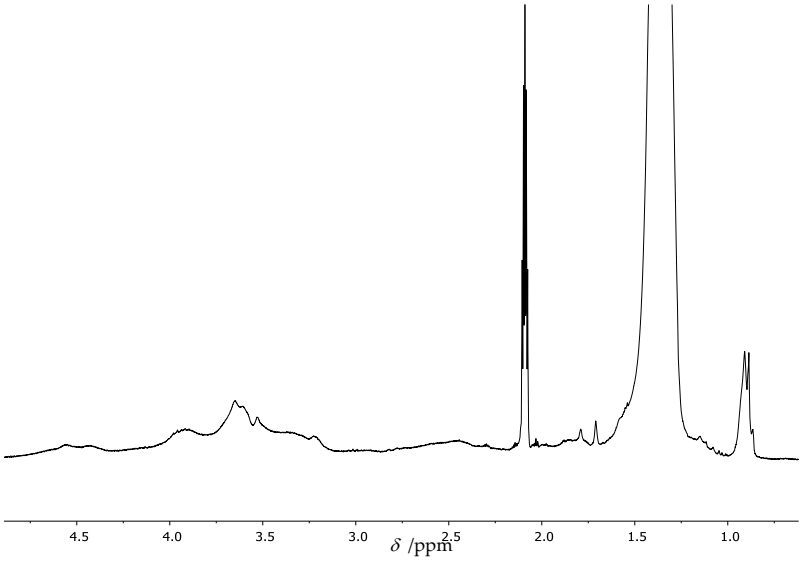

^{1}H-NMR spectrum of the esterification reaction based on PE-N$_6^+$.

Abbreviations

AgNP	Silver nanoparticle
ATR	Attenuated total reflection
ATRP	Atom transfer radical polymerization
AuNP	Gold nanoparticle
BA	*n*-butyl acrylate
Bomag	Butyloctylmagnesium
CCG	Catalyzed chain growth
CCTP	Coordinative chain transfer polymerization
CTA	Chain transfer agent
δ	Chemical shift
$Đ$	Dispersity
DCC	*N*,*N*'-Dicyclohexylcarbodiimide
DCE	1,2-Dichloroethane
DCTB	Trans-2-[3-(4-tert-butylphenyl)-2-methyl-2-propenylidene]
DLS	Dynamic light scattering
DMAP	4-Dimethylaminopyridine
DMF	Dimethylformamide
DSC	Differential scanning calorimetry
DVS	Dynamic vapor sorption
EMC	Equilibrium moisture content
ESI	Electrospray ionization
FTIR	Fourier-transform infrared spectroscopy
HABA	2-(4-hydroxylphenyl-azo)benzoic acid
HDPE	High-density polyethylene
HT-SEC	High-temperature size-exclusion chromatography
λ	Wavelength
LDPE	Low-density polyethylene
m/*z*	mass-to-charge
MA	Maleic anhydride
MALDI	Matrix-assisted laser desorption/ionization
MAO	Methylaluminoxane
m-CPBA	*meta*-Chloroperoxybenzoic acid

$\bar{M}_n$	Number average molar mass
MO	Methyl organge
M_p	Peak maximum molar mass
MS	Mass spectrometry
$\bar{M}_w$	Mass average molar mass
NMR	Nuclear magnetic resonance spectroscopy
NP	Nanoparticle
PBA	Poly(butyl acrylate)
PdNP	Palladium nanoparticle
PE	Polyethylene
PE-I	Iodo end-functional polyethylene
PE-N_3	Azide end-functional polyethylene
PE-NH_2	Amine end-functional polyethylene
PE_{vin}	Vinylic end-functional polyethylene
PE_{epo}	Epoxy end-functional polyethylene
PE-SH	Thiol end-functional polyethylene
PE_{TTC}	Trithiocarbonate end-functional polyethylene
PE-N	Temporary charged polyethylene
PE-N^+	Permanent charged polyethylene
PMDETA	*N*,*N*,*N*′,*N*′′,*N*′′-pentamethyldiethylenetriamine
ppm	Parts per million
PTC	Phase transfer catalyst
RAFT	Reversible addition-fragmentation chain transfer
SEM	Scanning electron microscopy
SiNP	Silica nanoparticle
TBAB	Tetrabutylammonium bromide
TBAI	Tetrabutylammonium iodide
TEM	Transmission electron microscopy
TGA	Thermogravimetric analysis
THF	Tetrahydrofuran
TOAB	Tetraoctylammonium bromide
TOF	Time of flight
TPPB	tetraphenylphosphonium bromide

TTC	Trithiocarbonyl
UV-vis	Ultraviolet–visible spectroscopy
WCA	Water contact angle
$wood_{alk}$	Alkyne modified wood
$wood_{carbo}$	Carboxyl modified wood
WPC	Wood-plastic composite

9 References

(1) Sauter, D. W.; Taoufik, M.; Boisson, C. Polyolefins, a Success Story. *Polymers* **2017**, *9*, 185.

(2) Seymour, R. B.; Cheng, T. *Advances in Polyolefins: The World's Most Widely used Polymers*, 1st ed.; Springer: Boston, MA, 1987.

(3) Echte, A. *Handbuch der Technischen Polymerchemie*; Wiley-VCH: Weinheim, 1993.

(4) Ziegler, K. Folgen und Werdegang einer Erfindung (Nobel-Vortrag). *Angew. Chem.* **1964**, *76*, 545–553.

(5) Tabone, M. D.; Cregg, J. J.; Beckman, E. J.; Landis, A. E. Sustainability Metrics: Life Cycle Assessment and Green Design in Polymers. *Environ. Sci. Technol.* **2010**, *44*, 8264–8269.

(6) Baier, M. C.; Zuideveld, M. A.; Mecking, S. Post-Metallocenes in the Industrial Production of Polyolefins. *Angew. Chem. Int. Ed.* **2014**, *53*, 9722–9744.

(7) Aggarwal, S. L.; Sweeting, O. J. Polyethylene: Preparation, Structure, and Properties. *Chem. Rev.* **1957**, *57*, 665–742.

(8) Tieke, B. *Makromolekulare Chemie: Eine Einführung*, 2nd ed.; Wiley-VCH: Weinheim, 2012.

(9) Hoogenboom, R. Temperature-Responsive Polymers: Properties, Synthesis and Applications. *Smart Polymers and their Applications*; pp 15–44.

(10) Bergbreiter, D. E.; Hobbs, C.; Hongfa, C. Polyolefin-Supported Recoverable/Reusable Cr(III)-Salen Catalysts. *J. Org. Chem.* **2011**, *76*, 523–533.

(11) Romanenko, I.; Norsic, S.; Veyre, L.; Sayah, R.; D'Agosto, F.; Raynaud, J.; Boisson, C.; Lacôte, E.; Thieuleux, C. Active and Recyclable Polyethylene-Supported Iridium-(N-Heterocyclic Carbene) Catalyst for Hydrogen/Deuterium Exchange Reactions. *Adv. Synth. Catal.* **2016**, *358*, 2317–2323.

(12) Gibson, V. C. Shuttling Polyolefins to a New Materials Dimension. *Science* **2006**, *312*, 703–704.

(13) Valente, A.; Mortreux, A.; Visseaux, M.; Zinck, P. Coordinative Chain Transfer Polymerization. *Chem. Rev.* **2013**, *113*, 3836–3857.

(14) Mazzolini, J.; Espinosa, E.; D'Agosto, F.; Boisson, C. Catalyzed chain growth (CCG) on a Main Group Metal: An Efficient Tool to Functionalize Polyethylene. *Polym. Chem.* **2010**, *1*, 793.
(15) Briquel, R.; Mazzolini, J.; Le Bris, T.; Boyron, O.; Boisson, F.; Delolme, F.; D'Agosto, F.; Boisson, C.; Spitz, R. Polyethylene Building Blocks by Catalyzed Chain Growth and Efficient End Functionalization Strategies, including Click Chemistry. *Angew. Chem. Int. Ed.* **2008**, *47*, 9311–9313.
(16) Kaneyoshi, H.; Inoue, Y.; Matyjaszewski, K. Synthesis of Block and Graft Copolymers with Linear Polyethylene Segments by Combination of Degenerative Transfer Coordination Polymerization and Atom Transfer Radical Polymerization. *Macromolecules* **2005**, *38*, 5425–5435.
(17) Nzahou, O. W.; Norsic, S.; D'Agosto, F.; Boisson, C. Monofunctional and Telechelic Polyethylenes Carrying Phosphonic Acid End Groups. *Macromol. Rapid Commun.* **2018**, 1800154.
(18) German, I.; Kelhifi, W.; Norsic, S.; Boisson, C.; D'Agosto, F. Telechelic Polyethylene from Catalyzed Chain-Growth Polymerization. *Angew. Chem. Int. Ed.* **2013**, *52*, 3438–3441.
(19) Hanton, S. D. Mass Spectrometry of Polymers and Polymer Surfaces. *Chem. Rev.* **2001**, *101*, 527–570.
(20) Gruendling, T.; Weidner, S.; Falkenhagen, J.; Barner-Kowollik, C. Mass Spectrometry in Polymer Chemistry: A State-of-the-Art Up-Date. *Polym. Chem.* **2010**, *1*, 599.
(21) Bauer, B. J.; Wallace, W. E.; Fanconi, B. M.; Guttman, C. M. "Covalent Cationization Method" for the Analysis of Polyethylene by Mass Spectrometry. *Polymer* **2001**, *42*, 9949–9953.
(22) Ebeling, B.; Ehlers, F.; Vana, P. Oberflächen nach Maß. *Nachr. Chem.* **2014**, *62*, 24–28.
(23) Ottersbach, P.; Schmitz, C.; Averdung, J.; Heinrich, L.; Gutsch, A. Von der Höhlenmalerei zur Schlüsseltechnologie: Nanoanwendung: Enormes Wirtschaftliches Potenzial. *Chem. unserer Zeit* **2005**, *39*, 54–59.
(24) Radhakrishnan, B.; Ranjan, R.; Brittain, W. J. Surface Initiated Polymerizations from Silica Nanoparticles. *Soft Matter* **2006**, *2*, 386.
(25) Kaseem, M.; Hamad, K.; Deri, F.; Ko, Y. G. Material Properties of Polyethylene/Wood Composites: A Review of Recent Works. *Polym. Sci. Ser. A* **2015**, *57*, 689–703.

(26) Tajvidi, M.; Najafi, S. K.; Shekaraby, M. M.; Motiee, N. Effect of Chemical Reagents on the Mechanical Properties of Natural Fiber Polypropylene Composites. *Polym. Compos.* **2006**, *27*, 563–569.
(27) Hullmann, A. Who is Winning the Global Nanorace? *Nat. Nanotech.* **2006**, *1*, 81–83.
(28) Sabella, S.; Brunetti, V.; Vecchio, G.; Galeone, A.; Maiorano, G.; Cingolani, R.; Pompa, P. P. Toxicity of Citrate-Capped AuNPs: An in Vitro and in Vivo Assessment. *J. Nanoparticle Res.* **2011**, *13*, 6821–6835.
(29) Li, W.-R.; Xie, X.-B.; Shi, Q.-S.; Zeng, H.-Y.; Ou-Yang, Y.-S.; Chen, Y.-B. Antibacterial Activity and Mechanism of Silver Nanoparticles on Escherichia Coli. *Appl. Microbiol. Biotechnol.* **2010**, *85*, 1115–1122.
(30) Tran, Q. H.; van Nguyen, Q.; Le, A.-T. Silver Nanoparticles: Synthesis, Properties, Toxicology, Applications and Perspectives. *Adv. Nat. Sci: Nanosci. Nanotechnol.* **2013**, *4*, 33001.
(31) Zeng, S.; Yong, K.-T.; Roy, I.; Dinh, X.-Q.; Yu, X.; Luan, F. A Review on Functionalized Gold Nanoparticles for Biosensing Applications. *Plasmonics* **2011**, *6*, 491–506.
(32) Dirix, Y.; Darribère, C.; Heffels, W.; Bastiaansen, C.; Caseri, W.; Smith, P. Optically Anisotropic Polyethylene–Gold Nanocomposites. *Appl. Opt.* **1999**, *38*, 6581.
(33) Milner, S. T. Polymer Brushes. *Science* **1991**, *251*, 905–914.
(34) Bieligmeyer, M.; Taheri, S. M.; German, I.; Boisson, C.; Probst, C.; Milius, W.; Altstädt, V.; Breu, J.; Schmidt, H.-W.; D'Agosto, F. *et al.* Completely Miscible Polyethylene Nanocomposites. *J. Am. Chem. Soc.* **2012**, *134*, 18157–18160.
(35) Damiron, D.; Mazzolini, J.; Cousin, F.; Boisson, C.; D'Agosto, F.; Drockenmuller, E. Poly(ethylene) Brushes Grafted to Silicon Substrates. *Polym. Chem.* **2012**, *3*, 1838–1845.
(36) Mecking, S. Olefin-Polymerisation durch Komplexe später Übergangsmetalle - ein Wegbereiter der Ziegler-Katalysatoren erscheint in neuem Gewand. *Angew. Chem.* **2001**, *113*, 550–557.
(37) McDaniel, M. P.; Rohlfing, D. C.; Benham, E. A. Long Chain Branching in Polyethylene from the Phillips Chromium Catalyst. *Polym. React. Eng.* **2003**, *11*, 101–132.
(38) McDaniel, M. P. A Review of the Phillips Supported Chromium Catalyst and Its Commercial Use for Ethylene Polymerization. *Advances in Catalysis* **2010**, *53*, 123–606.

(39) Natta, G.; Pino, P.; Mazzanti, G.; Giannini, U. A Crystallizable Organometallic Complex Containing Titanium and Aluminum. *J. Am. Chem. Soc.* **1957**, *79*, 2975–2976.
(40) Ziegler, K.; Holzkamp, E.; Breil, H.; Martin, H. Das Mülheimer Normaldruck-Polyäthylen-Verfahren. *Angew. Chem.* **1955**, *67*, 541–547.
(41) Ziegler, K.; Holzkamp, E.; Breil, H.; Martin, H. Polymerisation von Äthylen und anderen Olefinen. *Angew. Chem.* **1955**, *67*, 426.
(42) Natta, G. Von der Stereospezifischen Polymerisation zur Asymmetrischen Autokatalytischen Synthese von Makromolekülen (Nobel-Vortrag). *Angew. Chem.* **1964**, *76*, 553–566.
(43) Delferro, M.; Marks, T. J. Multinuclear Olefin Polymerization Catalysts. *Chem. Rev.* **2011**, *111*, 2450–2485.
(44) Böhm, L. L. Die Ethylenpolymerisation mit Ziegler-Katalysatoren 50 Jahre nach der Entdeckung. *Angew. Chem.* **2003**, *115*, 5162–5183.
(45) Kaminsky, W. Polymerization Catalysis. *Catal. Today* **2000**, *62*, 23–34.
(46) Senso, N.; Jongsomjit, B.; Praserthdam, P. Behaviors in Ethylene Polymerization of $MgCl_2$-SiO_2/$TiCl_4$/THF Ziegler-Natta Catalysts with differently treated SiO_2. *Molecules* **2011**, *16*, 1323–1335.
(47) Arlman, E. Ziegler-Natta Catalysis II. Surface Structure of Layer-Lattice Transition Metal Chlorides. *J. Catal.* **1964**, *3*, 89–98.
(48) Cossee, p. Ziegler-Natta catalysis I. Mechanism of Polymerization of α-Olefins with Ziegler-Natta Catalysts. *J. Catal.* **1964**, *3*, 80–88.
(49) Kaminsky, W.; Kopf, J.; Sinn, H.; Vollmer, H.-J. Extreme Bond Angle Distortion in Organozirconium Compounds Active Toward Ethylene. *Angew. Chem. Int. Ed.* **1976**, *15*, 629–630.
(50) Sinn, H.; Kaminsky, W.; Vollmer, H.-J.; Woldt, R. „Lebende Polymere" bei Ziegler-Katalysatoren Extremer Produktivität. *Angew. Chem.* **1980**, *92*, 396–402.
(51) Kaminsky, W.; Scholz, V. Progress of Olefin Polymerization by Metallocene Catalysts. *Macromol. Symp.* **2000**, *159*, 9–18.
(52) Kaminsky, W.; Miri, M.; Sinn, H.; Woldt, R. Bis(cyclopentadienyl)zirkon-Verbindungen und Aluminoxan als Ziegler-Katalysatoren für die Polymerisation und Copolymerisation von Olefinen. *Macromol. Rapid Commun.* **1983**, *4*, 417–421.
(53) Kaminsky, W.; Steiger, R. Polymerization of Olefins with Homogeneous Zirconocene/Alumoxane Catalysts. *Polyhedron* **1988**, *7*, 2375–2381.

(54) Brintzinger, H. H.; Fischer, D.; Mülhaupt, R.; Rieger, B.; Waymouth, R. M. Stereospecific Olefin Polymerization with Chiral Metallocene Catalysts. *Angew. Chem. Int. Ed.* **1995**, *34*, 1143–1170.

(55) McKnight, A. L.; Waymouth, R. M. Group 4 ansa- Cyclopentadienyl-Amido Catalysts for Olefin Polymerization. *Chem. Rev.* **1998**, *98*, 2587–2598.

(56) Gibson, V. C.; Spitzmesser, S. K. Advances in non-Metallocene Olefin Polymerization Catalysis. *Chem. Rev.* **2003**, *103*, 283–315.

(57) Chen, E. Y.-X.; Marks, T. J. Cocatalysts for Metal-Catalyzed Olefin Polymerization: Activators, Activation Processes, and Structure−Activity Relationships. *Chem. Rev.* **2000**, *100*, 1391–1434.

(58) Janiak, C.; Lassahn, P.-G.; Lozan, V. Metal Complexes for the Vinyl Addition Polymerization of Norbornene: New Compound Classes and Activation Mechanism with $B(C_6F_5)_3/AlEt_3$. *Macromol. Symp.* **2006**, *236*, 88–99.

(59) Kaminsky, W. Discovery of Methylaluminoxane as Cocatalyst for Olefin Polymerization. *Macromolecules* **2012**, *45*, 3289–3297.

(60) Sarzotti, D. M.; Marshman, D. J.; Ripmeester, W. E.; Soares, J. B. P. A Kinetic Study of Metallocene-Catalyzed Ethylene Polymerization using different Aluminoxane cocatalysts. *J. Polym. Sci., Part A: Polym. Chem.* **2007**, *45*, 1677–1690.

(61) Chen, E. Y.-X. Coordination Polymerization of Polar Vinyl Monomers by Single-site Metal Catalysts. *Chem. Rev.* **2009**, *109*, 5157–5214.

(62) Bochmann, M. The Chemistry of Catalyst Activation: The Case of Group 4 Polymerization Catalysts. *Organometallics* **2010**, *29*, 4711–4740.

(63) Kaminsky, W. The Discovery of Metallocene Catalysts and their Present State of the Art. *J. Polym. Sci., Part A: Polym. Chem.* **2004**, *42*, 3911–3921.

(64) Wieser, U.; Schaper, F.; Brintzinger, H.-H. Methylalumoxane (MAO)-Derived MeMAO−Anions in Zirconocene-Based Polymerization Catalyst Systems – A UV-Vis Spectroscopic Study. *Macromol. Symp.* **2006**, *236*, 63–68.

(65) Ivin, K. J.; Rooney, J. J.; Stewart, C. D.; Green, M. L. H.; Mahtab, R. Mechanism for the Stereospecific Polymerization of Olefins by Ziegler–Natta Catalysts. *J. Chem. Soc., Chem. Commun.* **1978**, 604–606.

(66) Green, M. L. H. Studies on Synthesis, Mechanism and Reactivity of some Organo-Molybdenum and -Tungsten Compounds. *Pure Appl. Chem.* **1978**, *50*, 27–35.
(67) Grubbs, R. H.; Coates, G. W. α-Agostic Interactions and Olefin Insertion in Metallocene Polymerization Catalysts. *Acc. Chem. Res.* **1996**, *29*, 85–93.
(68) Leatherman, M. D.; Svejda, S. A.; Johnson, L. K.; Brookhart, M. Mechanistic Studies of Nickel(II) Alkyl Agostic Cations and Alkyl Ethylene Complexes: Investigations of Chain Propagation and Isomerization in (α-diimine)Ni(II)-Catalyzed Ethylene Polymerization. *J. Am. Chem. Soc.* **2003**, *125*, 3068–3081.
(69) Brookhart, M.; Green, M. L. H.; Parkin, G. Agostic Interactions in Transition Metal Compounds. *PNAS* **2007**, *104*, 6908–6914.
(70) Bryliakov, K. P.; Talsi, E. P. Frontiers of Mechanistic Studies of Coordination Polymerization and Oligomerization of α-Olefins. *Coord. Chem. Rev.* **2012**, *256*, 2994–3007.
(71) Riedel, E.; Janiak, C. *Anorganische Chemie*, 8th ed.; de Gruyter: Berlin, 2011.
(72) Böhm, L.L. Reaction Model for Ziegler-Natta Polymerization Processes. *Polymer* **1978**, *19*, 545–552.
(73) Lechner, M. D.; Gehrke, K.; Nordmeier, E. H. *Makromolekulare Chemie*, 3rd ed.; Springer Spektrum: Berlin, 2003.
(74) Kempe, R. How to Polymerize Ethylene in a Highly Controlled Fashion? *Chemistry* **2007**, *13*, 2764–2773.
(75) Arriola, D. J.; Carnahan, E. M.; Hustad, P. D.; Kuhlman, R. L.; Wenzel, T. T. Catalytic Production of Olefin Block Copolymers via Chain Shuttling Polymerization. *Science* **2006**, *312*, 714–719.
(76) Britovsek, G. J. P.; Cohen, S. A.; Gibson, V. C.; Maddox, P. J.; van Meurs, M. Iron-Catalyzed Polyethylene Chain Growth on Zinc: Linear α-Olefins with a Poisson Distribution. *Angew. Chem. Int. Ed.* **2002**, *41*, 489–491.
(77) Britovsek, G. J. P.; Cohen, S. A.; Gibson, V. C.; van Meurs, M. Iron Catalyzed Polyethylene Chain Growth on Zinc: A Study of the Factors Delineating Chain Transfer versus Catalyzed Chain Growth in Zinc and Related Metal Alkyl Systems. *J. Am. Chem. Soc.* **2004**, *126*, 10701–10712.

(78) van Meurs, M.; Britovsek, G. J. P.; Gibson, V. C.; Cohen, S. A. Polyethylene Chain Growth on Zinc Catalyzed by Olefin Polymerization Catalysts: A Comparative Investigation of Highly Active Catalyst Systems Across the Transition Series. *J. Am. Chem. Soc.* **2005**, *127*, 9913–9923.

(79) Sita, L. R. Ex Uno Plures ("Out of One, Many"): New Paradigms for Expanding the Range of Polyolefins through Reversible Group Transfers. *Angew. Chem. Int. Ed.* **2009**, *48*, 2464–2472.

(80) D'Agosto, F.; Boisson, C. A RAFT Analogue Olefin Polymerization Technique Using Coordination Chemistry. *Aust. J. Chem.* **2010**, *63*, 1155.

(81) Quirk, R. P.; Lee, B. Experimental Criteria for Living Polymerizations. *Polym. Int.* **1992**, *27*, 359–367.

(82) Mani, G.; Gabbaï, F. P. A Neutral Chromium(III) Catalyst for the Living "Aufbaureaktion". *Angew. Chem. Int. Ed.* **2004**, *43*, 2263–2266.

(83) Bogaert, S.; Carpentier, J.-F.; Chenal, T.; Mortreux, A.; Ricart, G. Chlorolanthanocene-Dialkylmagnesium Systems for Styrene Bulk Polymerization and Styrene-Ethylene Block Copolymerization. *Macromol. Chem. Phys.* **2000**, *201*, 1813–1822.

(84) Rouholahnejad, F.; Mathis, D.; Chen, P. Narrowly Distributed Polyethylene via Reversible Chain Transfer to Aluminum by a Sterically Hindered Zirconocene/MAO. *Organometallics* **2010**, *29*, 294–302.

(85) Sarazin, Y.; Chenal, T.; Mortreux, A.; Vezin, H.; Carpentier, J.-F. Binary Cerium(IV) tert-Butoxides-Dialkylmagnesium Systems: Radical Versus Coordinative Polymerization of Styrene. *J. Mol. Catal. A: Chem.* **2005**, *238*, 207–214.

(86) Bogaert, S.; Chenal, T.; Mortreux, A.; Nowogrocki, G.; Lehmann, C. W.; Carpentier, J.-F. Neodymium(III) Complexes with Bulky ansa - Bis(cyclopentadienyl) Ligands: Synthesis and Use in Olefin Oligomerization. *Organometallics* **2001**, *20*, 199–205.

(87) Haas, I.; Kretschmer, W. P.; Kempe, R. Synthesis of Alumina-Terminated Linear PE with a Hafnium Aminopyridinate Catalyst. *Organometallics* **2011**, *30*, 4854–4861.

(88) Chenal, T.; Olonde, X.; Pelletier, J.-F.; Bujadoux, K.; Mortreux, A. Controlled Polyethylene Chain Growth on Magnesium Catalyzed by Lanthanidocene: A Living Transfer Polymerization for the Synthesis of Higher Dialkyl-Magnesium. *Polymer* **2007**, *48*, 1844–1856.

(89) Olonde, X.; Mortreux, A.; Petit, F.; Bujadoux, K. A Useful Method for the Synthesis of Neodymocene Homogeneous Catalysts for Ethylene Polymerization. *J. Mol. Catal.* **1993**, *82*, 75–82.
(90) Pelletier, J.-F.; Mortreux, A.; Olonde, X.; Bujadoux, K. Synthesis of New Dialkylmagnesium Compounds by Living Transfer Ethylene Oligo- and Polymerization with Lanthanocene Catalysts. *Angew. Chem. Int. Ed.* **1996**, *35*, 1854–1856.
(91) Ribeiro, R.; Ruivo, R.; Nsiri, H.; Norsic, S.; D'Agosto, F.; Perrin, L.; Boisson, C. Deciphering the Mechanism of Coordinative Chain Transfer Polymerization of Ethylene Using Neodymocene Catalysts and Dialkylmagnesium. *ACS Catal.* **2016**, *6*, 851–860.
(92) Binder, W. H.; Sachsenhofer, R. 'Click' Chemistry in Polymer and Material Science: An Update. *Macromol. Rapid Commun.* **2008**, *29*, 952–981.
(93) Lopez, R. G.; Boisson, C.; D'Agosto, F.; Spitz, R.; Boisson, F.; Bertin, D.; Tordo, P. Synthesis and Characterization of Macroalkoxyamines Based on Polyethylene. *Macromolecules* **2004**, *37*, 3540–3542.
(94) Nzahou, O. W.; Norsic, S.; Belaid, I.; Boisson, C.; D'Agosto, F. Amino End-Functionalized Polyethylenes and Corresponding Telechelics by Coordinative Chain Transfer Polymerization. *Macromolecules* **2017**, *50*, 8372–8377.
(95) Mazzolini, J.; Boyron, O.; Monteil, V.; D'Agosto, F.; Boisson, C.; Sanders, G. C.; Heuts, J. P. A.; Duchateau, R.; Gigmes, D.; Bertin, D. Polyethylene End Functionalization using Thia-Michael Addition Chemistry. *Polym. Chem.* **2012**, *3*, 2383.
(96) Mazzolini, J.; Boyron, O.; Monteil, V.; Gigmes, D.; Bertin, D.; D'Agosto, F.; Boisson, C. Polyethylene End Functionalization Using Radical-Mediated Thiol−Ene Chemistry: Use of Polyethylenes Containing Alkene End Functionality. *Macromolecules* **2011**, *44*, 3381–3387.
(97) Godoy Lopez, R.; Boisson, C.; D'Agosto, F.; Spitz, R.; Boisson, F.; Gigmes, D.; Bertin, D. New Functional Polyolefins: Towards a Bridge Between Catalytic and RAFT Polymerizations? *Macromol. Rapid Commun.* **2006**, *27*, 173–181.
(98) Maher, S.; Jjunju, F. P. M.; Taylor, S. Colloquium: 100 Years of Mass Spectrometry: Perspectives and Future Trends. *Rev. Mod. Phys.* **2015**, *87*, 113–135.

(99) Gross, J. H. *Mass Spectrometry: A Textbook*, 3rd ed.; Springer International Publishing: Cham, 2017.
(100) Fenn, J. B. Electrospray Wings for Molecular Elephants (Nobel lecture). *Angew. Chem. Int. Ed.* **2003**, *42*, 3871–3894.
(101) Tanaka, K. The Origin of Macromolecule Ionization by Laser Irradiation (Nobel lecture). *Angew. Chem. Int. Ed.* **2003**, *42*, 3860–3870.
(102) Awad, H.; Khamis, M. M.; El-Aneed, A. Mass Spectrometry, Review of the Basics: Ionization. *Appl. Spectrosc. Rev.* **2014**, *50*, 158–175.
(103) Konermann, L.; Ahadi, E.; Rodriguez, A. D.; Vahidi, S. Unraveling the Mechanism of Electrospray Ionization. *Anal. Chem.* **2013**, *85*, 2–9.
(104) Zenobi, R.; Knochenmuss, R. Ion Formation in MALDI Mass Spectrometry. *Mass Spectrom. Rev.* **1998**, *17*, 337–366.
(105) Karas, M.; Bahr, U.; Gießmann, U. Matrix-Assisted Laser Desorption Ionization Mass Spectrometry. *Mass Spectrom. Rev.* **1991**, *10*, 335–357.
(106) El-Aneed, A.; Cohen, A.; Banoub, J. Mass Spectrometry, Review of the Basics: Electrospray, MALDI, and Commonly Used Mass Analyzers. *Appl. Spectrosc. Rev.* **2009**, *44*, 210–230.
(107) Wollnik, H. Time-Of-Flight Mass Analyzers. *Mass Spectrom. Rev.* **1993**, *12*, 89–114.
(108) Peacock, P. M.; McEwen, C. N. Mass Spectrometry of Synthetic Polymers. *Anal. Chem.* **2004**, *76*, 3417–3427.
(109) Nielen, M. W.F. Maldi Time-of-Flight Mass Spectrometry of Synthetic Polymers. *Mass Spectrom. Rev.* **1999**, *18*, 309–344.
(110) Schriemer, D. C.; Li, L. Mass Discrimination in the Analysis of Polydisperse Polymers by MALDI Time-of-Flight Mass Spectrometry. 1. Sample Preparation and Desorption/Ionization Issues. *Anal. Chem.* **1997**, *69*, 4169–4175.
(111) Schriemer, D. C.; Li, L. Mass Discrimination in the Analysis of Polydisperse Polymers by MALDI Time-of-Flight Mass Spectrometry. 2. Instrumental Issues. *Anal. Chem.* **1997**, *69*, 4176–4183.
(112) Yalcin, T.; Wallace, W. E.; Guttman, C. M.; Li, L. Metal Powder Substrate-Assisted Laser Desorption/Ionization Mass Spectrometry for Polyethylene Analysis. *Anal. Chem.* **2002**, *74*, 4750–4756.

(113) Lin-Gibson, S.; Brunner, L.; Vanderhart, D. L.; Bauer, B. J.; Fanconi, B. M.; Guttman, C. M.; Wallace, W. E. Optimizing the Covalent Cationization Method for the Mass Spectrometry of Polyolefins. *Macromolecules* **2002**, *35*, 7149–7156.

(114) Wallace, W. E.; Blair, W. R. Matrix-Assisted Laser Desorption/Ionization Mass Spectrometry of Covalently Cationized Polyethylene as a Function of Sample Temperature. *Int. J. Mass spectrom.* **2007**, *263*, 82–87.

(115) Di Lena, F.; Quintanilla, E.; Chen, P. Measuring Rate Constants for Active Species in the Polymerization of Ethylene by MAO-Activated Metallocene Catalysts by Electrospray Ionization Mass Spectrometry. *Chem. Commun.* **2005**, 5757–5759.

(116) Moscato, B.; Landis, C. Are Carbodiimide-Quenched Polyethylene Distributions Representative of Bulk Polymer Samples? Analysis of Metallocene-Catalyzed Ethylene Polymerization by ESI-MS, MALDI, GPC and NMR. *Chem. Commun.* **2008**, 5785–5787.

(117) Cate, A. T.; Reinders, S. A.F.; Turkenburg, D. H.; Bruin, A.; D'Souza, F.; Donnelly, G. T.; Willemsen, P. R.; Maas, J. H.; van Bommel, K. J.C. High Density Hydrophilic and Hydrophobic Brush Coatings using a Polymeric Primer Layer. *Prog. Org. Coat.* **2009**, *64*, 221–224.

(118) Luzinov, I.; Minko, S.; Tsukruk, V. V. Responsive Brush Layers: From Tailored Gradients to Reversibly Assembled Nanoparticles. *Soft Matter* **2008**, *4*, 714.

(119) Barbey, R.; Lavanant, L.; Paripovic, D.; Schüwer, N.; Sugnaux, C.; Tugulu, S.; Klok, H.-A. Polymer Brushes via Surface-Initiated Controlled Radical Polymerization: Synthesis, Characterization, Properties, and Applications. *Chem. Rev.* **2009**, *109*, 5437–5527.

(120) Bell, A. T. The Impact of Nanoscience on Heterogeneous Catalysis. *Science* **2003**, *299*, 1688–1691.

(121) Zhao, B.; Brittain, W.J. Polymer Brushes: Surface-Immobilized Macromolecules. *Prog. Polym. Sci.* **2000**, *25*, 677–710.

(122) Zdyrko, B.; Luzinov, I. Polymer Brushes by the "Grafting to" Method. *Macromol. Rapid Commun.* **2011**, *32*, 859–869.

(123) Stamm, M. *Polymer Surfaces and Interfaces: Characterization, Modification and Applications*, 1st ed.; Springer: Berlin, 2008.

(124) Zapata, P. A.; Tamayo, L.; Páez, M.; Cerda, E.; Azócar, I.; Rabagliati, F. M. Nanocomposites based on Polyethylene and Nanosilver Particles Produced by Metallocenic "in situ" Polymerization: Synthesis, Characterization, and Antimicrobial Behavior. *Eur. Polym. J.* **2011**, *47*, 1541–1549.

(125) Lin, Y.; Jin, J.; Song, M. Preparation and Characterisation of Covalent Polymer Functionalized Graphene Oxide. *J. Mater. Chem.* **2011**, *21*, 3455–3461.

(126) Wang, L.; Feng, L.-X.; Xie, T. Novel Magnetic Polyethylene Nanocomposites Produced by Supported Nanometre Magnetic Ziegler-Natta catalyst. *Polym. Int.* **2000**, *49*, 184–188.

(127) Xiang, P.; Petrie, K.; Kontopoulou, M.; Ye, Z.; Subramanian, R. Tuning Structural Parameters of Polyethylene Brushes on Silicananoparticles in Surface-Initiated Ethylene "living" Polymerization and Effects on Silica Dispersion in a Polyolefin Matrix. *Polym. Chem.* **2013**, *4*, 1381–1395.

(128) Huebner, D.; Koch, V.; Ebeling, B.; Mechau, J.; Steinhoff, J. E.; Vana, P. Comparison of Monomethoxy-, Dimethoxy-, and Trimethoxysilane Anchor Groups for Surface-Initiated RAFT Polymerization from Silica Surfaces. *J. Polym. Sci., Part A: Polym. Chem.* **2015**, *53*, 103–113.

(129) Ghosh, S.; Goswami, S. K.; Mathias, L. J. Surface Modification of Nano-Silica with Amides and Imides for Use in Polyester Nanocomposites. *J. Mater. Chem. A* **2013**, *1*, 6073.

(130) Peng, Z.; Li, Q.; Li, H.; Hu, Y. Polyethylene-Modified Nano Silica and Its Fine Dispersion in Polyethylene. *Ind. Eng. Chem. Res.* **2017**, *56*, 5892–5898.

(131) Li, Y.-F.; Liu, Y.-X.; Wang, X.-M.; Wu, Q.-L.; Yu, H.-P.; Li, J. Wood-Polymer Composites Prepared by the in situ Polymerization of Monomers within Wood. *J. Appl. Polym. Sci.* **2011**, *119*, 3207–3216.

(132) Kumar, V.; Tyagi, L.; Sinha, S. Wood Flour–Reinforced Plastic Composites: A Review. *Rev. Chem. Eng.* **2011**, *27*, 441.

(133) Lu, J. Z.; Wu, Q.; Negulescu, I. I. Wood-Fiber/High-Density-Polyethylene Composites: Compounding Process. *J. Appl. Polym. Sci.* **2004**, *93*, 2570–2578.

(134) Keener, T.J.; Stuart, R.K.; Brown, T.K. Maleated Coupling Agents for Natural Fibre Composites. *Composites Part A* **2004**, *35*, 357–362.

(135) Zhang, Y.; Li, H. Functionalization of High Density Polyethylene with Maleic Anhydride in the Melt State through Ultrasonic Initiation. *Polym. Eng. Sci.* **2003**, *43*, 774–782.
(136) Lu, B.; Chung, T. C. Synthesis of Maleic Anhydride Grafted Polyethylene and Polypropylene, with Controlled Molecular Structures. *J. Polym. Sci. A Polym. Chem.* **2000**, *38*, 1337–1343.
(137) Balazs, A. C.; Emrick, T.; Russell, T. P. Nanoparticle Polymer Composites: Where Two Small Worlds Meet. *Science* **2006**, *314*, 1107–1110.
(138) Kumar, S. K.; Jouault, N.; Benicewicz, B.; Neely, T. Nanocomposites with Polymer Grafted Nanoparticles. *Macromolecules* **2013**, *46*, 3199–3214.
(139) Peng, W.; Rossner, C.; Roddatis, V.; Vana, P. Gold-Planet–Silver-Satellite Nanostructures Using RAFT Star Polymer. *ACS Macro Lett.* **2016**, *5*, 1227–1231.
(140) Rossner, C.; Ebeling, B.; Vana, P. Spherical Gold-Nanoparticle Assemblies with Tunable Interparticle Distances Mediated by Multifunctional RAFT Polymers. *ACS Macro Lett.* **2013**, *2*, 1073–1076.
(141) Ebeling, B.; Vana, P. RAFT-Polymers with Single and Multiple Trithiocarbonate Groups as Uniform Gold-Nanoparticle Coatings. *Macromolecules* **2013**, *46*, 4862–4871.
(142) Palza, H. Antimicrobial Polymers with Metal Nanoparticles. *Int. J. Mol. Sci.* **2015**, *16*, 2099–2116.
(143) Christensen, C. H.; Nørskov, J. K. Chemistry. Green Gold Catalysis. *Science* **2010**, *327*, 278–279.
(144) Garcia, M. A. Surface Plasmons in Metallic Nanoparticles: Fundamentals and Applications. *J. Phys. D: Appl. Phys.* **2011**, *44*, 283001.
(145) Link, S.; El-Sayed, M. A. Size and Temperature Dependence of the Plasmon Absorption of Colloidal Gold Nanoparticles. *J. Phys. Chem. B* **1999**, *103*, 4212–4217.
(146) Cushen, M.; Kerry, J.; Morris, M.; Cruz-Romero, M.; Cummins, E. Evaluation and Simulation of Silver and Copper Nanoparticle Migration from Polyethylene Nanocomposites to Food and an Associated Exposure Assessment. *J. Agric. Food. Chem.* **2014**, *62*, 1403–1411.
(147) Zhang, Y.; Li, H.; Dong, J.-Y.; Hu, Y. Facile Synthesis of Chain End Functionalized Polyethylenes via Epoxide Ring-Opening and Thiol–ene Addition Click Chemistry. *Polym. Chem.* **2014**, *5*, 105–115.

(148) Kolb, H. C.; Finn, M. G.; Sharpless, K. B. Click-Chemie: Diverse chemische Funktionalität mit einer Handvoll guter Reaktionen. *Angew. Chem.* **2001**, *113*, 2056–2075.
(149) Friebolin, H.; Thiele, C. M. *Ein- und Zweidimensionale NMR-Spektroskopie: Eine Einführung*, 5th ed.; Wiley-VCH-Verl.: Weinheim, 2013.
(150) Norsic, S.; Thomas, C.; D'Agosto, F.; Boisson, C. Divinyl-end-Functionalized Polyethylenes: Ready Access to a Range of Telechelic Polyethylenes through Thiol-ene Reactions. *Angew. Chem. Int. Ed.* **2015**, *54*, 4631–4635.
(151) Mangiante, G.; Alcouffe, P.; Burdin, B.; Gaborieau, M.; Zeno, E.; Petit-Conil, M.; Bernard, J.; Charlot, A.; Fleury, E. Green Nondegrading Approach to Alkyne-Functionalized Cellulose Fibers and Biohybrids thereof: Synthesis and Mapping of the Derivatization. *Biomacromolecules* **2013**, *14*, 254–263.
(152) Hill, C. A. S.; Mallon, S. The Chemical Modification of Scots Pine with Succinic Anhydride or Octenyl Succinic Anhydride. I. Dimensional Stabilisation. *Holzforschung* **1998**, *52*, 427–433.
(153) Müller, G.; Schöpper, C.; Vos, H.; Kharazipour, A.; Polle, A. FTIR-ATR Spectroscopic Analyses of Changes in Wood Properties During Particle- and Fibreboard Production of Hard- and Softwood Trees. *Bioresour.* **2009**, *4*, 49–71.
(154) Parker, F. S. *Applications of Infrared, Raman, and Resonance Raman Spectroscopy in Biochemistry*; Plenum Press: New York, 1983.
(155) Krimm, S.; Liang, C. Y.; Sutherland, G. B. B. M. Infrared Spectra of High Polymers. II. Polyethylene. *The Journal of Chemical Physics* **1956**, *25*, 549–562.
(156) Kaßel, M.; Gerke, J.; Ley, A.; Vana, P. Surface Modification of Wood Flour via ARGET ATRP and Its Application as Filler in Thermoplastics. *Polymers* **2018**, *10*, 354.
(157) Stöber, W.; Fink, A.; Bohn, E. Controlled Growth of Monodisperse Silica Spheres in the Micron Size Range. *J. Colloid Interface Sci.* **1968**, *26*, 62–69.
(158) Rogers, H. R.; Hill, C. L.; Fujiwara, Y.; Rogers, R. J.; Mitchell, H. L.; Whitesides, G. M. Mechanism of Formation of Grignard Reagents. Kinetics of Reaction of Alkyl Halides in Diethyl Ether with Magnesium. *J. Am. Chem. Soc.* **1980**, *102*, 217–226.

(159) Reuben D. Rieke; S. E. Bales; P. M. Hudnall; T. P. Burns; G. S. Poindexter. Highly Reactive Magnesium for the Preparation of Grignard Reagents: 1-Norbornane Acid. *Org. Synth.* **1979**, *59*, 85.
(160) Schlenk, W.; Schlenk, W. Über die Konstitution der Grignardschen Magnesiumverbindungen. *Ber. dtsch. Chem. Ges. A/B* **1929**, *62*, 920–924.
(161) Wagner, J.; Peng, W.; Vana, P. Polyethylene-Grafted Gold and Silver Nanoparticles Using Catalyzed Chain Growth (CCG). *Polymers* **2018**, *10*, 407.
(162) Shen, W.; Qiu, Q.; Wang, Y.; Miao, M.; Li, B.; Zhang, T.; Cao, A.; An, Z. Hydrazine as a Nucleophile and Antioxidant for Fast Aminolysis of RAFT Polymers in Air. *Macromol. Rapid Commun.* **2010**, *31*, 1444–1448.
(163) Fink, J.; Kiely, C. J.; Bethell, D.; Schiffrin, D. J. Self-Organization of Nanosized Gold Particles. *Chem. Mater.* **1998**, *10*, 922–926.
(164) Hiramatsu, H.; Osterloh, F. E. A Simple Large-Scale Synthesis of Nearly Monodisperse Gold and Silver Nanoparticles with Adjustable Sizes and with Exchangeable Surfactants. *Chem. Mater.* **2004**, *16*, 2509–2511.
(165) Kade, M. J.; Burke, D. J.; Hawker, C. J. The Power of Thiol-Ene Chemistry. *J. Polym. Sci. A Polym. Chem.* **2010**, *48*, 743–750.
(166) Shan, J.; Zhao, Y.; Granqvist, N.; Tenhu, H. Thermoresponsive Properties of N -Isopropylacrylamide Oligomer Brushes Grafted to Gold Nanoparticles: Effects of Molar Mass and Gold Core Size. *Macromolecules* **2009**, *42*, 2696–2701.
(167) Li, W.; Cai, X.; Kim, C.; Sun, G.; Zhang, Y.; Deng, R.; Yang, M.; Chen, J.; Achilefu, S.; Wang, L. V. *et al.* Gold Nanocages Covered with Thermally-Responsive Polymers for Controlled Release by High-Intensity Focused Ultrasound. *Nanoscale* **2011**, *3*, 1724–1730.
(168) Rossner, C.; Glatter, O.; Vana, P. Stimulus-Responsive Planet–Satellite Nanostructures as Colloidal Actuators: Reversible Contraction and Expansion of the Planet–Satellite Distance. *Macromolecules* **2017**, *50*, 7344–7350.
(169) Bergbreiter, D. E.; Chandran, R. Polyethylene-Bound Rhodium(I) Hydrogenation Catalysts. *J. Am. Chem. Soc.* **1987**, *109*, 174–179.
(170) Bergbreiter, D. E. Using Soluble Polymers to Recover Catalysts and Ligands. *Chem. Rev.* **2002**, *102*, 3345–3384.

(171) Hobbs, C.; Yang, Y.-C.; Ling, J.; Nicola, S.; Su, H.-L.; Bazzi, H. S.; Bergbreiter, D. E. Thermomorphic Polyethylene-Supported Olefin Metathesis Catalysts. *Org. Lett.* **2011**, *13*, 3904–3907.

(172) Niu, Z.; Peng, Q.; Gong, M.; Rong, H.; Li, Y. Oleylamine-Mediated Shape Evolution of Palladium Nanocrystals. *Angew. Chem. Int. Ed.* **2011**, *50*, 6315–6319.

(173) Staudt, B. H.; Wagner, J.; Vana, P. Cationic End-Functional Polyethylene via Catalyzed Chain Growth: Synthesis, Mass Spectrometry, and Applications. *Macromolecules* **2018**, *51*, 8469–8476.

(174) Axelsson, J.; Scrivener, E.; Haddleton, D. M.; Derrick, P. J. Mass Discrimination Effects in an Ion Detector and Other Causes for Shifts in Polymer Mass Distributions Measured by Matrix-Assisted Laser Desorption/Ionization Time-of-Flight Mass Spectrometry. *Macromolecules* **1996**, *29*, 8875–8882.

(175) Zhang, L.; Cool, L. R.; Wesdemiotis, C.; Weiss, R. A.; Cavicchi, K. A. Syntheses of Quaternary Ammonium-Containing, Trithiocarbonate RAFT Agents and Hemi-telechelic Cationomers. *Polym. Chem.* **2014**, *5*, 1180–1190.

(176) Zhang, L.; Tang, Q.; Weiss, R. A.; Cavicchi, K. A. Synthesis and Characterization of Quaternary Phosphonium-Containing, Trithiocarbonate RAFT Agents. *Polym. Chem.* **2014**, *5*, 5492–5500.

(177) Rahman, M.; Brazel, C. The Plasticizer Market: An Assessment of Traditional Plasticizers and Research Trends to Meet New Challenges. *Prog. Polym. Sci.* **2004**, *29*, 1223–1248.

(178) Appendini, P.; Hotchkiss, J. H. Review of Antimicrobial Food Packaging. *Innov. Food Sci. Emerg. Technol.* **2002**, *3*, 113–126.

(179) Bergbreiter, D. E.; Blanton, J. R. Functionalized Ethylene Oligomers as Phase-Transfer Catalysts. *J. Org. Chem.* **1985**, *50*, 5828–5833.

(180) Neises, B.; Steglich, W. Einfaches Verfahren zur Veresterung von Carbonsäuren. *Angew. Chem.* **1978**, *90*, 556–557.

(181) Sonntag, N. O. V. The Reactions of Aliphatic Acid Chlorides. *Chem. Rev.* **1953**, *52*, 237–416.

(182) Matyjaszewski, K.; Xia, J. Atom Transfer Radical Polymerization. *Chem. Rev.* **2001**, *101*, 2921–2990.

(183) Tilley, T. D.; Andersen, R. A. Pentamethylcyclopentadienyl Derivatives of the Trivalent Lanthanide Elements Neodymium, samarium, and ytterbium. *Inorg. Chem.* **1981**, *20*, 3267–3270.

(184) Weber, W. G.; McLeary, J. B.; Sanderson, R. D. Facile Preparation of Bis(thiocarbonyl)disulfides via Elimination. *Tetrahedron Lett.* **2006**, *47*, 4771–4774.